ANALYSIS OF VARIOUS MICROSTRIP PRINTED GEOMETRIES USING CLOSED-FORM GREEN'S FUNCTIONS

A THESIS SUBMITTED TO
THE GRADUATE SCHOOL OF NATURAL AND APPLIED SCIENCES
OF
MIDDLE EAST TECHNICAL UNIVERSITY

BY
İREM ÜLKÜ

IN PARTIAL FULLFILLMENT OF THE REQUIREMENTS
FOR
THE DEGREE OF MASTER OF SCIENCE
IN
ELECTRICAL AND ELECTRONICS ENGINEERING

SEPTEMBER 2013

Approval of the thesis:

ANALYSIS OF VARIOUS MICROSTRIP PRINTED GEOMETRIES USING CLOSED-FORM GREEN'S FUNCTIONS

submitted by **İREM ÜLKÜ** in partial fulfillment of the requirements for the degree of **Master of Science in Electrical and Electronics Engineering Department, Middle East Technical University** by,

Prof. Dr. Canan Özgen
Dean, Graduate School of **Natural and Applied Sciences** _____

Prof. Dr. Gönül Turhan Sayan
Head of Department, **Electrical and Electronics Engineering** _____

Prof. Dr. Gülbin Dural
Supervisor, **Electrical and Electronics Engineering, METU** _____

Assoc. Prof. Dr. Lale Alatan
Co-Supervisor, **Electrical and Electronics Engineering, METU** _____

Examining Committee Members:

Prof. Dr. Mustafa Kuzuoğlu
Electrical and Electronics Engineering Dept., METU _____

Prof. Dr. Gülbin Dural
Electrical and Electronics Engineering Dept., METU _____

Assoc. Prof. Dr. Lale Alatan
Electrical and Electronics Engineering Dept., METU _____

Prof. Dr. Gönül Turhan Sayan
Electrical and Electronics Engineering Dept., METU _____

Assoc. Prof. Dr. Özlem Özgün
Electrical and Electronics Engineering Dept., TED Univ. _____

Date: _____

I hereby declare that all information in this document has been obtained and presented in accordance with academic rules and ethical conduct. I also declare that, as required by these rules and conduct, I have fully cited and referenced all material and results that are not original to this work.

Name, Last name :

Signature :

ABSTRACT

ANALYSIS OF VARIOUS MICROSTRIP PRINTED GEOMETRIES USING CLOSED-FORM GREEN'S FUNCTIONS

Ülkü, İrem

M. S., Department of Electrical and Electronics Engineering

Supervisor: Prof. Dr. Gülbin Dural

Co-Supervisor: Doç. Dr. Lale Alatan

August 2013, 116 Pages

In general, current distributions for different microstrip structures such as Single Microstrip Line (SML), Coupled Microstrip Line (CML) and Microstrip Patch Antenna (MPA) are obtained by using Method of Moments (MoM) in conjuction with closed-form spatial domain Green's functions. Specifically, MPA is designed to obtain a Wideband Microstrip Patch Antenna (WMPA). The current distribution is acquired by the same analysis and bandwidth is obtained from the return loss graph for this WMPA. Standard MPA and WMPA bandwidths are compared.

First, MoM analysis is used to find the current distribution of SML. Then, current distribution on CML is found, in that case by considering the interaction between the lines. Afterward, current distribution on MPA is calculated. Finally, WMPA is obtained by opening two parallel slots on the metal patch of standard MPA. Current distribution on WMPA is found by using matrix deleting method such that there is no need to re-execute software program for this new geometry. Thereafter, bandwidth of WMPA is obtained from the return loss graph. Bandwidth values for standard MPA and WMPA are compared and the increase in bandwidth is observed.

Keywords: Method of Moments, Green's functions, coupled microstrip line, microstrip patch antenna, wideband microstrip patch antenna.

ÖZ

ÇEŞİTLİ MİKROŞERİT YAPILARIN KAPALI-FORMDA GREEN FONKSİYONLARI KULLANILARAK İNCELENMESİ

Ülkü, İrem

Yüksek Lisans, Elektrik ve Elektronik Mühendisliği Bölümü

Tez Yöneticisi: Prof. Dr. Gülbin Dural

Ortak Tez Yöneticisi: Doç. Dr. Lale Alatan

Ağustos 2013, 116 Sayfa

Genel olarak, Mikroşerit Hat (MH), Kuplajlanmış Mikroşerit Hat (KMH) ve Mikroşerit Yama Anten (MYA) gibi mikroşerit yapıların akım dağılımları Moment Metodu (MM) ile birlikte gerçek uzaydaki kapalı form Green fonksiyonları kullanılarak bulunmuştur. Özel olarak ise, Geniş Bant Yama Antenleri (GBYA) MYA kullanılarak tasarlanmış, aynı analizler kullanılarak akım dağılımları bulunmuş, geri dönüş kayıbı grafiği çizilmiş ve buradan bantgenişliği hesaplanmıştır. Standart MYA bantgenişliği değeri ile GBYA bantgenişliği değeri karşılaştırılmıştır.

İlk önce, MM analizi kullanılarak MH üzerindeki akım dağılımları bulunmuştur. İkinci olarak, KMH üzerindeki akım dağılımı bulunmuştur, burada hatlar arasındaki etkileşim de göz ününde bulundurulmuştur. Daha sonra, MYA üzerindeki akım dağılımı bulunmuştur. Son olarak, standart MYA üzerinde iki paralel yarık açılarak GBYA elde edilmiştir. Matriks silme yöntemi kullanılarak GBYA üzerindeki akım dağılımı bulunmuştur bu nedenle bilgisayar programını yeni geometri yapısı için yeniden çalıştırmaya gerek kalmamıştır. Buradan geri dönüş kaybı grafiği GBYA için çizdirilmiş ve bantgenişliği hesaplanmıştır. Standart MYA bantgenişliği değeri ile GBYA bantgenişliği değeri karşılaştırılarak, bantgenişliği artışı gözlemlenmiştir.

Anahtar Kelimeler: Moment Methodu, Green fonksiyonları, Kuplajlanmış Mikroşerit Hatlar, Mikroşerit Yama Anten, Geniş Bant Yama Anten.

To my family,

ACKNOWLEDGEMENT

First of all I want to thank my supervisor Prof. Dr. Gülbin Dural. I want to express my gratitude to her due to the entire support and assistance she gave me throughout my thesis study. In addition to the technical and scientific support she ensures, her positive standpoint and encouragement keep my motivation always at the highest level. Due to this positive approach, I always believe that there should be a solution to every problem. Moreover, my supervisor spends significant effort to help me in various issues that eases my study. This thesis study cannot be completed without all these precious supports and assistances of my supervisor. Therefore, I present my endless appreciation to her.

Especially, I want to thank my co-supervisor Assoc. Prof. Dr. Lale Alatan. I want to present my appreciation one by one due to the facts that she never rejects me even though she is very busy, spends her valuable time to my thesis study, sometimes works on my software program for hours, never gives up when problems arise and points out the right way every time when I get lost. I can ask all the questions on my mind to her then all these confusions are removed. Therefore, throughout my thesis study I always feel self confident about my studies. She gives information about all substantial details and alerts me to all possible consequences, so I can be aware of everything in the study. I cannot achieve the desired results without her guidance. This thesis study cannot be completed without all these precious supports and assistances of my co-supervisor. Therefore, I present my endless appreciation to her.

I want to thank Şefika Özkal Piroğlu who studied similar subjects in her thesis. She helps me a lot to the software programming part of my study and does not hesitate to share her valuable experience with me. I also grateful to graduate assistant Ömer Bayraktar who shares his knowledge with me. I also want to thank Prof. Dr. Yusuf Ziya Umul who makes an effort to solve my problems and interests to all stages of my study. I want to thank my dear teacher Canan Kamacıoğlu, she supports me both morally and technically throughout my study. I can share all my problems with her and she always try to find out solutions, I am grateful to her.

I want to express my deepest gratitude to my family. They try to ease my life in every way during my thesis study. They always believe me and respect my decisions. They know all my experiences through my study and they try to ensure the highest level of support to me. I want to thank both my mother and my father due to their precious support and love, without them I cannot achieve this exhausting process.

I also express my gratitude to whom I forget to mention here but help me in my thesis study somehow.

TABLE OF CONTENTS

LIST OF FIGURES

CHAPTER 1

INTRODUCTION

In microwave circuits the wavelength is very close to the dimensions of circuit components and frequency of application generally exists within 300MHz-300GHz frequency range where wavelength is in between 1mm-1m. Circuit components are not very small relative to the wavelength as in the case of lumped-circuit model for low frequencies.

By a printed circuit, it should be understood that circuit patterns are printed or etched on a dielectric slab by photolithographic technology or screen printing technology. Microwave printed circuits (MPC) are constructed by using technologies that are constructed for low frequencies where lumped elements are valid. Here, distributed circuit elements are used instead of lumped elements. The difference between printed circuit board (PCB) and MPC is the electrical/physical features of the dielectric. Both PCBs and MPCs enable complex connections between circuit components. A matter of fact this is the most important advantage of microstrip circuits. Multilayer and complex circuits can be constructed easily and less costly [1].

In monolithic microwave integrated circuits (MMIC), monolithic is defined as placing active/passive elements, components and interconnects on a dielectric substrate by using a deposition scheme [2]. These deposition schemes can be epitaxy, ion implantation, sputtering, evaporation, diffusion and etc. MMICs are generally constructed by using GaAs semiconductor substrate [3].

Coaxial line is modified and flat-strip coaxial line is constructed during World War II and some applications are performed. First commercial slotted line application is realized by Hewelett-Packard Co as known [1]. Even so, before the year 1949, flat-strip coaxial lines are considered to be used only for transmission. Robert M. Barrett realized that in addition to the transmission usage, flat-strip coaxial lines can also be used to develop microwave components such as filters, directional couplers, etc. [4]. That means printed circuit application can also be applied to flat-strip coaxial lines. MPCs are appeared like that. This study is carried out in Air Force Cambridge Research Center and it can be considered that MPCs are first developed for airborne applications. In year 1954, first MPC symposium is realized at Tufts University. In this symposium subjects such as striplines, microstriplines, filters, couplers, power dividers and hybrid rings are presented [1]. Afterwards, Transactions on Microwave Theory and Techniques constituted a special issue that includes the studies presented in the symposium.

In microstrip structures, fundamental propagation mode is not transverse electromagnetic (TEM). Therefore, phase velocity and characteristic impedance change by frequency and it creates some problems. However, there is a way to draw propagation mode to TEM. If the

cross section relative to wavelength could be reduced, the advantages of microstrip structures can be utilized easily [5].

First known study for microstrip patch antenna is performed by Deschamps, Cutton and Baissinot in year 1950 [6]. In year 1974, a study is published that is about conformal microstrip antennas and arrays [7]. In this study, it is aimed to use microstrip antennas in aircrafts, missiles and rockets. Experimental studies about rectangular and circular patch antennas are published as well [1]. In year 1979, a study that is related with cavity model appeared. Again in the same year, a workshop is designed for microstrip antennas at New Mexico State University. Afterwards, IEEE Transactions on Antenna and Propagation is constructed a special issue about microstrip antennas in year 1981 [1]. While microstrip circuits are developed throughout the years, a special type of them which is microstrip antennas are developed as well. Nowadays, in most microstrip circuits, microstrip antennas are used. The advantages, disadvantages and usage areas of microstrip antennas will be described in this thesis in detail later. Patch antenna can be fed by microstrip line, coaxial line or by slot. Radiation loss, surface wave loss, dielectric loss and metallization loss should be taken into account while analyzing microstrip patch antennas. Here, radiation loss is the lost energy due to the space wave radiation. Surface wave is the energy that is used in surface. In this study, mainly the aim is finding the current distribution on microstrip patch antenna. This distribution can be found by using Green's functions in that media. Then, by using the found current distribution, radiation pattern and any other parameter of the antenna can be acquired.

Full-wave analysis methods are defined such as Method of Moments (MoM), Finite Element Method (FEM) and Finite-Difference Time-Domain Method (FDTD). Nowadays the computers are super fast and solution of full-wave methods get easier. A full-wave MoM is employed in the analysis of this thesis study. In [8] it is demonstrated that MoM is the best method that can be used for planar multilayered printed structures, so in this study MoM is used for the analysis. In order to construct MoM, first integral equation that defines the real problem should be defined. Integral equation is simply the integral representation of field quantities that are written in terms of Green's function and current density. Integral equation can be electric field integral equation (EFIE), magnetic field integral equation (MFIE) or mixed potential integral equation (MPIE). In EFIE, kernel is the Green's function of electric field and in MFIE kernel is the Green's function of magnetic field. On the other hand, in MPIE, kernel is the Green's functions of scalar/vector potentials. The most appropriate integral equation that is used for MoM should be MPIE, because the Green's function in its kernel is less singular than the Green's functions in EFIE and MFIE kernels. Clearly, this is a significant computational advantage which is the main criteria. The analysis of microstrip circuits can be performed very accurately by using EM simulation tools that include numerical techniques. Then, overall circuit response can be obtained. A computer simulation uses full-wave analysis, so all interconnections and radiations can be taken into account.

In this thesis study, different microstrip structures are analyzed using MoM which employs closed-form Green's functions, in general. Therefore, these microstrip structures should be introduced and described firstly. Microstrip lines and microstrip antennas are explained. The advantages, disadvantages and the usage areas of microstrip structures are discussed. Afterwards, possible future applications together with analysis methods are presented. In

Chapter 1, it is aimed to introduce microstrip structures so that reader can have an idea about microstrip structures in different aspects.

In Chapter 2, it is aimed to introduce MoM so that the reader can understand the general application procedure of MoM.

Closed-form spatial domain Green's functions are used in MoM application. In Chapter 3, spatial domain Green's functions are discussed. In Chapter 3, it is aimed to discuss the procedure for obtaining the closed-forms of spatial domain Green's functions so that the reader can understand why spatial domain Green's functions are used in MoM application rather than spectral domain Green's functions.

In Chapter 4, the method applied to find the current distribution on the single microstrip line is explained. The formulation is given together with the MoM application procedure. In Chapter 4, it is aimed to introduce the procedure of the analysis for single line case so that the reader can understand the application of MoM to single line for finding the current distribution on the metal line.

In Chapter 5, the analyses are described in order to find the current distribution on the coupled microstrip line. The formulation is given together with the MoM application procedure. The interaction between parallel lines should be taken into account for this case. In Chapter 5, it is aimed to introduce the procedure of the analysis for coupled line case so that the reader can understand the application of MoM to coupled line for finding the current distribution on the parallel metal lines.

In Chapter 6, the procedure of the analysis for microstrip patch antenna is given.

The main aim of this thesis study is to analyze wideband microstrip patch antenna and to compare the bandwidths of standard patch antenna and this wideband patch antenna. In order to obtain such an aim, the analyses for various microstrip structures are analyzed up to now. In Chapter 7, a wideband patch antenna is designed from the standard patch antenna by opening parallel slots at two non-radiating edges. In this chapter, the analyses are described in order to find the current distribution on the wideband microstrip patch antenna. The formulation is given together with the MoM application procedure. After finding current distribution, bandwidth is obtained for wideband patch antenna and this bandwidth is compared with standard patch antenna bandwidth. In Chapter 7, it is aimed to introduce the procedure of the analysis for wideband microstrip patch antenna case so that the reader can understand the calculation of bandwidth for wideband microstrip patch antenna.

In conclusion, the final results and acquirements are discussed. The comment on the comparison of wideband and standard patch antenna bandwidths are provided.

1.1 Advantages and Disadvantages of Microstrip Antennas

Microstrip lines and antennas have many advantages nowadays. Before going into details of the history of microstrip structures, these advantages as well as the disadvantages will be

discussed. Specifically, microstrip antennas can be considered to gather a general idea about microstrip structures. Advantages of microstrip antennas are as follows; they have light weight, low cost, ease of fabrication, ease of integration with MMIC (Monolithic Microwave Circuits) fabrication technology which leads to low manufacturing cost, conformability on curved surfaces and they are suitable for arrays. Although microstrip antennas have many advantages that lead them to be popular in wide area of applications, they have some disadvantages such as narrow bandwidth, low gain, relatively large size particularly at lower frequencies due to the fact that the operation frequencies are related to electrical size of the antenna [9]. The recent researches are mainly based to the improvement on these disadvantages. In order to improve the bandwidth, first solution would be the increase in substrate thickness, but here surface power increases while the radiation power decreases. Another method will be the suppression of surface waves by using magneto-dielectric substrate. One popular research on the improvement of bandwidth is the usage of EBG (electromagnetic bandgap) structures for eliminating the surface waves, therefore the bandwith is improved. New geometries and genetic algorithm based optimization methods are the other methods for bandwith improvement. The increase in the gain of the microstrip antennas can be achieved by again using EBG antennas. Here reducing the surface waves will lead to a reduction in side lobe levels which in turn improves the gain of the antenna. FSS (Frequency Selective Surface) are also studied for the improvement in gain. Lens covering can be another method for gain improvement. The last disadvantage which is mentioned earlier is the relatively large size of the microstrip antennas. Inductive/capacitive loading and the usage of magneto-dielectric substrates can lead to miniaturization [10].

Surface wave propagation is a significant problem that is observed in microstrip antennas. It reduces the gain and bandwidth while increasing the end-fire radiation and cross polarization which are all unwanted situations in an antenna. Surface waves also reduce the ability of the miniaturization of antennas as well as the integration with MMICs [11]. Using the EBG structures, bandgap is constructed around the operating frequency which stops the surface waves and the energy that is consumed in surface waves can be used in radiation.

1.2 Application Areas of Microstrip Antennas

Due to the advantages of microstrip antennas, they have very wide range of applications for many areas. Microstrip antennas can be used in televisions, broadcast radios, mobile systems, satellite communications, global positioning systems (GPS), radio-frequency identification (RFID), multiple-input multiple-output (MIMO) systems, surveillance systems, radar systems, future space communications, high-velocity aircrafts, missiles, rockets, remote sensing, WiMAX/WLAN applications, biological imaging and etc. Microstrip antennas are compatible with embedded antennas in handle hand wireless devices such as cellular phones and pagers. They are also used in aircraft, satellite and missile applications.

Recently, various machining techniques such as MPCB, CMOS, LTCC and MEMS are developed. Since, microstrip antennas are highly related with such machining techniques,

they are developed as well such as active antennas, reconfigurable antennas, meta-material based antennas and THz antennas.

1.3 Analysis Methods

Rectangular microstrip patch antennas can be analyzed by using either analytical methods or numerical methods. Most frequently used analytical methods are *Transmission Line Model* and *Cavity Model* [1]. In transmission line model, patch can be considered and modeled as a transmission line which connects two parallel slots. In cavity model, the dielectric substrate is considered and modeled as a cavity that has magnetic walls. These analytical models are approximate methods, yet they are easy to apply. However, surface waves, coupling effects and fringing fields cannot be taken into account in such analytical models. They are not very accurate, so they cannot reflect the real behavior of the patch antenna. Numerical methods can be defined as *Full-wave Analysis*, in general. In full-wave analysis methods, the obtained equations are solved numerically, so they are more realistic than the approximate analytical methods. On the other hand, the application of the numerical methods are not so easy. The computational time can be a problem in many cases. Therefore, while using the numerical techniques the main aim is to obtain a fast solution. The most frequently used full-wave analysis methods are Finite Element Method (FEM), Method of Moments (MoM), Finite Difference Time Domain Method (FTDT). In this thesis study, MoM is used which is a full-wave method.

CHAPTER 2

METHOD OF MOMENTS

In numerical solutions, first an integral, differential or integro-differential equation that defines the physical problem should be constructed. Then, by discritizing the unknown function the integral or differential equation is transformed into a matrix equation. This is the main idea in Method of Moments (MoM) as well, since MoM is also a numerical solution. As indicated earlier, the selected numerical method that will be used in this study is Method of Moments. In this chapter, Method of Moments (MoM) will be described.

2.1 The Method of Moments (MoM)

Some studies were known before 1960's about Method of Moments. However, the significant works that are related to Method of Moments were presented at the middle of 1960's [12, 13, 14]. These studies helped the construction of Method of Moments. Finally, R.F. Harrington introduced Method of Moments by his works at 1967 [15] and 1968 [16].

In electromagnetic modeling, Method of Moments is the most preferred numerical method for radiation and scattering problems. In general, it is aimed to transfer an operator equation into a matrix equation and then solve this matrix equation by an appropriate method. Method of Moments has high accuracy and it is suitable for complex geometries as well. In electromagnetic applications, it is generally used for solving integral equations. It can be regarded as the numerical solution of exact integral equation, so it inherently contains everything that integral equation has and it is considered as full-wave solution [17]. In equation (1) an inhomogeneous equation is presented. Here, L is a linear operator. It is generally an integro-differencial operator. Moreover, $g(x)$ is the source and this is a known function [18]. The aim here is to find out unknown function f.

$$L(f(x)) = g(x) \tag{1}$$

Before going into details of Method of Moment's formulation, inner product $\langle u, v \rangle$ should be defined, because it will be used later. The inner product of two functions u and v is defined in equation (2) and the sign * means complex conjugate [19].

$$\langle u, v \rangle = \int_{\Omega} u v^{*} d\Omega \tag{2}$$

In equation (3), the properties of inner product are shown.

$$\begin{aligned} &\langle u,v\rangle = \langle v,u\rangle \\ &\langle \alpha u+\beta v,h\rangle = \alpha\langle u,h\rangle + \beta\langle v,h\rangle \quad \alpha \text{ and } \beta \text{ are scalars} \\ &\langle f^{*},f\rangle > 0 \quad if \quad f\neq 0 \\ &\langle f^{*},f\rangle = 0 \quad if \quad f = 0 \end{aligned} \tag{3}$$

The solution of equation (1) depends on the properties of the operator. If the operator L is positive definite, then the relation in equation (4) should be satisfied.

$$\langle f(x)^{*}, L(f(x))\rangle > 0 \tag{4}$$

Method of Moments application can be divided into four basic steps. Now, these steps are described.

Step 1:

First an equation should be constructed that defines the physical problem. In this study, this equation will be MPIE.

Step 2:

It is clear that $f(x)$ function is unknown and the main aim is to find this function. The basic logic of Method of Moments is to expand the unknown function in terms of known functions. Therefore, $f(x)$ function is expanded in terms of a known function set $f(x)_1, f(x)_2, ..., f(x)_N$ in L domain. These known functions are known as basis functions. Basis functions are selected to reflect the characteristics of the unknown function. They can be either scalar or vector. Furthermore, they can be sub-sectional or entire-domain. In equation (5) this expansion is presented.

$$f(x) = \sum_{n=1}^{N} \alpha_n f(x)_n \tag{5}$$

In equation (5), $\alpha_n's$ are unknown coefficients. When these coefficients are obtained, $f(x)$ function can be uniquely defined. The summation in equation (5) is a finite solution practically. If the summation is infinite, then the solution will be the exact one. As the N value is increased, the solution will become closer to the exact solution. Here, the memory size of the computer should be taken into account. Since the operator L is linear, by using equation (1) and equation (5) the equation (6) can be constructed.

$$\sum_{n=1}^{N} \alpha_n L(f(x)_n) = g(x) \tag{6}$$

Step 3:

Error function which is sometimes called as residual is shown in equation (7).

$$R(x) = \left[\sum_{n=1}^{N} \alpha_n L(f(x)_n) \right] - g(x) \tag{7}$$

In this step, the aim is to minimize this error function $R(x)$, because this error function shows the difference between the result of the approximation that is realized in step 2 and the exact known function $g(x)$. For the minimization, a value that is similar to the average of the error function is defined across the domain of the problem and this value is equated to zero [20]. Now, it is time to define the weighting functions. Weighting functions $w(x)_1, w(x)_2, ..., w(x)_N$ are defined across the range of operator L. The selection of weighting functions will be discussed later in this chapter, but a detailed study can be found in the reference [21]. Each weighting function $w(x)_m$ is multiplied with the error function $R(x)$ then the inner product of this multiplication is taken and it is equated to zero [19]. This procedure can be redefined as weighting the error function and equating this weighted function to zero. Here, this weighted function is similar to the average of the error function and it can be the exact average if appropriate weights are used and equation (8) shows the final form after this operation is applied.

$$\sum_{n=1}^{N} \alpha_n \langle w(x)_m, L(f(x)_n) \rangle = \langle w(x)_m, g(x) \rangle \quad for \quad m = 1,2,...., N \tag{8}$$

By means of reducing the error function across the domain of the problem, the projection of error function across the range space of the operator L should be zero. This can be realized by taking the inner product of error function with each weighting function of the weighting function set which is defined across the range space of operator L and equating this inner product to zero [1]. This method is called the weighted residuals. If point matching is used which will be described later, then error functions are zero only at N discrete points.

In equation (8) shows an equation set with N number of equations and the equations in this set can be written in matrix form. In equation (9), this matrix form is presented that is obtained by rearranging the equations in equation (8) into a matrix form.

$$[A_{mn}][\alpha_n] = [g_m] \tag{9}$$

$[A_{mn}]$ is called Method of Moments matrix and it can be written in detailed which is shown in equation (10).

$$[A_{mn}] = \begin{bmatrix} \langle w(x)_1, L(f(x)_1) \rangle & \langle w(x)_1, L(f(x)_2) \rangle & ... \\ \langle w(x)_2, L(f(x)_1) \rangle & \langle w(x)_2, L(f(x)_2) \rangle & ... \\ . & . & . \\ . & . & . \\ . & . & . \end{bmatrix} \tag{10}$$

The detailed forms of matrices $[\alpha_n]$ and $[g_m]$ are shown in equation (11).

$$[\alpha_n]=\begin{bmatrix}\alpha_1\\ \alpha_2\\ .\\ .\\ .\end{bmatrix}, \quad [g_m]=\begin{bmatrix}\langle w(x)_1, g(x)\rangle\\ \langle w(x)_2, g(x)\rangle\\ .\\ .\\ .\end{bmatrix} \tag{11}$$

If $[A_{mn}]$ matrix is non-singular, then the inverse matrix $[A_{mn}]^{-1}$ can be defined and this inverse can be used to find out unknown α_n's. Equation (12) represents the equation that will end up with these unknown α_n's.

$$[\alpha_n]=[A_{mn}]^{-1}[g_m] \tag{12}$$

For a detailed representation, the elements in $[A_{mn}]$ matrix can be defined explicitly, and this representation is provided in equation (13).

$$A_{mn}=\langle w(x)_m, L\{f\}\rangle=\int_a^b w(x)_m L\{f(x)_n\}dx \tag{13}$$

Similar explicit expression can be defined for $[g_m]$ matrix as well, which is given in equation (14).

$$g_m=\langle w(x)_m, g(x)\rangle=\int_a^b w(x)_m g(x)dx \tag{14}$$

Integrals in equations (13) and (14) are generally required to be evaluated by numerical methods due to the fact that it is in general hard or not possible to evaluate such integrals analytically [22]. It should be noted here that if Galerkin's Method of Moments is used that will be discussed later the resulted $[A_{mn}]$ matrix will be symmetric.

Step 4:

In this last step, it is aimed to solve the matrix equation in equation (12). Gaussian elimination, LU decomposition or other similar methods can be used. However, taking directly the inverse of matrix $[A_{mn}]$ and multiplying this value with matrix $[g_m]$ can be another method.

The choice of basis and testing functions is very important in Method of Moments. In general the factors such as accuracy of the solution, the ease in the calculation of matrix entries, suitability with problem geometry are taken into account. Furthermore, convergence of the resulted matrix should be considered. Basis functions should be linearly independent and they must satisfy the physical behaviors of the unknown function mathematically [16]. If unknown function becomes zero at the boundaries, then basis functions must be zero correspondingly. The ease in the calculation of matrix entries that are given in equations (13) and (14) should also be considered. On the other hand, weighting functions should also be

linearly independent. By adjusting the weighting functions appropriately, the reduction of error function to zero can be achieved, for more detail reference can be investigated [21].

2.1.1 Basis Functions

There are two types of basis functions present in Method of Moments. These are entire-domain basis functions and sub-domain basis functions. The choice between these two is based on the situation of the problem and the unknown function to be represented. Two types are both defined in this part. The one that is used in this study will be sub-domain basis functions.

a) Sub-domain Basis Functions

First the domain of the problem is divided into an arbitrary number of sub-domains either with same or different domain sizes. Afterwards, each sub-domain is matched with a function. These functions are called sub-domain functions. Sub-domain functions are defined only on the sub-domain that they belong to and they are assigned to zero for the remaining sub-domains. Representing the unknown function in this case is very realistic due to the fact that even small variations can be taken into account by considering sub-domains. Figure-1 illustrates the graphical representation of sub-domain basis functions.

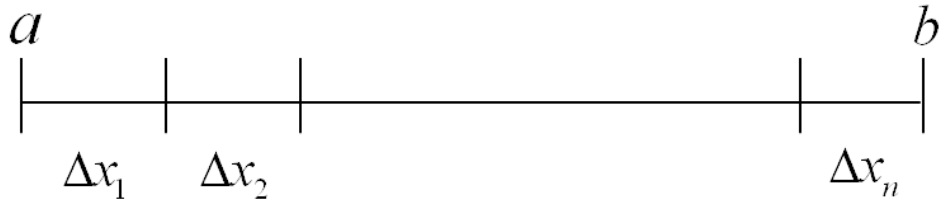

Figure- 1 Graphical Representation of Sub-domian Basis Functions

The representation in Figure-1 can be explained mathematically. For example, the domain $[a,b]$ is divided into N sub-domains and the unknown function can be defined in terms of different $f_n(x)$ sub-domain functions and this defined unknown function is shown in

equation (15). Here each of these $f_n(x)$ sub-domain functions is defined in different sub-domains.

$$f(x)=\sum_{n=1}^{N}\alpha_n f_n(x)=\begin{cases}\alpha_1 f_1(x) & x\in\Delta x_1\\ \alpha_2 f_2(x) & x\in\Delta x_2\\ . & \\ . & \\ \alpha_N f_N(x) & x\in\Delta x_N\end{cases} \tag{15}$$

Now, the most frequently used sub-domain basis functions are briefly discussed.

Pulse Basis Functions:

Let the domain range is defined as $0\le x\le 1$ and it is divided into $N+1$ equally sized domain. Equation (16) shows the width and equation (17) shows the center point of one sub-domain.

$$h_x=\frac{1}{N+1} \tag{16}$$

$$x_m=\frac{m}{N+1},\quad m=1,2,3,... \tag{17}$$

Pulse functions are defined in equation (18) and they are orthogonal.

$$P(x-x_m)=\begin{cases}1 & for\quad x_m-\frac{h_x}{2}\le x\le x_m+\frac{h_x}{2}\\ 0 & elsewhere\end{cases} \tag{18}$$

The graphical representation of the pulse functions are illustrated in Figure-2.

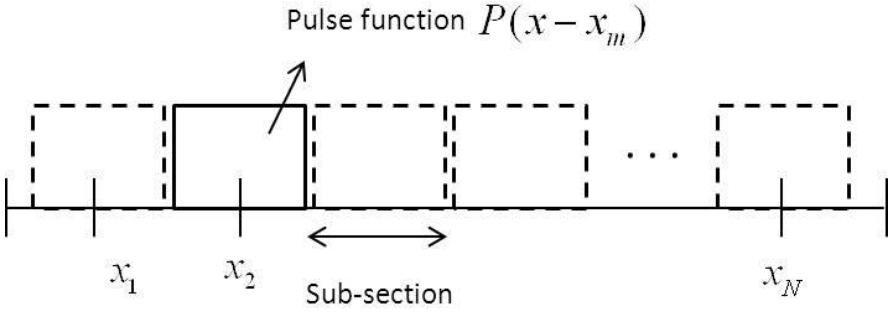

Figure- 2 Graphical Representation of Pulse Basis Functions for a Particular Case

It should be noted here that the choice of basis function have to be compatible with the unknown function that will be represented. Indeed, pulse functions can be differentiated only once. Therefore, a twice differentiable unknown function cannot be represented by pulse functions.

Triangular Basis Functions:

Triangular basis functions are twice differentiable and they are defined in equation (19).

$$T(x-x_m)=\begin{cases}\dfrac{x-x_{m-1}}{x_m-x_{m-1}} & for \quad x_{m-1}\le x\le x_m\\ \dfrac{x_{m+1}-x}{x_{m+1}-x_m} & for \quad x_m\le x\le x_{m+1}\\ 0 & elsewhere\end{cases} \tag{19}$$

Figure-3 shows the graphical representation of triangular basis functions in a particular case again such that the amplitudes and sub-domain lengths are equal.

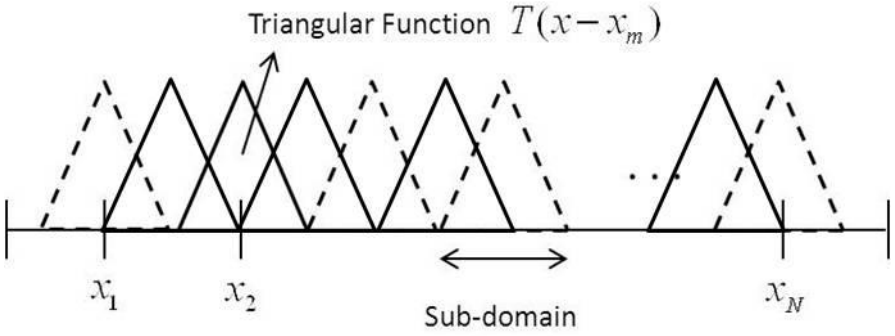

Figure-3 Graphical Representation of Triangular Basis Functions for a Particular Case

It is clear from Figure-3 that one triangular function is defined in two adjoining sub-domains, because it exists in both of these regions. Therefore, triangular functions are not orthogonal.

For two dimensional sub-domain basis functions, only roof-top basis functions will be analyzed, because roof-top basis functions are chosen to be used in this thesis study. The usage of roof-top basis function is easy and it is appropriate to represent the unknown function in the physical problem of this study.

Roof-top Basis Functions:

They are the most frequently used basis functions. They are piecewise functions in x-direction that are triangular functions and pulse functions in y-direction. Piecewise linear functions that are chosen to represent the unknown function in the x-direction are defined in equation (20) and the pulse functions in the y-direction are defined in equation (21).

$$f_{1m}(x) = \begin{cases} (x - x_{m-1})/h_x & for \quad x_{m-1} \le x \le x_m \\ (x_{m+1} - x)/h_x & for \quad x_m \le x \le x_{m+1} \\ 0 & otherwise \end{cases} \tag{20}$$

Where, $x_m - x_{m-1} = h_x = x_{m+1} - x_m$

$$f_{2n}(y) = \begin{cases} 1 & for \quad y_n - \dfrac{h_y}{2} \le y \le y_n + \dfrac{h_y}{2} \\ 0 & elsewhere \end{cases} \tag{21}$$

The graphical representation of the roof-top function is illustrated in Figure-4.

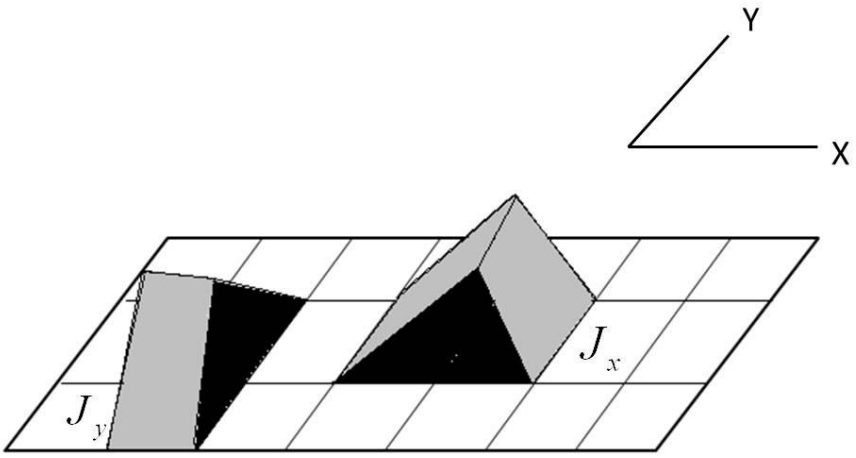

Figure-4 Graphical Representation of Roof-top Basis Function

Roof-top functions are discussed further in this thesis, so the given information is enough for this part.

b) Entire domain Basis Functions

In this case, basis functions are defined across the entire domain of the problem. The orthogonal functions such as Bessel functions, Legendre functions, Chebyshev polynomials, Power series, sine and cosine functions, Maclourin series and etc. can be used for entire domain basis functions. Even less number of basis functions can satisfy the desired accuracy in entire domain basis functions when compared to the sub-domain basis functions. If the expansion functions are the eigenfunctions of the problem, then an efficient analysis can be obtained [23]. Entire domain basis function selection is appropriate when the change of the approximated unknown function across the domain is small. Therefore, entire domain basis functions cannot be used for the approximation of high and rapidly changing functions. For instance, if entire domain is defined as such $x \in [a,b]$ and all basis functions are defined in this range as well, then these basis functions are treated as entire domain basis functions.

2.1.2 Weighting Functions

There are varieties of weighting function models that can be used in MoM analysis. In this part, these models will be presented.

a) Point Matching Method (Collocation Method)

In this method, Dirac delta functions are chosen as weighting functions. Weighting functions are defined in equation (22). If domain is defined as $[a,b]$, then the weighting functions w_m have to be defined in the range of $[a,b]$ as well.

$$w_m(x) = \delta(x - x_m) \text{ for } m = 1,2,...,N \tag{22}$$

As explained earlier, error function is weighted that is similar to taking the average. Moreover, the inner product of this average like value is calculated and it is equated to zero. In point matching method, instead of the average of the function, the values at discrete points are more used. Here, N discrete point values of error function across range $[a,b]$ are equated to zero. Therefore, it is not possible to control the error function at continuous values between a and b. In equation (23), the inner product is shown where the error function is equated to zero at selected N points across the interval $[a,b]$ [19].

$$\langle w_m, R \rangle = \int_a^b R(x)\delta(x - x_m)dx = 0 \tag{23}$$

This method may suffer in terms of accuracy and the boundary conditions are matched only at the selected points across the domain [18]. The accuracy can be increased by selecting more points. On the other hand, it should be indicated that this method is the simplest one among the alternatives. It is even not necessary to calculate the integral and this is proved in equations (24) and (25). By investigating these equations, it can be observed that the integrals are assigned to a value directly and the calculation is unnecessary.

$$A_{mn} = \int_a^b \delta(x - x_m) L\{f_n(x)\}dx = L\{f_n\}_{X=X_m} \tag{24}$$

$$G_m = \int_a^b \delta(x - x_m) g(x)dx = g(x)_{X=X_m} \tag{25}$$

Although this method provides advantage computationally, the degree of accuracy can be low. In Figure-5, the illustration of point matching method is given.

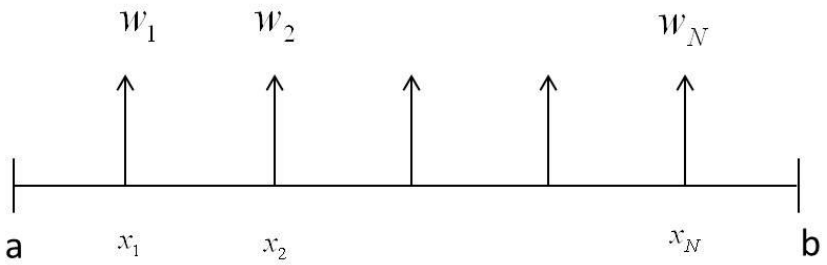

Figure-5 Graphical Representation of Point Matching Method Weighting Functions

In this method weighting functions are defined at arbitrary discrete points and error function is equated to zero only at these discrete points. In one respect, this application can be considered as a simplification.

b) Sub-sectional Collocation Method

This method is the more advance state of the previous method in terms of the accuracy. In that case weighting functions are defined as N pulses in a given range. Instead of having N discrete points in the point matching method, in sub-sectional collocation method the error function is equated to zero at N sub-sections. Again in the continuous values between these sub-sections, the error function cannot be controlled. In equation (26) the weighting function is defined and it is illustrated that the inner product of the error function is equal to zero across the sub-sections.

$$w_m(x) = \begin{cases} 1 & x \in \Omega_m \\ 0 & elsewhere \end{cases} \quad \text{and} \quad \int_{\Omega_m} R(x)dx = 0 \qquad m = 1,2,3,....,N \tag{26}$$

In Figure-6, the illustration of sub-sectional collocation method is provided.

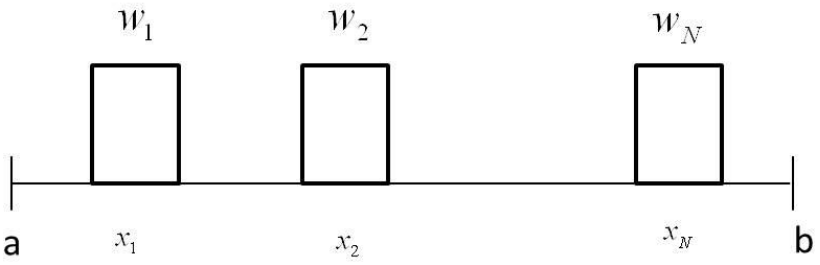

Figure-6 Graphical Representation of Sub-sectional Collocation Method Weighting Functions

In this method, the integrals cannot be eliminated as in the case of point matching method. Even they are one dimensional, it is still required to calculate the integrals.

c) Galerkin's Method

In Galerkin's method, weighting functions are chosen as equal to the basis functions. Moreover, Galerkin's method is one of the most frequently used methods for selecting the weighting function. Equation (27) shows the weighting functions. Equations (28) and (29) define the matrix entries.

$$w_m = f_m \qquad m = 1,2,...,N \tag{27}$$

$$A_{mn} = \langle f_m, L\{f_n\} \rangle \tag{28}$$

$$g_m = \langle f_m, g \rangle \tag{29}$$

This method enables the boundary conditions to be satisfied across the solution domain. Instead of controlling the error function only at specified discrete points or sections as used in previous methods, here error function can be controlled in the overall range. Furthermore, it is not necessary to decide on the selection of weighting functions. However, the most important advantage of the Galerkin's method is obtaining a symmetric matrix at the end of the application. Computational time can be improved significantly by this symmetric matrix. However, method has a disadvantage in terms of integral values. Here, integrals has complex forms and evaluation of them can be very time consuming and sometimes impossible. Therefore, this method should be selected by first observing the resulted integrals. The reason why this method is selected in this thesis study is explained in another part. Yet, it is clearly seen that the most important reason is the coordination of method with the problem

that is studied in the thesis. Additionally, the computational time can be reduced by the resulted symmetric matrix.

CHAPTER 3

GREEN'S FUNCTIONS IN PLANARLY LAYERED MEDIA

First, general review of Green's functions should be provided since they are used in analyses. In linear time-invariant systems, if the impulse response of the system is known then response of an arbitrary input signal can be found easily. Simply, the convolution integral of impulse response and input signal provide the response of this source. In electromagnetic problems, it is aimed to find out the field distribution that is created by an arbitrary source. Here, Green's function can be considered as the impulse response of the impulse source. However, if the field distribution that is created by an arbitrary source is intended to be found, then the linearity of Maxwell's equations should be proven. The nonlinearity of Maxwell's equations can only be caused by the electrical properties of the medium. Therefore, in linear media, Maxwell's equations are linear. The detailed proof can be found in the reference [1].

A detailed explanation of obtaining dyadic Green's function of electric field from scalar Green's function of electric field, obtaining dyadic Green's function of electric field from scalar/vector potentials (MPIE) and spectral domain Green's function in layered media are provided in appendix A.1, A.2 and A.3, respectively. Although these calculations are not performed in this thesis study, presentation of these calculations in a detailed manner could ease the understanding of further concepts. Therefore, they are presented in the appendix part.

Since spatial domain Green's functions will be used in the MoM analysis of microstrip structures, they are necessary for this thesis study. Therefore, before introducing the MoM application, spatial domain Green's functions are presented in this chapter. First a general review of Green's functions will be given in this chapter. Then, spatial domain Green's functions in layered media will be discussed. Sommerfeld integral and Sommerfeld identity are introduced. The importance of Sommerfeld identity is explained. At the end of this chapter, reader can understand the physical meaning of the spatial domain Green's function formula and the reason why spatial domain Green's function is used in the MoM application instead of spectral domain Green's function.

3.1 Spatial Domain Green's Functions in Layered Media

The reason why spatial domain values are needed and why MoM should be applied to the spatial domain Green's functions will be clear in the next section. After finding the spectral domain dyadic Green's functions, inverse Fourier transform or inverse Hankel transform should be used in order to obtain spatial domain Green's functions from spectral domain

counterparts. Both inverse Fourier transform and inverse Hankel transform are called in general as Sommerfeld integrals. First, spectral to spatial domain transformations will be investigated. Let's assume a scalar field component for example as $f(\mathbf{r}) \equiv f(\rho, z)$, where $\rho = \hat{\mathbf{x}}x + \hat{\mathbf{y}}y$. Then, transformations are shown in equations (30) and (31).

$$Ff(\mathbf{r}) \equiv \tilde{f}(\mathbf{k}_\rho; z) = \int_{-\infty}^{\infty}\int_{-\infty}^{\infty} f(\mathbf{r}) e^{jk_x x} e^{jk_y y} dxdy \tag{30}$$

$$F^{-1}\tilde{f}(\mathbf{k}_\rho; z) \equiv f(\mathbf{r}) = \frac{1}{(2\pi)^2}\int_{-\infty}^{\infty}\int_{-\infty}^{\infty} \tilde{f}(k_\rho; z) e^{-jk_x x} e^{-jk_y y} dk_x dk_y \tag{31}$$

Where, $k_\rho = \hat{x}k_x + \hat{y}k_y, k_\rho = \sqrt{k_x^2 + k_y^2}$

Equation (31) is called the Sommerfeld integral. In order to find the Fourier transform of the spherical wave function $\frac{e^{-jkr}}{r}$, Sommerfeld identity in equation (32) will be used [24]. This identity eases our analysis significantly and this will be explained later. Sommerfeld identity is shown in equation (32).

$$\frac{e^{-jkr}}{r} = \frac{1}{2\pi j}\int_{-\infty}^{\infty}\int_{-\infty}^{\infty} \frac{e^{-jk_z|z|}}{k_z} e^{-jk_x x} e^{-jk_y y} dk_x dk_y \tag{32}$$

Where, $r = \sqrt{x^2 + y^2 + z^2}$, $\quad k_z = \sqrt{k^2 - k_x^2 - k_y^2}$

It can be seen from equation (31) that k_ρ can be used instead of two independent variables x and y. If Cartesian coordinates are transformed into Cylindrical coordinates as $k_x = k_\rho \cos\alpha,\ k_y = k_\rho \sin\alpha,\ x = \rho\cos\varphi,\ y = \rho\sin\varphi$ and jacobian determinant is used as $dk_x dk_y = k_\rho d\alpha dk_\rho$, then the expression in equation (31) will become the one in equation (33).

$$\begin{aligned} f(\mathbf{r}) &= \frac{1}{(2\pi)^2}\int_{-\infty}^{\infty}\int_{-\infty}^{\infty} \tilde{f}(k_\rho; z) e^{-j(k_x x + k_y y)} dk_x dk_y = \\ &\frac{1}{(2\pi)^2}\int_{0}^{\infty}\int_{0}^{2\pi} \tilde{f}(k_\rho; z) e^{-jk_\rho \rho\cos(\alpha-\varphi)} k_\rho d\alpha dk_\rho \end{aligned} \tag{33}$$

After further arrangements, the expression in equation (34) can be obtained, without explaining the details the final form is shown [24].

$$f(\mathbf{r}) = \frac{1}{2\pi}\int_{0}^{\infty} \tilde{f}(k_\rho; z)\mathbf{J}_0(k_\rho\rho) k_\rho dk_\rho \tag{34}$$

In equation (34), $\mathbf{J}_0$ is called zero order Bessel function and it corresponds to cylindrical standing wave. By using the expressions in equation (35) and (36), equation (34) can be changed to an alternative form which is provided in equation (37).

$$\mathbf{J}_0(u) = \frac{1}{2}\left[\mathbf{H}_0^{(1)}(u) + \mathbf{H}_0^{(2)}(u)\right] \tag{35}$$

$$\mathbf{H}_0^{(1)}(u) = -\mathbf{H}_0^{(2)}(e^{-j\pi}u) \tag{36}$$

Final form is shown in equation (63).

$$f(\mathbf{r}) = \frac{1}{4\pi}\int_{-\infty}^{\infty} \tilde{f}(k_\rho; z)\mathbf{H}_0^{(2)}(k_\rho\rho)k_\rho dk_\rho \tag{37}$$

e^{jwt} time dependence is assumed throughout this thesis study. $\mathbf{H}_0^{(1)}$ and $\mathbf{H}_0^{(2)}$ are zero order first kind and second kind Hankel functions and they correspond to inward and outward cylindrical travelling waves, respectively. Equations (34) and (37) are in general called as Sommerfeld integrals.

As a matter of fact, MoM can be applied etiher to the spectral domain or to the spatial domain. Now, both of these cases will be discussed together with the advantages and disadvantages.

If MoM is applied to a spectral domain Green's function, an advantage can be utilized. Spectral domain Green's functions can be used in closed forms. In this case, the integrals that are belonging to inner products are defined along the infinite domain and only double integrals of complex functions remain [8]. Additionally, one integral can be transformed to polar coordinates from Cartesian coordinates. However, the time consuming integral part cannot be eliminated. Therefore, in spite of all these arrangements, computationally efficient analysis in the spectral domain is not possible.

If MoM is applied to spatial domain Green's function without any further arrangement, then each matrix element is composed of five-dimensional integrals. Two of them come from inner product, two of them come from convolution integral and one is the Sommerfeld integral and come from the Green's function directly. By applying some simplifications, this five-dimensional integral can be reduced to three-dimensional one. This simplification is transforming the convolution integral between Green's function and basis function to a convolution integral between basis and testing function and it will be discussed later. Moreover, instead of the required infinite range in spectral domain, in spatial domain integrals in MoM matrix elements are defined across finite domains [25]. However, Sommerfeld integral that is the time consuming and oscillatory function remains the same, so this case is not computationally efficient as well.

Up to now, it can be seen that there is no much difference between applying MoM to spatial domain or spectral domain in terms of computational advantage. However, the studies that are published in year 1988 by Fang and his friends [26] and in year 1991 by Chow and his friends [27] completely change the situation in this field of study. According to these studies,

if the spatial domain Green's functions could be expressed in closed forms, it would be possible to eliminate the time consuming part. If spatial domain Green's functions are written in closed forms, then three-dimensional integral is reduced to two-dimensional integral and it is defined across the finite range. Here, it is not necessary to take the integrals of Green's functions which is the only time consuming part in the analysis. Therefore, the question is how to express the spatial domain Green's functions in closed forms? Before answering this question, the spatial domain Green's function will be analyzed by observing its singularities.

$$\mathbf{G}^{A,q}(\rho) = \frac{1}{4\pi} \int_{SIP} \mathbf{H}_0^{(2)}(k_\rho \rho) \tilde{\mathbf{G}}^{A,q}(\rho) k_\rho dk_\rho \tag{38}$$

Where, $k_\rho^2 = k_x^2 + k_y^2$. Here ρ is a variable in cylindrical coordinates, G is the spatial domain Green's function and $\tilde{G}$ is the spectral domain Green's function. Equation (38) shows the general representation of spatial domain Green's function. SIP is called Sommerfeld integration path and it is illustrated in Figure-7.

The integration path needs to be deformed as shown in Figure-7 due to the branch-point and pole singularities of the integrand.

- The function $\mathbf{H}_0^{(2)}(k_\rho \rho)$ has a logarithmic branch-point singularity at point $k_\rho = 0$.
- The value $k_z = \sqrt{k^2 - k_\rho^2}$ has algebraic branch-point singularity at points $k_\rho = \pm k_0$.

Branch-point singularities correspond to the radiating modes in the outermost layer, because it requires the layer to be unbounded. Pole singularities correspond to guided modes in the dielectric layers [8].

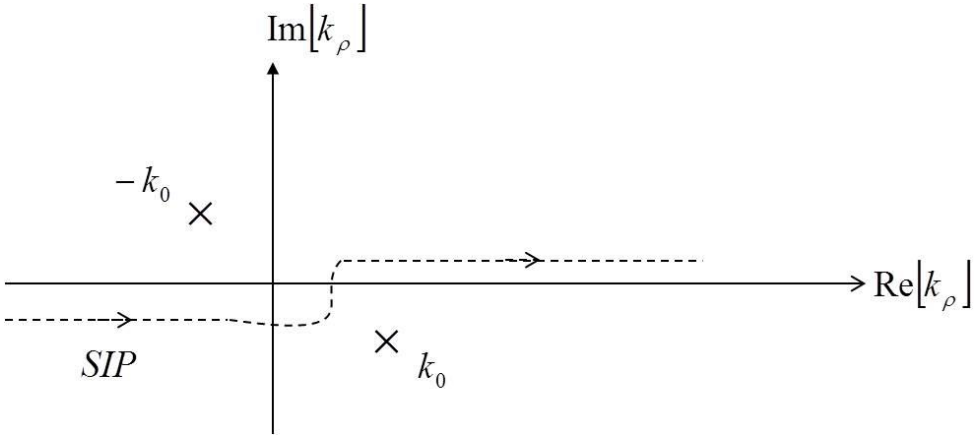

Figure-7 Illustration of Sommerfeld Integration Path (SIP)

Now, writing spatial domain Green's functions in closed form can be discussed. After finding the closed form spatial domain Green's functions, these values will be used in the solution of MPIE by MoM and computationally efficient solutions can be achieved. It can be seen from equation (38) that spatial domain Green's functions are expressed in terms of spectral domain Green's functions. Closed-form spectral domain Green's functions are known for layered media, so the evaluation of the spatial domain Green's function requires the numerical computation of the Sommerfeld integral. However, this integral is an oscillatory integral and the calculation of this integral is computationally very expensive [28]. If spectral domain Green's functions are arranged properly, then it is possible to eliminate the Sommerfeld integral completely and get rid of the numerical evaluation of this integral. Hence, if spectral domain Green's functions could be approximated in terms of complex exponentials, then integral of this resulted expression which is the summation of complex exponentials can be computed analytically. After spectral domain Green's functions are approximated in terms of complex exponentials, the inverse Hankel transform can be computed analytically by using the previously mentioned Sommerfeld identity. In order to use Sommerfeld identity, integral should contain an exponential expression. Indeed, this is the reason why the spectral domain Green's functions are approximated to exponential forms. This idea is first suggested in year 1988 by a published paper [26]. In this paper writing spectral domain Green's functions in terms of the summation of complex exponentials by using Prony's method is explained. Then, by using this approximation, Sommerfeld identity is utilized in order to express spatial domain Green's functions in closed forms [26]. Then, this study is improved by Chow et al. [27]. This study is only valid for finding vector and scalar potentials of HED (Horizontal Electric Dipole)'s over thick substrates, so it has a very limited application area. However, this study is very important in terms of the usage of the main idea. Then, this study is improved by a paper that is published in year 1992 which is valid for arbitrary thickness where both substrate and super-strate exist [29]. In year 1995, a study is published that is aimed to find Green's functions of vector and scalar potentials for HED, HMD (Horizontal Magnetic Dipole), VED (Vertical Electric

Dipole) and VMD (Vertical Magnetic Dipole) sources that means all available source types in planar layered medium where they located over an arbitrary layer [30]. In other words, in this study instead of only HED all source types are considered and there is no restriction on layer numbers as well. Furthermore, in early studies [26, 27] original Prony's method was used in order to make an approximation. However, in this method excessive sampling numbers are required, so it cannot be responded to fast changes. Consequently, in this study an alternative method which is called Generalized Pencil of Functions (GPOF) method is offered and more robust method is developed [30]. In year 1996 another paper is published. This study is about converting the process of approximating spectral domain Green's functions in terms of complex exponentials to a more efficient and robust process and a two-level approximation approach is developed. This method is definitely more computationally efficient and robust when compared to the old method as proven in the paper [31]. In year 1997, a study is published which discussed the observed problems during the usage of closed form spatial domain Green's functions for the geometries with vertical metallization and two methods are developed for this situation [32]. The study in year 2003 stated that after certain distance the spectral domain approximation could deviate. They made a comprehensive investigation about this issue together with the main reasons of this problem [33]. In year 2005, a paper is published that is about analyzing the process of obtaining closed form Green's functions in detail [34]. In year 2008, a paper is published which detects the fact that far field results are not very accurate due to the lack of proper closed form representations of lateral waves [35]. In year 2009, the studies headed towards different sides. Because of the requirements of the recent scientific developments, the studies proceed to different fields. A study published in this year discussed the applications of closed form Green's functions in planar layered media so far. Alteration of the method that is used for this approximation which is called DCIM is investigated and the applicability of this method to the artificial materials is analyzed [36]. The continuation of the study in year 2009 was published in year 2010 which developed the two-level approximation approach to a three-level approximation approach (three-level DCIM) [37]. The main aim is to develop a method that is valid for all ranges including the far-field and for all material types including LHM (Left-handed Material). The assumption in this study is that the combination of spherical waves could be used to represent lateral waves appropriately and it is discussed in the reference in detailed [37].

The method that is used to find out spatial domain Green's functions in closed forms is discussed throughout the historical perspective. Now it is time to explain how the spectral domain Green's functions are approximated in terms of complex exponentials.

GPOF method is the one that is used to express spectral domain Green's functions in terms of complex exponentials in this thesis study. This method requires uniform sampling like the other less computationally efficient methods that are used in early works such as Prony's method and least square Prony's method. This uniform sampling should be understood as the uniform sampling of a complex valued function across a real variable. If this sampling process is performed across the variable k_ρ, then the resulted complex exponentials are in terms of k_ρ. However, the complex exponentials that are written in terms of k_ρ cannot be useful for our analysis because the aim is to find out the same exponentials used in the Sommerfeld identity. The exponentials in the Sommerfeld identity are in terms of k_z, so in

order to use Sommerfeld identity, the resulted exponentials should be in terms of k_z. If this approximated complex exponential expression in terms of k_z is inserted instead of the spectral Green's function inside the integral in equation (38), then the required form the Sommerfeld identity is achieved. Then, instead of calculating the integral in equation (38), by inserting the equivalent value of Sommerfeld identity the integral evaluation is completely eliminated.

As intended, in order to obtain exponentials in terms of k_z, a deformed path is constructed on k_ρ plane such that the real variable t is used to obtain values on complex k_z plane. In equation (39), the mathematical representation of this mapping process is shown.

$$k_z = k\left[-jt + \left(1 - \frac{t}{T_0}\right)\right], \qquad 0 \le t \le T_0 \tag{39}$$

Here T_0 is the truncation point.

This deformed path is obtained by deforming the SIP path. Here a path is constructed that is away from surface wave poles (SWP) (for details reference should be examined [38]). Let this deformed path is called as C_{ap}, and it is illustrated together with SIP in Figure-8. C_{ap} can be obtained by deforming the SIP, because no singularity is experienced during the deformation [27]. Sampling of spectral domain Green's functions should be performed along SIP or a path that is deformed from SIP appropriately [8].

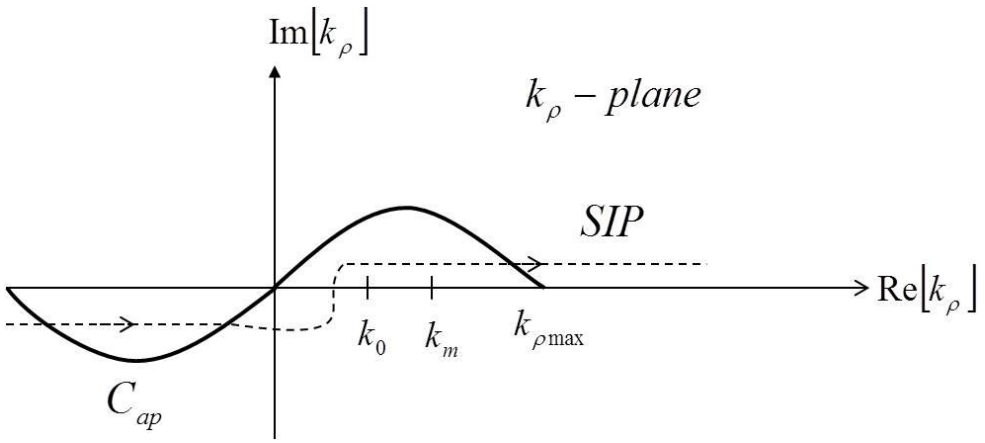

Figure-8 Illustration of C_{ap} Path together with SIP

As seen from equation (39), Green's functions are sampled uniformly as $t \in [0, T_0]$. In this process, exponentials in terms of t are approximated by taking values along C_{ap} path in the k_ρ plane with the fact that $k_{\rho\max} = k\left[1 + T_0^2\right]^{1/2}$. Then, these exponentials can be transformed to the case where they are written in terms of k_z, again as seen from equation (39). This application is called one-level approximation approach [31]. The reason why it is called as one-level is because of the fact that complex function is approximated in between 0 and T_0, and beyond T_0 is not considered. Advanced method is also developed that is more efficient than one-level approach. In order to catch even smaller changes in the k_ρ, the sample size should be very high. Spectral domain Green's functions can vary fast in small distances. Additionally, GPOF method requires uniform sampling, so one-level approach requires thousands of samples [8]. Moreover, in order to reflect the asymptotic behavior of Green's functions T_0 should be selected large [39]. Large T_0 already means large samples and it increases the computational time. Since Green's functions have a slowly varying behavior, it is not so efficient to take large number of samples. Therefore, two-level approach is developed [31]. According to the two-level approach, approximation is performed along C_{ap1} and C_{ap2} one by one which are shown in Figure-9. First approximation is realized along C_{ap1} path and afterwards C_{ap2} path is used [19].

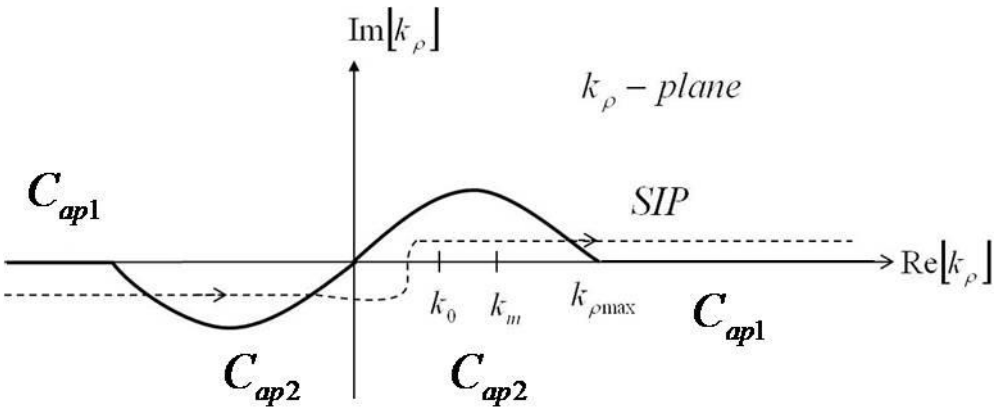

Figure-9 Illustration of C_{ap1} and C_{ap2} Path together with SIP

Parametric equations of C_{ap1} and C_{ap2} paths are shown in equations (40) and (41).

$$\text{For } C_{ap1} \quad k_{zi} = -jk_i\left[T_{02} + t\right] \qquad 0 \le t \le T_{01} \tag{40}$$

$$\text{For } C_{ap2} \quad k_{zi} = k_i\left[-jt + \left(1 - \frac{t}{T_{02}}\right)\right] \qquad 0 \le t \le T_{02} \tag{41}$$

A rapid change is observed up to $k_\rho = k_{\max}$, then the remaining part shows a smoother structure [36]. This fact is taking into consideration while developing the new method and two separate paths are considered. Region is divided into two parts by taking into account this behavior and sampling is performed according to these two paths. C_{ap1} path is the part where quasi-static terms are extracted which means extracting the asymptotic behavior of the approximated function [34]. The details will not be discussed in this study, so reader can examine the reference for details [32]. Additionally, the detailed description of two-level approach that can be transformed into multi-level approximation approach easily can be found in the reference [36].

After applying the two-level approach, spectral domain Green's functions are approximated in terms of complex exponentials as shown in equation (42) and it should be noted that the exponentials are in terms of k_z as desired.

$$\tilde{G} \cong \frac{1}{j2\varepsilon_i k_{zi}}\left[e^{-jk_{zi}|z|} + \sum_{n=1}^{N_1} a_{1n} e^{-\alpha_{1n} k_{zi}} + \sum_{n=1}^{N_2} a_{2n} e^{-\alpha_{2n} k_{zi}}\right] \tag{42}$$

Here a_{1n} and α_{1n} are the coefficient and exponent that are obtained from the first approximation along C_{ap1}, respectively. a_{2n} and α_{2n} are the coefficient and exponent that are obtained from the second approximation along C_{ap2}, respectively. These coefficients and exponents are complex constants and k_{zi} is the propagation constant in the source layer. N_1 and N_2 are number of exponentials that are used in the approximation. The aim is to write down spatial domain Green's functions in closed form expressions. For this reason, approximated spectral domain Green's functions in equation (42) are substituted into the Sommerfeld identity in equation (38). A small example should be given in order to explain the process. For simplicity, one-level approach is used and the resulted spectral domain Green's function is given in equation (43).

$$\tilde{G} = \frac{1}{2jk_z}\sum_{m=1}^{N} a_m e^{-b_m k_z} \tag{43}$$

Furthermore, the Sommerfeld identity is re-written in equation (44).

$$\frac{e^{-jkr}}{r} = \frac{1}{2j}\int_{SIP} H_0^{(2)}(k_\rho \rho)\frac{e^{-jk_z|z|}}{k_z} k_\rho dk_\rho \tag{44}$$

Spatial domain Green's function expression is given in equation (45).

$$G = \frac{1}{4\pi}\int_{SIP} H_0^{(2)}(k_\rho \rho)\tilde{G}(k_\rho) k_\rho dk_\rho \tag{45}$$

By substituting the spectral domain Green's function in equation (43) into the expression in equation (45), the resulted expression for spatial domain Green's function is written in equation (46).

$$G = \frac{1}{4\pi}\left\{\frac{1}{2j}\sum_{m=1}^{N} a_m \int_{SIP} \frac{e^{-b_m k_z}}{k_z} H_0^{(2)}(k_\rho \rho) k_\rho dk_\rho\right\} \tag{46}$$

In equation (46), the power of the exponential term $e^{-b_m k_z}$ is multiplied and divided by j and the $e^{-jk_z(-jb_m)}$ term is obtained. Then the transformation that is provided in equation (47) is applied to this final expression.

$$-jb_m = |z| \tag{47}$$

Afterwards, the final expression which is obtained after the transformation is given in equation (48). Since this expression fits entirely with the Sommerfeld identity that is given in equation (44), the integral part is removed and instead of it the expression $\frac{e^{-jkr}}{r}$ is used.

$$G = \frac{1}{4\pi}\underbrace{\left\{\sum_{m=1}^{N} a_m \frac{1}{2j}\int_{SIP} \frac{e^{-b_m k_z}}{k_z} H_0^{(2)}(k_\rho \rho) k_\rho dk_\rho\right\}}_{\sum_{m=1}^{N} a_m \frac{e^{-jkr_m}}{r_m}} \tag{48}$$

Where $r_m^2 = \rho^2 + (-jb_m)^2 = \rho^2 - b_m^2$. Now, the simple example is terminated and the final form of the spatial domain Green's function that is obtained from two-level approximation approach is given in equation (49) in a general representation.

$$G \cong \frac{1}{4\pi\varepsilon_i}\left[\frac{e^{-jk_i r}}{r} + \sum_{n=1}^{N_1} a_{1n}\frac{e^{-jk_i r_{1n}}}{r_{1n}} + \sum_{n=1}^{N_2} a_{2n}\frac{e^{-jk_i r_{2n}}}{r_{2n}}\right] \tag{49}$$

Where, $r_{1n} = \sqrt{x^2 + y^2 - \alpha_{1n}^2}$ and $r_{2n} = \sqrt{x^2 + y^2 - \alpha_{2n}^2}$ are the complex distances. k_i is the wavenumber that belongs to source layer. The spectral domain approximation expression in equation (42) is the expression that is obtained from the direct sampling of spectral domain Green's function.

In order to find out the complex coefficients a_{1m}, a_{2m} and exponents b_{1m}, b_{2m} a software program which is written in Fortran is used. This program is written for the study in the reference [30] and will be used for our study as well. These complex coefficients and exponents are used as inputs into the program that is written for this thesis study.

A couple of numerical examples regarding the use of spatial domain closed-form Green's functions will be presented. In Figure-10, a three-layer microstrip line is illustrated. First layer is considered as the ground plane at the bottom which is PEC (Perfect Electric

Conductor), second layer is the dielectric layer with a specific permittivity and the third one is the air. For this structure in Figure-10, two-level approximation approach is applied in order to find the Green's functions of vector and scalar potentials G_{xx}^{A} and G_q, respectively. From the approximation, the complex coefficients a_m and b_m are obtained then they are used to find the Green's functions. In the approximation the frequency is taken as $1GHz$, $\varepsilon_{r1}=4$, $\varepsilon_{r2}=1$ and $d_1=0.02032cm$. In the approximation, the source is considered as HED.

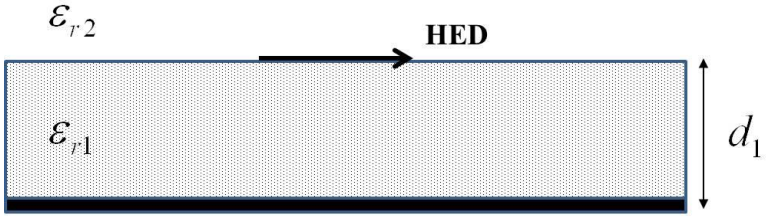

Figure-10 The Illustration of 3-Layer Microstrip Line Structure

Magnitudes of vector Green's function G_{xx}^{A} and scalar Green's function G_q can be plotted. These Green's functions will be used in the analysis that will be discussed in the next chapter. They will be used as inputs to the software program. For details, next chapter should be investigated.

Magnitude of the vector Green's function G_{xx}^{A} is plotted in Figure-11. Here the logarithm of the magnitude of G_{xx}^{A} is plotted with respect to the logarithm of $k_0\rho$. Logarithm is used in order to obtain more clear figures with large scales.

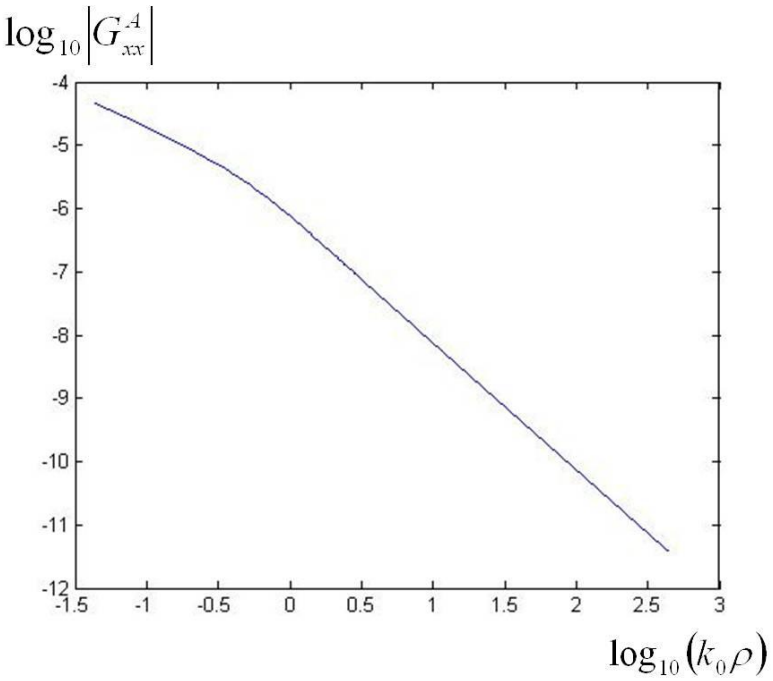

Figure-11 Magnitude of the Green's Function of Vector Potential, G_{xx}^{A}

Magnitude of the scalar Green's function G_q is also plotted in Figure-12.

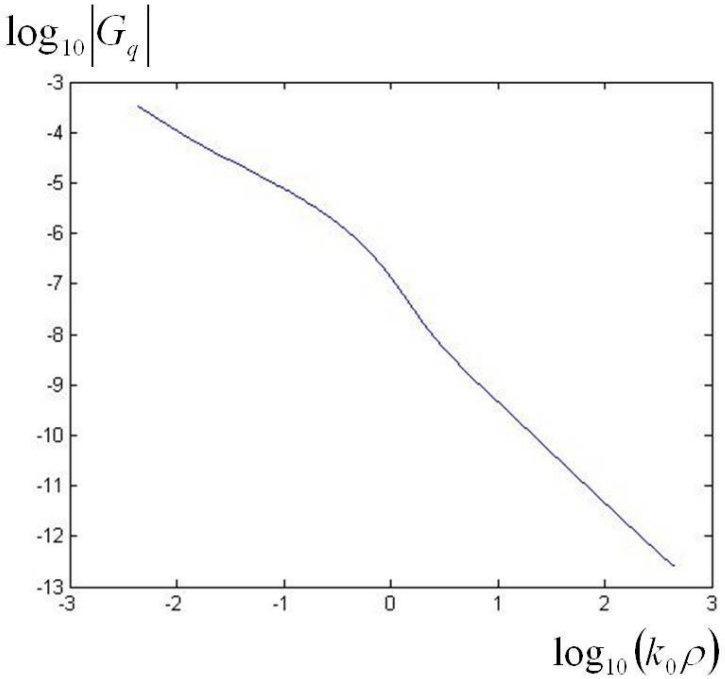

Figure-12 Magnitude of the Green's Function of Scalar Potential, G_q

The Green's function plots are compared with the ones in the reference [22] and a good agreement is observed. In the reference, the obtained values are already compared with published results [30].

CHAPTER 4

ANALYSIS OF A MICROSTRIP LINE ON PLANARLY LAYERED MEDIA – SINGLE LINE CASE

In this chapter field analysis and current distribution of planar layered media will be discussed for single line case. First single line microstrip will be discussed. Then, MPIE formulation in planar layered media will be explained for single line case. Afterwards singularity extraction, parameter calculations for single microstrip line and software implementation will be explained as well.

4.1 Brief Explanation of Single Line Case

While making the MoM analysis by using spatial domain closed-form Green's functions, first the MPIEs for layered structures should be obtained. MPIE is written in terms of vector and scalar potential Green's functions. Then, the unknown current density values that are included in MPIE are written in terms of known basis functions. Afterwards, boundary conditions are used and this process is called testing. Galerkin MoM method will be used. The reason why MPIE should be used is explained. Additionally, the process of obtaining closed forms of spatial domain Green's functions is explained as well. After applying MoM, the resulted matrix equation is solved in order to find out the current distribution on the single line conductor. Indeed, the main aim is finding this current distribution. Once the current distribution on the line is obtained, then all the parameters that define the circuit uniquely can be found by using this current distribution. In Figure-13, a microstrip line which has single conductor is illustrated.

The microstrip line in Figure-13 can be considered as a 3-layered structure. First layer is the ground plane. Ground plane is a perfect electric conductor (PEC) and it is positioned at the bottom of the microstrip structure. Second layer is composed of dielectric substrate that is on the ground plane. In this 3-layer structure, there is no superstrate, yet this is the simplest one. The third layer is the air which is on the dielectric substrate. On the dielectric substrate, a single line conductor is located which is composed of metal. This conductor has a width of w and this width is small compared to the operating wavelength. The main aim of the study is to find out the current distribution on this single line conductor. As seen from Figure-13, the current distribution on this metal conductor is approximated as rooftop functions. In this study, it is assumed that the behavior of the current distribution can be approximately reflected by rooftop functions and the basis functions are chosen in this way. It should be noted that this rooftop function approximation is appropriate to reflect the behavior of the current density on the conductor. All studies that are related to this study uses rooftop

functions and accurate results are obtained. At the right and left terminals, loads are located. Load currents are approximated as half rooftop functions. In this study, different load terminations will be tested such as open, short and matched then results corresponding to these different load combinations will be presented. Load impedances are defined as left load impedance and right load impedance Z_L and Z_R, respectively. During the analysis, additional load equations are obtained to the resulted matrix equation. The reason why these load equations should be added will be described together with how they can be calculated. Lastly, microstrip line is fed with a coaxial probe at an arbitrary point on the conductor, this arbitrary point is generally assumed as 1 cm from the load where the operating frequency is 1GHz. The function representing the source current is illustrated in Figure-13, and this function is chosen in order to model the discontinuity in the source current at the probe location. In the analysis, the point where the source is applied will be changed and the corresponding results will be presented.

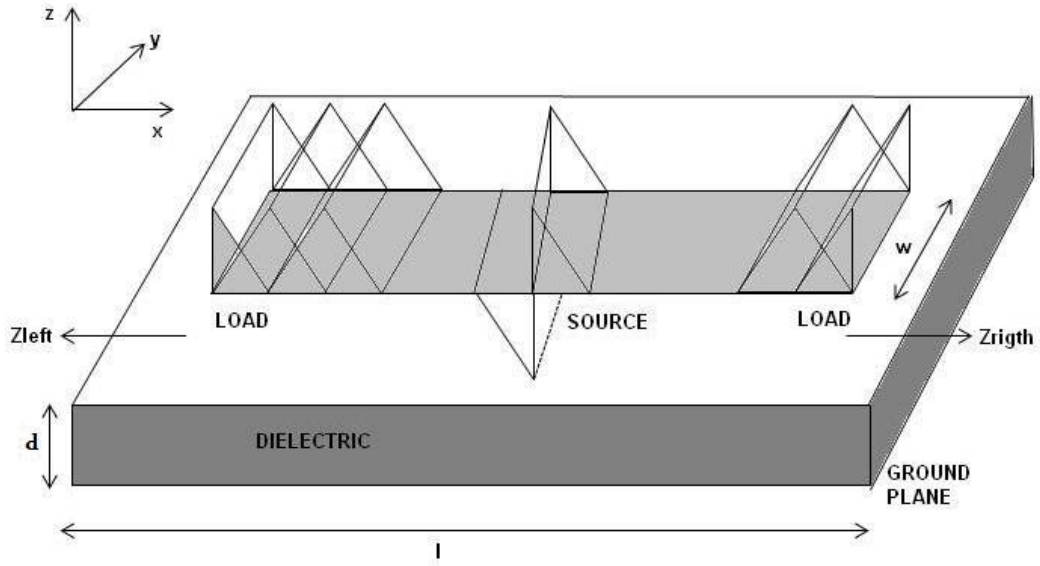

Figure-13 Illustration of Single Conductor Microstrip Line

In the software program, the location of the source point with respect to the loads is defined as a parameter, so by changing its value the results can be observed easily. In this study it is assumed that dielectric layer and ground plane extend to infinity without any border. Therefore, there are no boundaries observed in transverse direction. Conductors are assumed to be lossless. The thickness of the dielectric substrate can be shown with d. The width of single line conductor metal is shown with w and this value is small. Since the width of the conductor metal is small compared to the operating wavelength, current distribution is

observed only in the x direction and it is assumed that the current distribution in the y direction can be neglected [40]. On the other hand, if the width of the conductor is not small compared to the wavelength, then the current distribution in the y direction cannot be neglected and this situation will be analyzed in this thesis as well. However, in this single line conductor case, the current distribution in the y direction will be ignored. Therefore, the current distribution in the y direction is assumed to be uniform. It is clear from Figure-13 that in x direction current distribution is taken as piecewise linear function and in the y direction the current distribution is taken as uniform which corresponds to rooftop functions.

4.1.1 MPIE Formulation in Planar Layered Media

Tangential component of electric field on the conductor metal can be expressed in terms of scalar and vector potentials and associated Green's functions. Besides, scalar and vector potentials can be expressed in terms of induced surface current densities (J) [19]. The electric field expression can be written as shown in equation (50).

$$E_x = -j\omega G_{xx}^A * J_x + \frac{1}{j\omega}\frac{\partial}{\partial x}\left[G_q * \nabla . J\right] \tag{50}$$

Since the surface current density in y direction is neglected, the assumption in equation (51) is valid.

$$\nabla = \frac{\partial \hat{a}x}{\partial x} + \frac{\partial \hat{a}y}{\partial y} + \frac{\partial \hat{a}z}{\partial z} \rightarrow \frac{\partial \hat{a}x}{\partial x} \tag{51}$$

Therefore, the x directed electric field expression can be written as shown in equation (52).

$$E_x = -j\omega G_{xx}^A * J_x + \frac{1}{j\omega}\frac{\partial}{\partial x}\left[G_q * \frac{\partial}{\partial x} J_x\right] \tag{52}$$

As seen from equation (52), electric field is created only in the x direction in this case. G_{xx}^A expression represents the x directed vector potential located at r that is created from x directed electric dipole of unit strength (HED) located at r'. G_q is the Green's function for scalar potential. J_x represents x directed surface current density and this is unknown. The value that is desired to be found is this current density value J_x. This unknown J_x value can be approximated by the linear combination of known basis functions. This approximation is provided in equation (53). Here N represents the number of known basis functions that are used in order to approximate the unknown function with linear combination. Therefore, unknown function is expanded in terms of chosen and known basis functions, as shown in equation (53).

$$J(x,y) = \sum_{n=1}^{N} I_n J_{xn}(x,y) + J_s(x,y) \tag{53}$$

Equation (53) can be analyzed in detail. The coefficients of basis functions are defined as I_n and they are unknowns. After realizing the expansion, then these coefficients are desired to be found. This is because of the fact that now J_x unknown values are written in terms of basis functions. Basis functions are defined as $J_{xn}(x,y)$ and they are chosen from known functions. It is expected from these basis functions to reflect the behavior of the unknown function. Therefore, the behavior of J_x which is the surface current density created on the conductor metal should be reflected by a properly chosen basis function. In Figure-13, the chosen basis functions for this study is already illustrated on the conductor and they will be explained in detail. It is time to give some information about the selection of these basis functions. Since basis functions are used to approximate unknown current densities, their derivatives should approximate charge densities [1]. The selected basis functions should satisfy the continuity of current and at the same time they should satisfy the charge conservation on the conductor. Rooftop basis functions are defined along rectangular cells. No charge loss or gain can be observed in these rectangular cells and it is expected that the total charge in the circuit have to be zero. Because of all these reasons, basis functions together with source and load basis functions are chosen as illustrated in Figure-13, the detailed explanation of this selection of basis functions can be found in the reference [1]. Furthermore, the half rooftop functions that are chosen for source and loads are piecewise continuous while rooftop functions that are chosen for the remaining parts of the conductor are piecewise differentiable and again for the details reference should be examined [41]. The basis function for the source is defined as J_s and this is completely a known function. J_s does not have any unknown coefficient. Since the source that is applied by us has to be known and this is under our control, there are no unknowns for the source basis function [41].

Galerkin's MoM is used, so testing functions $J_{xm}(x,y)$ are same as chosen basis functions $J_{xn}(x,y)$. After this Galerkin's MoM, the resulted matrix is a symmetric matrix and this symmetry enables computational efficiency. If equation (53) is substituted into equation (52), then the expression in equation (54) is acquired.

$$E_x = -j\omega G_{xx}^A * \left[\sum_n I_n J_{xn}(x,y) + J_s(x,y) \right] + \frac{1}{j\omega} \frac{\partial}{\partial x} \left\{ G_q * \frac{\partial}{\partial x} \left[\sum_n I_n J_{xn}(x,y) + J_s(x,y) \right] \right\} \tag{54}$$

By expanding equation (54), equation (55) will be obtained.

$$E_x = -j\omega G_{xx}^A * J_s(x,y) + \frac{1}{j\omega} \frac{\partial}{\partial x} \left[G_q * \frac{\partial}{\partial x} J_s(x,y) \right] + \sum_n I_n \left\{ -j\omega G_{xx}^A * J_{xn}(x,y) + \frac{1}{j\omega} \frac{\partial}{\partial x} \left[G_q * \frac{\partial}{\partial x} J_{xn}(x,y) \right] \right\} \tag{55}$$

Now, the next step in the process will be the testing process. This is the testing of expression in equation (55) with $J_{xm}(x,y)$ and this testing procedure is given in equation (56).

$$\left\langle J_{xm}(x,y), E_x \right\rangle = 0 \tag{56}$$

In order to construct equation (56), boundary conditions should be taken into account. According to the boundary condition, tangential electric field on the conductor of microstrip line should be zero, because conductor metal is assumed to be PEC and on the PEC the tangential electric field must be zero. Since in this case there is only x directed electric field is considered, in the testing procedure only E_x will be used to satisfy boundary condition. This testing equation could be considered as the minimization of residual [1]. In equation (56), number of the constituted equations is equal to the number of unknowns. Now, if E_x in equation (55) is substituted into equation (56), the final form is provided in equation (57).

$$\begin{aligned} &j\omega\left\langle J_{xm}(x,y), G_{xx}^{A} * J_s(x,y)\right\rangle - \frac{1}{j\omega}\left\langle J_{xm}(x,y), \frac{\partial}{\partial x}\left[G_q * \frac{\partial}{\partial x} J_s(x,y)\right]\right\rangle = \\ &\sum_n I_n \left\{ - j\omega\left\langle J_{xm}(x,y), G_{xx}^{A} * J_{xn}(x,y)\right\rangle + \frac{1}{j\omega}\left\langle J_{xm}(x,y), \frac{\partial}{\partial x}\left[G_q * \frac{\partial}{\partial x} J_{xn}(x,y)\right]\right\rangle\right\} \end{aligned} \tag{57}$$

The chosen basis functions are piecewise differentiable. Therefore, the differentiation can be transferred onto the testing functions as shown in equations (58) and (59) by using integration by parts.

$$\left\langle J_{xm}(x,y), \frac{\partial}{\partial x}\left[G_q * \frac{\partial}{\partial x} J_s(x,y)\right]\right\rangle = -\left\langle \frac{\partial}{\partial x} J_{xm}(x,y), G_q * \frac{\partial}{\partial x} J_s(x,y)\right\rangle \tag{58}$$

$$\left\langle J_{xm}(x,y), \frac{\partial}{\partial x}\left[G_q * \frac{\partial}{\partial x} J_{xn}(x,y)\right]\right\rangle = -\left\langle \frac{\partial}{\partial x} J_{xm}(x,y), G_q * \frac{\partial}{\partial x} J_{xn}(x,y)\right\rangle \tag{59}$$

If the final simplifications in equations (58) and (59) are substituted into equation (57) and if both sides are divided by $-j\omega$, then the final form of equation (57) could be expressed as in equation (60).

$$\begin{aligned} &\sum_n I_n \left\{ \left\langle J_{xm}(x,y), G_{xx}^{A} * J_{xn}(x,y)\right\rangle - \frac{1}{\omega^2}\left\langle \frac{\partial}{\partial x} J_{xm}(x,y), G_q * \frac{\partial}{\partial x} J_{xn}(x,y)\right\rangle\right\} = \\ &-\left\langle J_{xm}(x,y), G_{xx}^{A} * J_s(x,y)\right\rangle + \frac{1}{\omega^2}\left\langle \frac{\partial}{\partial x} J_{xm}(x,y), G_q * \frac{\partial}{\partial x} J_s(x,y)\right\rangle \end{aligned} \tag{60}$$

Further simplifications can be possible if the convolution integrals over Green's function and basis function inside the inner product in equation (60) are transformed to the convolution integrals over basis and testing functions. By this transformation, the convolution integral can be evaluated analytically, because this time Green's function is not involved in the convolution integral. The final simplified form of equation (60) after this convolution

integral transformation is shown in equation (61). Calculating the convolution integral analytically is only possible by such a convolution integral transformation. After finding the results of convolution integrals analytically, then inner products of these results and the Green's functions will be evaluated. All analytic convolution calculations including load basis and testing functions for single conductor case are given in a very detailed fashion in references, so here the details are not covered once more [20, 23].

$$\sum_n I_n \left\{ \left\langle G_{xx}^A, J_{xm}(x,y) * J_{xn}(x,y) \right\rangle - \frac{1}{\omega^2} \left\langle G_q, \frac{\partial}{\partial x} J_{xm}(x,y) * \frac{\partial}{\partial x} J_{xn}(x,y) \right\rangle \right\} = \\ - \left\langle G_{xx}^A, J_{xm}(x,y) * J_s(x,y) \right\rangle + \frac{1}{\omega^2} \left\langle G_q, \frac{\partial}{\partial x} J_{xm}(x,y) * \frac{\partial}{\partial x} J_s(x,y) \right\rangle \tag{61}$$

In order to give an example, an arbitrary inner product term in equation (61) will be written in an explicit form, which is provided in equation (62).

$$\left\langle G_{xx}^A, J_{xm} * J_{xn} \right\rangle = \iint du dv G_{xx}^A(u,v) \iint dx dy J_{xm}(x-u, y-v) J_{xn}(x,y) \tag{62}$$

In equation (62), the second double integral inside is the convolution integral of basis and testing functions which is the result of the convolution integral transformation in equation (61) and it is evaluated analytically. The first double integral outside in equation (62) is the inner product integral between the analytically obtained convolution result and the Green's function. This integral cannot be evaluated analytically and numerical calculation is necessary. This numerical integral is realized by using Gauss Quadrature Method in the software program [42].

The expression in equation (61) is a matrix equation. After solving this matrix equation, unknown coefficients that are defined as I_n are found. Afterwards, these I_n values are substituted into equation (53) and unknown surface current densities that are defined as J_x are uniquely determined. The resulted matrix equation will be explained in detailed later, now the basis functions will be analyzed.

- **Basis Functions:**

As indicated previously, rooftop functions are selected in this study as basis functions. Additionally, the reason of this choice was explained. Rooftop functions are triangular functions in longitudinal direction and uniform in transverse direction [19]. These rooftop basis functions are given in equation (63) in a mathematical form and shown in Figure-14.

$$J_{xn}(x,y) = \begin{cases} \frac{1}{wh_x}\left[(1-n)h_x + x\right] & (n-1)h_x \le x \le nh_x, \quad |y| \le \frac{w}{2} \\ \frac{1}{wh_x}\left[(1+n)h_x - x\right] & nh_x \le x \le (n+1)h_x, \quad |y| \le \frac{w}{2} \\ 0 & elsewhere \end{cases} \tag{63}$$

Basis functions in equation (63) are illustrated in Figure-14.

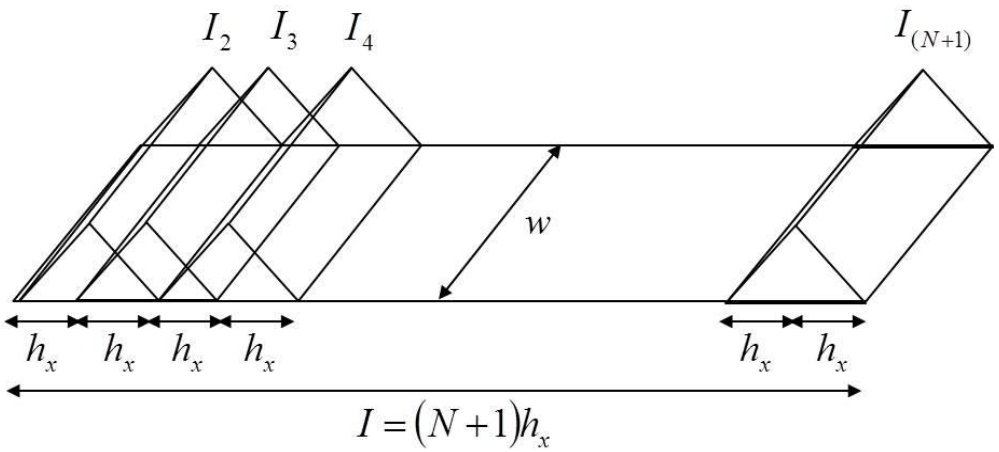

Figure-14 Illustration of Rooftop Basis Functions on the Conductor

As seen from Figure-14, the value of h_x is determined by the length of the conductor and the chosen number of basis function. Now, the issue of basis function selection can be discussed. The selection of basis function directly affects the rate of convergence of the integrals in MoM matrix elements [40]. Moreover, some features that are listed below should be satisfied by the selected basis and testing functions.

- Summation of the order of differentiability for basis and testing functions in the direction of current polarization should equal to one or greater than one.
- Any even function that has order of singularity less than one or any piecewise continuous function could be used in the direction orthogonal to the current polarization.

In order to add the contributions of source and load to the current density that is desired to be found, the corresponding basis functions should be selected appropriately. Then, they should be associated with the remaining basis functions. Now, these basis functions for source and load contributions will be discussed.

- **Source Basis Functions:**

For the source, sawtooth like function is chosen as basis function. In order to reflect the behavior of the source, such basis function is selected. Here, this function shows a discontinuity that accounts for the vertical current provided by the probe. The mathematical expression of the source basis function is shown in equation (64).

$$J_s(x,y)=\begin{cases}\dfrac{1}{wh_x}\left[(a-1)h_x-x\right] & (a-1)h_x\le x\le ah_x,\quad |y|\le\dfrac{w}{2}\\ \dfrac{1}{wh_x}\left[(a+1)h_x-x\right] & ah_x\le x\le (a+1)h_x,\quad |y|\le\dfrac{w}{2}\\ 0 & \textit{elsewhere}\end{cases} \tag{64}$$

In equation (64), the parameter a represents the excitation point in terms of number of h_x. By using different values for a, the feed point where the source in applied can be changed easily and the results can be observed on the software program. The illustration of the source basis function that is defined in equation (64) is provided in Figure-15.

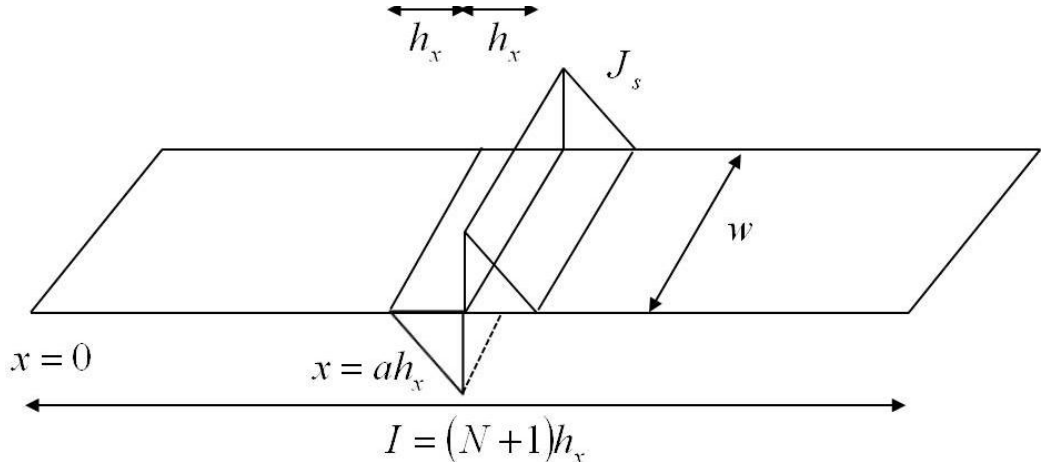

Figure-15 Illustration of Source Basis Function on the Conductor

- **Load Basis Functions:**

Load basis functions are chosen as half rooftop functions. Half rooftop functions have triangular functions in longitudinal direction and uniform functions in transverse direction. The mathematical representation which is similar to the one for rooftop functions is provided in equations (65) and (66) that are for left load and right load, respectively.

$$J_{lL}(x,y)=\begin{cases}-\dfrac{1}{wh_x}\left[x-h_x\right] & 0\le x\le h_x,\quad |y|\le\dfrac{w}{2}\\ 0 & \textit{elsewhere}\end{cases} \tag{65}$$

$$J_{lR}(x,y)=\begin{cases}\dfrac{1}{wh_x}\left[x-Nh_x\right] & Nh_x \le x \le (N+1)h_x, \quad |y| \le \dfrac{w}{2} \\ 0 & elsewhere\end{cases} \tag{66}$$

N is the number of basis functions. In single conductor microstrip line case, load basis functions that are used in both terminations should be associated with the basis functions of the remaining parts of the conductor. Therefore, two additional equations are needed at two load terminations for constructing such a relation. In order to write these equations, boundary conditions at the terminals of the conductor should be taken into account. When load impedance and line current are multiplied, voltage difference between line and ground is obtained. Hence, the voltage values found at the load terminations can be expressed in terms of load impedances, coefficients of load expansion functions and coefficients of other expansion functions [41]. By using an approach that is based on transmission line analysis, load impedances can be associated with the surface current densities on the conductor. Finite differencing approach will be used as well. Total voltage $V(x)$ and total current $I(x)$ on the conductor can be related by using first-order differential equations provided in equations (67) and (68).

$$\frac{dI(x)}{dx} = -YV(x) \tag{67}$$

$$\frac{dV(x)}{dx} = -ZI(x) \tag{68}$$

Where, $Y = j\beta / Z_0$ and $Z = j\beta Z_0$, shunt admittance and series impedance per unit length of the line, respectively.

Characteristic impedance Z_0 and propagation constant β of the line can be found by using quasi-static analysis and details are not provided here [19]. Derivatives in the equations (67) and (68) can be calculated with finite differencing. The resulted equations can be associated with each at the load terminations $x = x_l$ and $x = x_r$, the final equations are acquired which are shown in equations (69) and (70).

$$I_1\left[1+ j\beta h_x \frac{Z_{lL}}{Z_c} - \frac{\beta^2 h_x^2}{2}\right] - I_2 = 0 \tag{69}$$

$$I_{N+1} + I_{N+2}\left[1+ j\beta h_x \frac{Z_{lR}}{Z_c} - \frac{\beta^2 h_x^2}{2}\right] = 0 \tag{70}$$

Where,

Z_{lL} = Load impedance of the left end of the line

Z_{lR} = Load impedance of the right end of the line

Z_c = Characteristic impedance of the line

β = Propagation constant

Equations (69) and (70) should be added to the matrix equation and then this final matrix equation should be solved for I_n values. In this way, current distribution on the microstrip line conductor which is terminated with complex load impedances Z_{lL} and Z_{lR} is determined uniquely. These complex load impedances will have different values depending on the loads that are used in the analysis. In the software program, these impedance values can be changed easily and the corresponding results could be observed eventually. The illustration of the load basis functions is presented in Figure-16.

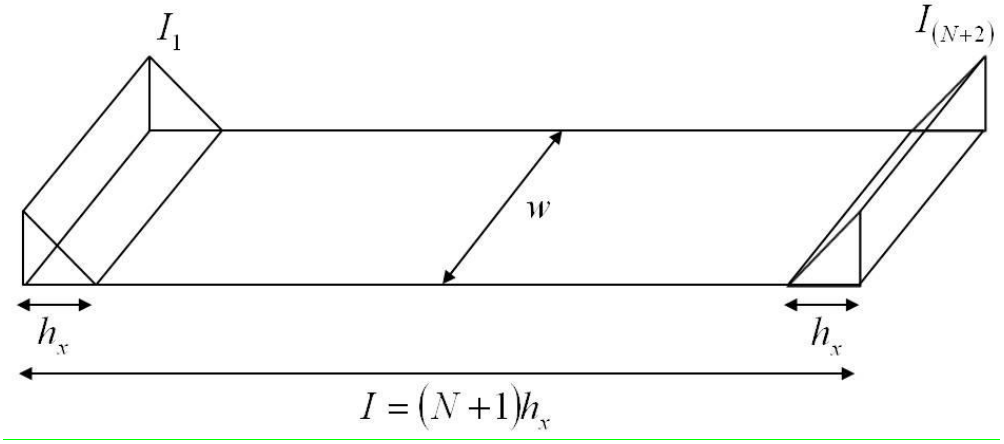

Figure-16 Illustration of Load Basis Functions on the Conductor

- **Derivative of Basis Function:**

Derivatives of basis functions are needed while the electric field due to the scalar potential and these derivatives are provided in equation (71).

$$\frac{d}{dx} J_{xn}(x,y) = \begin{cases} \dfrac{1}{wh_x} & (n-1)h_x \le x \le nh_x, \quad |y| \le \dfrac{w}{2} \\ -\dfrac{1}{wh_x} & nh_x \le x \le (n+1)h_x, \quad |y| \le \dfrac{w}{2} \\ 0 & \textit{elsewhere} \end{cases} \tag{71}$$

- **Derivative of Source Basis Function:**

Derivative of the source basis function is also needed like the derivative of shifted testing function. Therefore, the derivative expression of this source basis function is provided in equation (72).

$$\frac{d}{dx}J_s(x,y)=\begin{cases}-\dfrac{1}{wh_x} & (a-1)h_x \le x \le ah_x, \quad |y| \le \dfrac{w}{2} \\ -\dfrac{1}{wh_x} & ah_x \le x \le (a+1)h_x, \quad |y| \le \dfrac{w}{2} \\ 0 & elsewhere \end{cases} \tag{72}$$

- **Derivative of Load Basis Functions:**

Lastly, derivative of load basis functions are presented in equations (73) and (74).

$$\frac{d}{dx}J_{lL}(x,y)=\begin{cases}-\dfrac{1}{wh_x} & 0 \le x \le h_x, \quad |y| \le \dfrac{w}{2} \\ 0 & elsewhere \end{cases} \tag{73}$$

$$\frac{d}{dx}J_{lR}(x,y)=\begin{cases}\dfrac{1}{wh_x} & Nh_x \le x \le (N+1)h_x, \quad |y| \le \dfrac{w}{2} \\ 0 & elsewhere \end{cases} \tag{74}$$

By using these given basis functions and their derivatives, all desired convolution integrals could be evaluated analytically [20, 23]. Figure-17 illustrates the derivatives of rooftop and half rooftop functions.

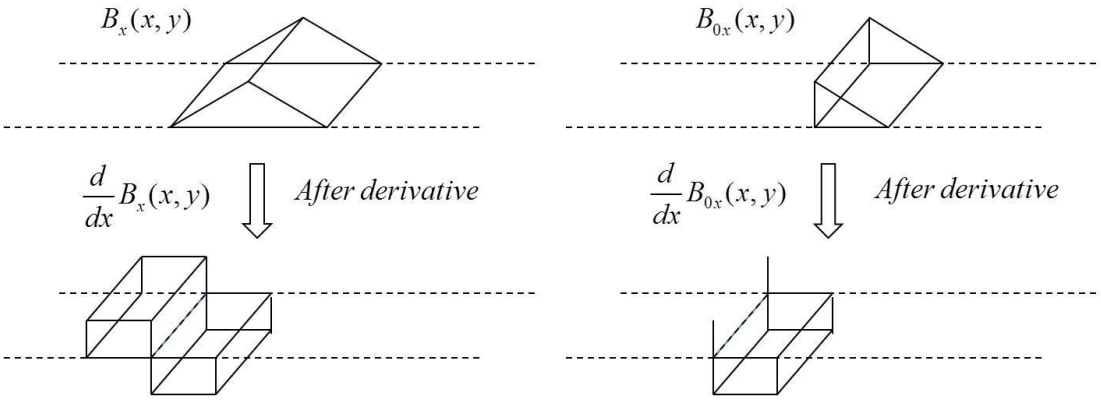

Figure-17 Illustration of the Derivative of Basis Functions

4.1.2 Singularity Extraction

The closed-form spatial domain Green's function expression is shown in equation (75). This expression will be used in MoM application and it is the general designation which contains both vector and scalar potential Green's functions.

$$G \cong \sum_{n=1}^{N} a_n \frac{e^{-jkr_n}}{r_n} \tag{75}$$

Where, $r_n = \sqrt{\rho^2 - b_n^2}$.

The complex coefficients a_n and b_n that are acquired during the process of obtaining closed-form spatial domain Green's functions are data sets of complex numbers. These complex coefficients are obtained from a software program which is written in FORTRAN, such that these coefficients will be the inputs of the MoM application. In these complex data sets, the last terms are called as direct terms and for these direct terms always $a_n = 1$ and $b_n = 0$ have to be satisfied. However, if the Green's function expression in equation (75) is investigated carefully, it is clear that at the direct term the denominator of Green's function should equal to zero ($r \to 0$). Consequently, always a singularity is observed in the direct term. In order to eliminate this singularity, numerical integrals in equation (59) should be evaluated by extracting the direct terms. Then, the effects of these direct terms should be added analytically to the integral expression. For this reason, first the Taylor series expansion of the direct term is written. The Taylor series expansion of the exponential e^{-jkr} at the point $r = 0$ is given in equation (76).

$$e^{-jkr} = 1 + (-jkr) + \frac{(-jkr)^2}{2!} + \ldots = \sum_{n=0}^{\infty} \frac{(-jkr)^n}{n!} \tag{76}$$

If both sides of the expression in equation (76) are divided by r, the final form is shown in equation (77).

$$\frac{e^{-jkr}}{r} = \frac{1}{r} + (-jk) + r\left[\frac{(-jk)^2}{2!} + \ldots\right] \tag{77}$$

Equation (77) is the series expansion of an arbitrary exponential by using Taylor series expansion. Since, the integral will be evaluated numerically without including the direct term, the integral of the direct term should be evaluated analytically by using this series expansion. Analytical calculation of such integrals is only possible by this series expansion approaches and otherwise only numerical calculation could be considered. However, it should be noted that this is a series approximation, so the contributions of the third term and the following terms are very small to the general expression with respect to the contributions of the first two terms when $r \to 0$. Hence, the contributions of third term and the following terms are ignored. Only first two terms will be used in the analysis. Now, in equation (77) instead of the expression in the left side of the equation, the expression in the right side of the equation will be used by accounting only the first two terms. The integral of this expression in the right side should be calculated with respect to the variable r. As seen from equation (77), the second term is a constant that is independent of the variable r, so it can be used directly. Thereof, second term can be directly taken out of the integral as a constant. Integral with respect to variable r should be evaluated analytically only for the first term which is already a function of r. Let, rewrite the first term in equation (78).

$$\frac{1}{r} = \frac{1}{\sqrt{x^2 + y^2}} \tag{78}$$

For evaluating the integral of equation (78) analytically, "Method of Kantorovich for isolating singularities" will be used, the details are not discussed here and they can be found in the reference [22]. Both the source and observation points are located at point $z = 0$. After applying "Method of Kantorovich for isolating singularities" to the expression in equation (78) when $r \to 0$ (x and $y \to 0$), the final result is presented in equation (79) [22].

$$\begin{aligned}\int_{y_1}^{y_2}\int_{x_1}^{x_2} \frac{1}{\sqrt{x^2 + y^2}} dxdy = {} & y_2 \log\left[\frac{-x_1 + \sqrt{x_1^2 + y_2^2}}{-x_2 + \sqrt{x_2^2 + y_2^2}}\right] + y_1 \log\left[\frac{-x_2 + \sqrt{x_2^2 + y_1^2}}{-x_1 + \sqrt{x_1^2 + y_1^2}}\right] + \\ & x_2 \log\left[\frac{-y_1 + \sqrt{x_2^2 + y_1^2}}{-y_2 + \sqrt{x_2^2 + y_2^2}}\right] + x_1 \log\left[\frac{-y_2 + \sqrt{x_1^2 + y_2^2}}{-y_1 + \sqrt{x_1^2 + y_1^2}}\right]\end{aligned} \tag{79}$$

Consequently, by adding equation (79) together with the second term in equation (77) to each of the numerically evaluated integrals in equation (59), without having any trouble for the singularity in the direct term, the contribution of the direct term is added analytically to

the general expression. The parts in the integral excluding the direct term are already evaluated numerically. Only the contribution of the direct term is added afterwards analytically. By this way, the singularity problem is solved. If the contribution of the direct term would be evaluated numerically as well, then singularity will arise and the denominator will go to infinity.

4.1.3 Software Implementation

When the matrix equation in equation (59) is solved, then the unknown coefficient I_n's are found. Afterwards, by using these coefficients the basis functions can be expressed uniquely, so that the current distribution on the line is found. It should be stated that all these calculations are written with program in MATLAB® software. First, matrix equation should be constructed from the expression in equation (59). The matrix equation which identifies the infrastructure of the software program is discussed below as well. The MoM matrix equation is given in equation (80).

$$Ax = b \tag{80}$$

Here A is N X N matrix. x and b are N X 1 matrices. The elements of these matrices A, x and b are shown in equations (81), (82) and (83), respectively.

$$A_{mn} = \left\langle G_{xx}^{A}, J_{xm}(x,y) * J_{xn}(x,y) \right\rangle - \frac{1}{\omega^2} \left\langle G_q, \frac{\partial}{\partial x} J_{xm}(x,y) * \frac{\partial}{\partial x} J_{xn}(x,y) \right\rangle \tag{81}$$

$$x_n = I_n \tag{82}$$

$$b_m = -\left\langle G_{xx}^{A}, J_{xm}(x,y) * J_s(x,y) \right\rangle + \frac{1}{\omega^2} \left\langle G_q, \frac{\partial}{\partial x} J_{xm}(x,y) * \frac{\partial}{\partial x} J_s(x,y) \right\rangle \tag{83}$$

Where, $m = 2,3,...,(N+1)$, $n = 2,3,...,(N+1)$. N is the number of basis functions. Number of testing functions is equal to number of basis functions. As indicated before, the convolution integrals that are inside the matrix elements of A and b matrices such as $J_{xm}(x,y) * J_{xn}(x,y)$, $\frac{\partial}{\partial x} J_{xm}(x,y) * \frac{\partial}{\partial x} J_{xn}(x,y)$, $J_{xm}(x,y) * J_s(x,y)$ and $\frac{\partial}{\partial x} J_{xm}(x,y) * \frac{\partial}{\partial x} J_s(x,y)$ should be evaluated analytically. Then, the double integrals of the obtained values from analytical calculations and the Green's functions G_{xx}^{A} and G_q are evaluated. While evaluating these integrals, the analytical calculation is not possible, so numerical calculation has to be used to take these integrals. In the constructed software program, numeric integrals are evaluated by using Gauss Quadrature [42]. It should be noted that the convolution integrals depends on the distance between the basis and the testing functions, not on the absolute locations of them. Therefore, when the convolution integral of

the first testing function with each of the basis functions are computed, all other convolution integral combinations are known. Therefore, once the first row of the matrix is constructed, the remaining part of the matrix can be filled by using the entries of the first row. As mentioned previously, unique solution can be obtained if and only if the effects of the loads at two terminations of the microstrip line are taken into account. Loads are represented by half rooftop basis functions. The coefficients of these half rooftop functions should be associated with other basis functions. Consequently, two additional equations that are given in equations (68) and (69) should be added to the matrix equation. These equations include the coefficients of load basis and testing functions which are I_1 and $I_{(N+2)}$.

4.2 Numerical Application

The analysis for a single microstrip line structure is presented. In this part, the results that are obtained from the application of this analysis are given and associated comments on these results are presented. A single line microstrip structure that analyses are applied is illustrated in Figure-18.

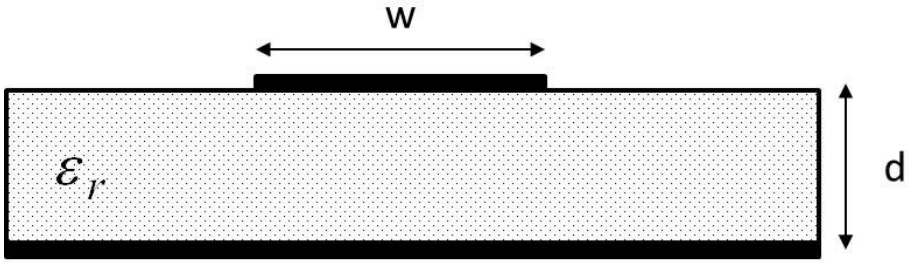

Figure-18 Single Microstrip Line Structure

The parameters that are used in the analysis are given as follows:

$f = 1\,GHz$
$\varepsilon_r = 4.0$
$d = 0.02032\,cm$
$w = 0.08128\,cm$
$l = 12\,cm$
$z_c = 32.035\,\Omega$

The magnitudes of closed form spatial domain vector and scalar potentials are illustrated in Figure-11 and Figure-12. These values are used as inputs in the analysis. Now, the obtained results are presented with graphical representation.

In Figure-19, the amplitude of the current distribution on the line is illustrated when two terminals of the line are match loaded, line is fed at 1cm from the left and 50 basis functions are used. For matched load case, it is expected to obtain current distribution as constant throughout the line. This result approximately represents the expected behavior. Only small amount of fluctuation occurs and the general structure of the amplitude distribution is almost constant. At the feeding point, a source discontinuity is observed. This result is also expected in matched load case.

In Figure-20, the amplitude of the current distribution on the line is illustrated when two terminals of the line are match loaded again, line is fed at 6cm from the left and 50 basis functions are used. When the location of the feeding point is changed, it is expected to observe a shift in source discontinuity. In the figure, this shift can be observed.

In Figure-21, the amplitude of the current distribution on the line is illustrated when two terminals of the line are open circuited, line is fed at 1cm from the left and 50 basis functions are used. For open circuit termination case, it is expected to observe current as zero at the termination points. Moreover, it is expected to observe maximum. These expected results can be acquired from the given figure. Current amplitudes are zero at the terminations and a peak current is observed as well. At the source feeding point, discontinuity can be realized.

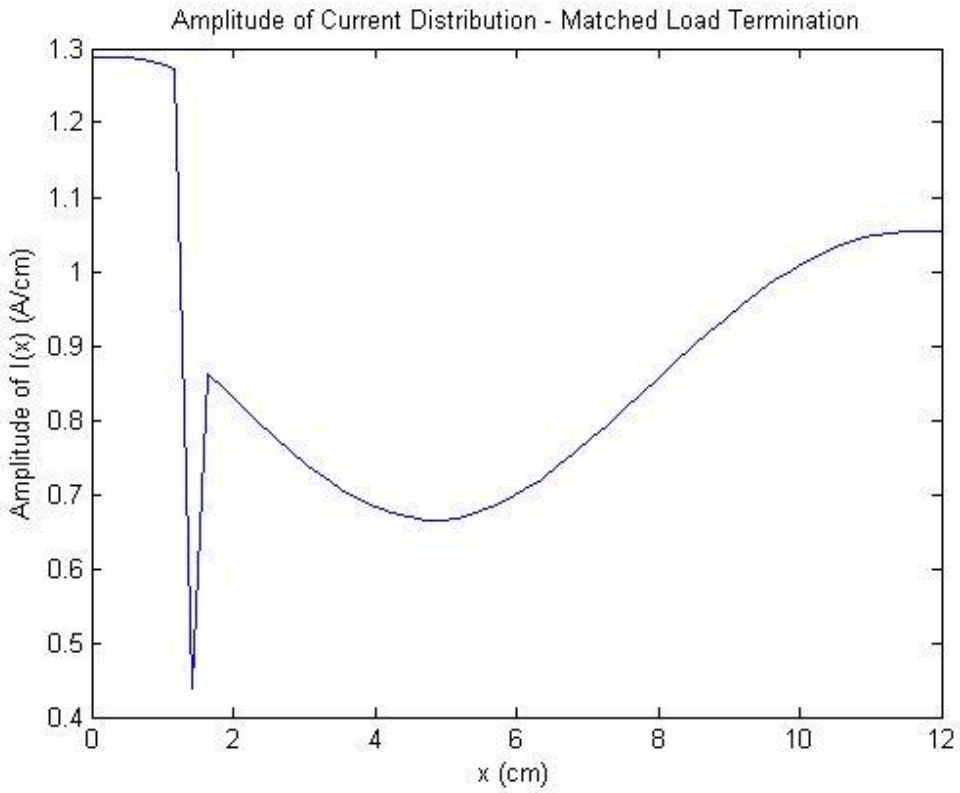

Figure-19 Amplitude of Current Distribution with Match Load Terminations, Excited at 1cm from Left, 50 Basis Functions

In Figure-22, the amplitude of the current distribution on the line is illustrated when two terminals of the line are open circuited, line is fed at 6cm from the left and 50 basis functions are used. When the feeding point is changed for open circuit termination case, a shift in source discontinuity should be observed and this shift can be seen from the given figure. Again at the termination points, the current values are zero as expected.

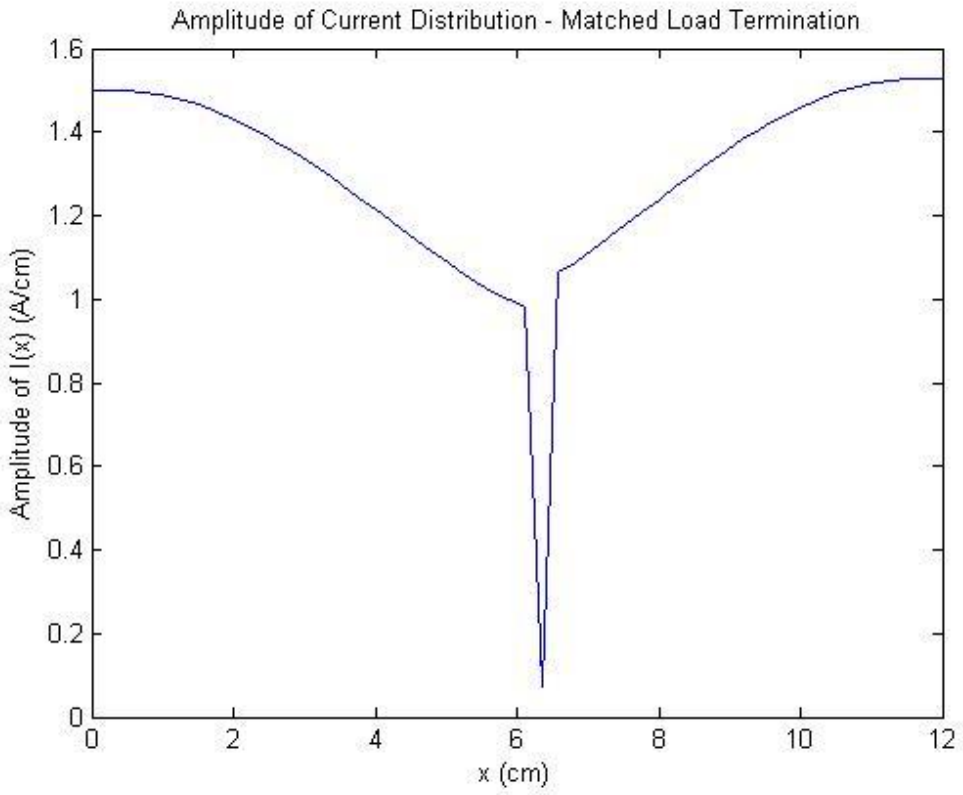

Figure-20 Amplitude of Current Distribution with Match Load Terminations, Excited at 6cm from Left, 50 Basis Functions

In Figure-23, the amplitude of the current distribution on the line is illustrated when two terminals of the line are short circuited, line is fed at 1cm from the left and 50 basis functions are used. For short circuit case, it is expected to observe maximum current values at the termination points. Additionally, zero current should be observed. These expected results can be acquired from the given figure. $2cm$ offset can also be observed for the source.

In Figure-24, the amplitude of the current distribution on the line is illustrated when two terminals of the line are short circuited, line is fed at 6cm from the left and 50 basis functions are used. When the feeding point is changed, a shift is be observed for the source point. Again at the termination points maximum current amplitudes are observed.

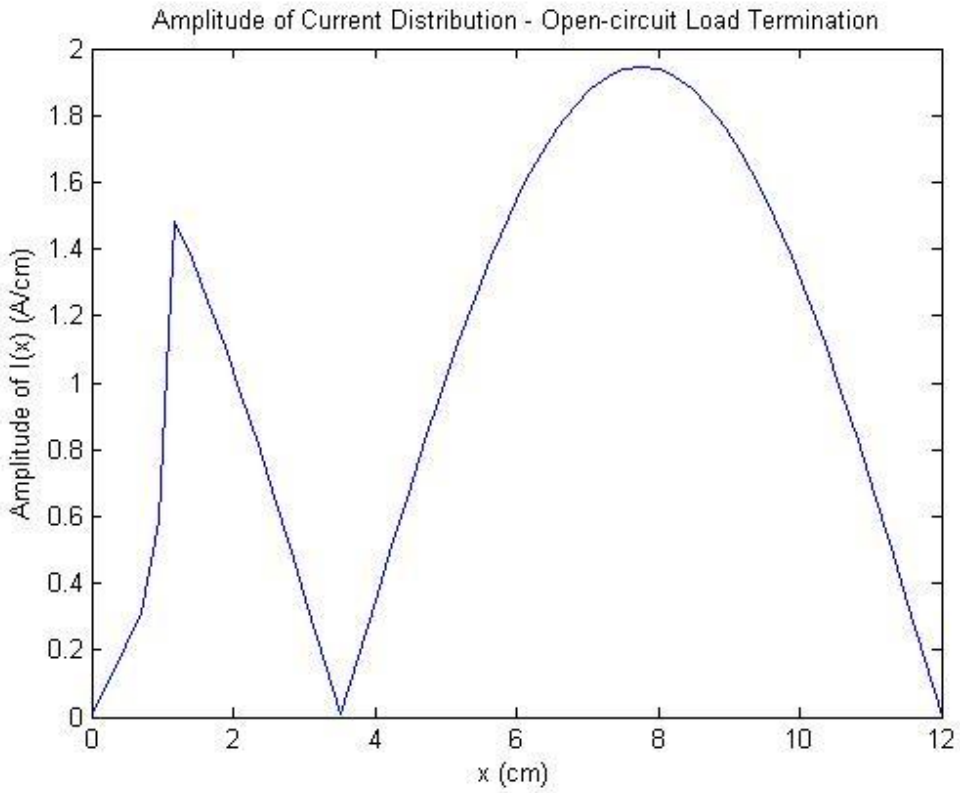

Figure-21 Amplitude of Current Distribution with Open Circuit Terminations, Excited at 1cm from Left, 50 Basis Functions

In these figures mainly the effect of the location of feed point is observed. Moreover, the effect of the termination loadings can be observed. From now on, by using these data the resulted parameters can be calculated. The main parameter calculations will be performed for patch antenna case. However, for a single line, the main parameter calculation techniques are presented.

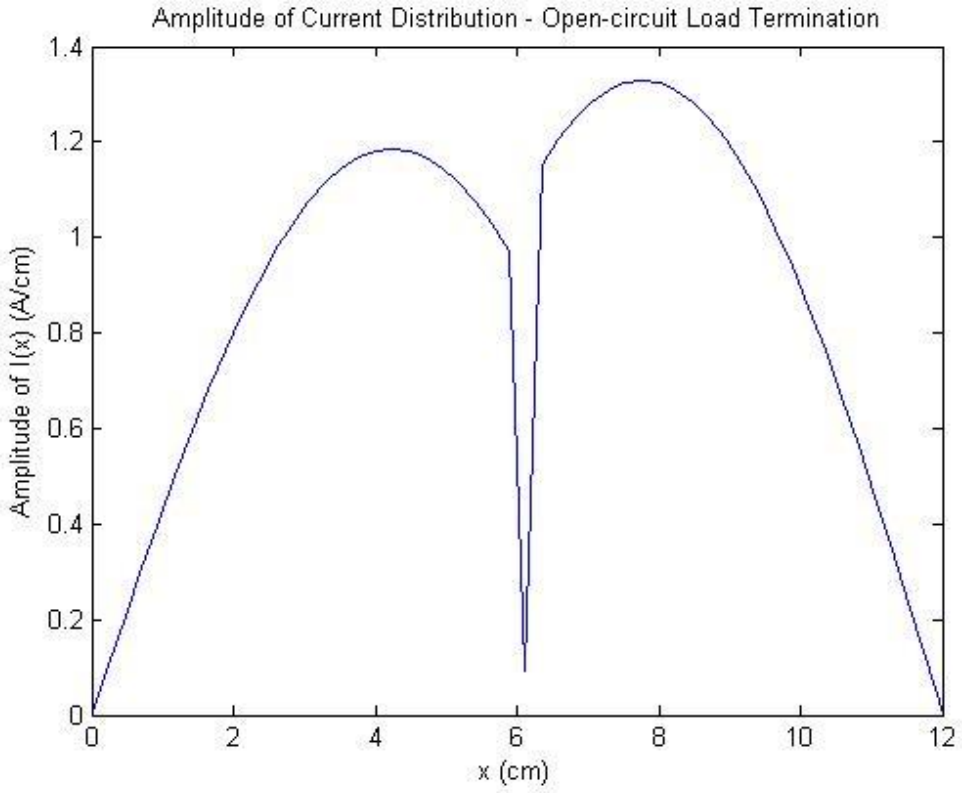

Figure-22 Amplitude of Current Distribution with Open Circuit Terminations, Excited at 6cm from Left, 50 Basis Functions

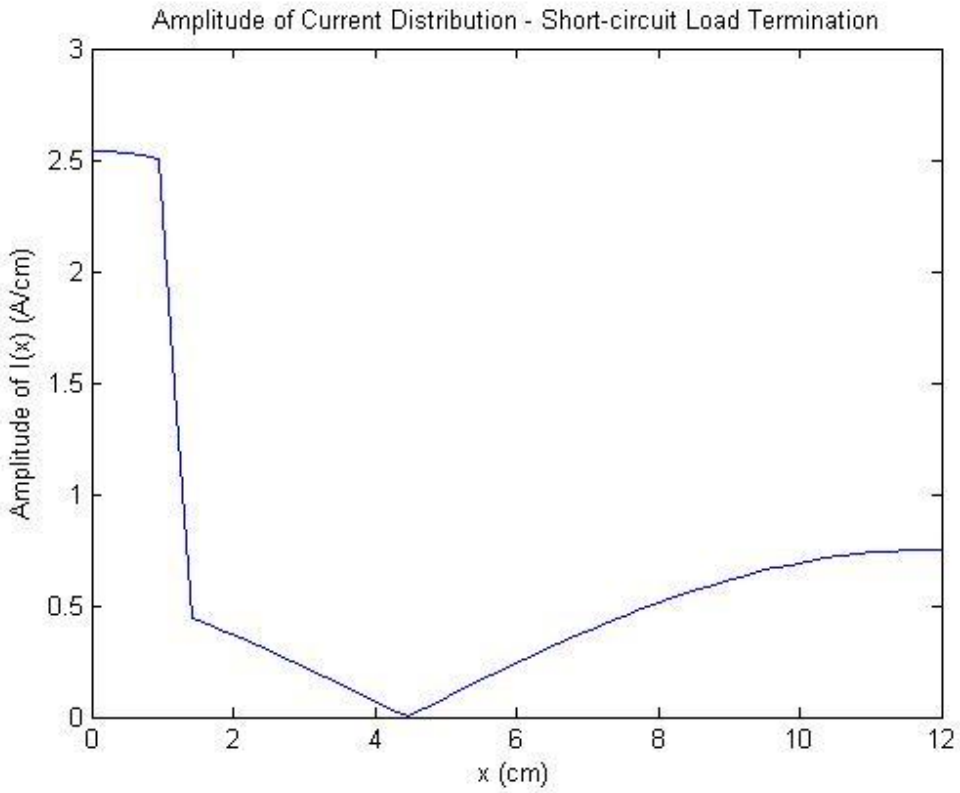

Figure-23 Amplitude of Current Distribution with Short Circuit Terminations, Excited at 1cm from Left, 50 Basis Functions

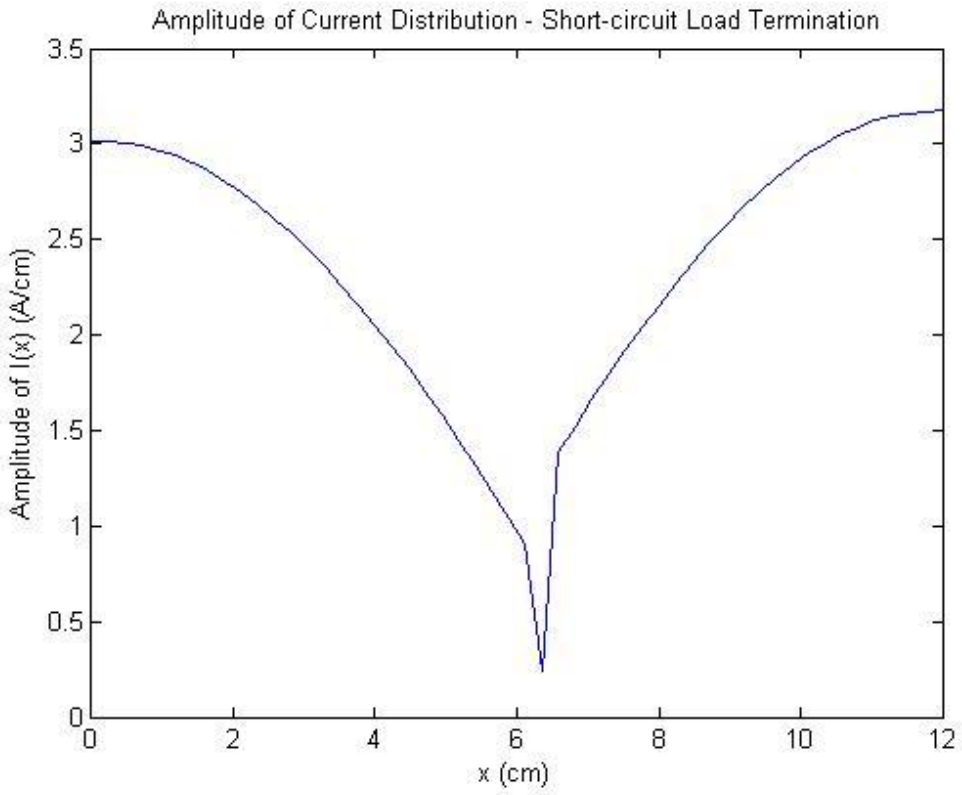

Figure-24 Amplitude of Current Distribution with Short Circuit Terminations, Excited at 6cm from Left, 50 Basis Functions

CHAPTER 5

ANALYSIS OF A MICROSTRIP LINE ON PLANARLY LAYERED MEDIA – COUPLED LINE CASE

In this chapter, the current distribution on parallel coupled lines are calculated by using closed form Green's functions in spatial domain via Galerkin's MoM. First parallel coupled lines are explained. The formulation for this kind of structures will be described and an information will be given regarding to the software application. Lastly, the results that are obtained from the analysis are presented in terms of graphs.

5.1 Parallel Coupled Line Structures

The general form of a parallel coupled line structure is shown in Figure-25. In the previous chapter, analysis of the single line microstrip structure is provided. Now, two lines are located as parallel to each other to form a coupled line pair. For such an arrangement, there will be an interaction between these two lines and this coupling effect should be taken into account while performing the analysis.

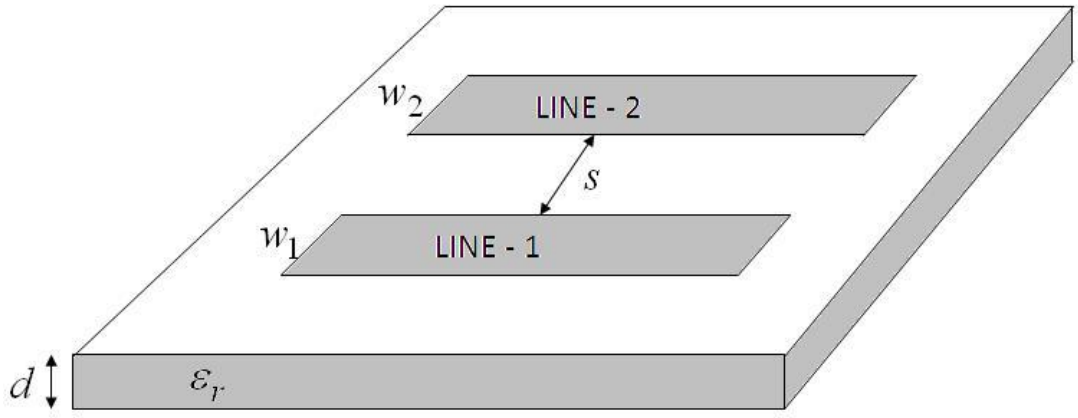

Figure-25 Parallel Coupled Line Structure

5.2 Formulation

In the coupled line case, total current can be expressed as the summation of the currents on each line together with the source current. This total current expression is shown in equation (84).

$$J_x(x,y)=\sum_n I_{1n}J_{1xn}(x,y)+\sum_n I_{2n}J_{2xn}(x,y)+J_s(x,y) \tag{84}$$

Feeding should be only on one line and there will be no source included on the second line. The currents that are created on the line without the source are due to the effect of the currents on the line with the source. This effect is called as coupling effect. According to the terminology, the line that is excited by a source is called as active line and the other one without source is called as passive line. The current on the passive line is created only by the currents on the active line that are due to the source excitement.

Assume that line-1 is the active line which means feeding is on line-1;

J_{1xn} and J_{2xn} are basis functions of active and passive lines, respectively. I_{1n} and I_{2n} are the basis function coefficients of active and passive lines, respectively. It is aimed to find out these coefficients at the end of the analysis. Since similar analysis will be performed for this case as the analysis of single line case, a detailed explanation of the theory will not be provided in this chapter. Detailed presentation can be found in the previous chapter. Recall the tangential electric field formula which is given in equation (85).

$$E_x=-j\omega G_{xx}^A * J_x+\frac{1}{j\omega}\frac{\partial}{\partial x}\left[G_q * \frac{\partial}{\partial x}J_x\right] \tag{85}$$

Expression of J_x in equation (84) is substituted in equation (131). Afterwards, E_x expression should be tested with testing functions J_{1xm} and J_{2xm} according to the MoM analysis. Since there are two testing functions belonging to two lines, testing operation should be performed twice. These testing operations are given in equation (86) and equation (87).

$$\langle J_{1xm}, E_x \rangle = 0 \tag{86}$$

$$\langle J_{2xm}, E_x \rangle = 0 \tag{87}$$

If equation (84) and equation (85) are substituted into equation (86) and equation (87), then two equations are obtained. These two equations are shown in equation (88) and equation (89).

$$\sum_n I_{1n}\left\{\left\langle G_{xx}^A, J_{1xm} * J_{1xn}\right\rangle - \frac{1}{\omega^2}\left\langle G_q, \frac{d}{dx}J_{1xm} * \frac{d}{dx}J_{1xn}\right\rangle\right\}$$
$$+\sum_n I_{2n}\left\{\left\langle G_{xx}^A, J_{1xm} * J_{2xn}\right\rangle - \frac{1}{\omega^2}\left\langle G_q, \frac{d}{dx}J_{1xm} * \frac{d}{dx}J_{2xn}\right\rangle\right\} = \tag{88}$$
$$-\left\langle G_{xx}^A, J_{1xm} * J_s\right\rangle + \frac{1}{\omega^2}\left\langle G_q, \frac{d}{dx}J_{1xm} * \frac{d}{dx}J_s\right\rangle$$

$$\sum_n I_{1n}\left\{\left\langle G_{xx}^A, J_{2xm} * J_{1xn}\right\rangle - \frac{1}{\omega^2}\left\langle G_q, \frac{d}{dx}J_{2xm} * \frac{d}{dx}J_{1xn}\right\rangle\right\}$$
$$+\sum_n I_{2n}\left\{\left\langle G_{xx}^A, J_{2xm} * J_{2xn}\right\rangle - \frac{1}{\omega^2}\left\langle G_q, \frac{d}{dx}J_{2xm} * \frac{d}{dx}J_{2xn}\right\rangle\right\} = \tag{89}$$
$$-\left\langle G_{xx}^A, J_{2xm} * J_s\right\rangle + \frac{1}{\omega^2}\left\langle G_q, \frac{d}{dx}J_{2xm} * \frac{d}{dx}J_s\right\rangle$$

In equations (88) and (89), convolution integrals should be calculated. As in the case of single line in previous chapter, these integrals are calculated analytically. Since the analytical calculation technique is given in previous chapter, a detailed analysis will not be given in this chapter. Detailed analytical calculation of the convolution integrals for parallel coupled line case can be found in the references [20, 23].

5.3 Software Implementation

Equations (88) and (89) should be solved in order to obtain the unknown basis function coefficients I_{1n} and I_{2n}. As performed in previous chapter for single line case, each of these equations are first defined in terms of matrix equations and then these matrix equations are solved. Software program is constructed such that it can identify active and passive lines automatically by using the information that which line is fed. The location of the source on an arbitrary part of the line can be assigned easily. Therefore, the effect of the location of the source can be observed easily. The distance between two parallel lines can also be assigned to the software program easily, so the effect of this distance can be observed easily as well. It is expected that by increasing the distance between the lines, the coupling effect between the lines should be decreased. On the other hand, if this distance is decreased, then the coupling effect between the lines should be strengthened. Software program outputs the current distributions on both the active and passive lines as a graphical representation together with the required data. The software program is very similar to the program for single line case in previous chapter. Calculation of integrals and the general structure of the program are same as previous method. Therefore, detailed explanation is not necessary in this chapter.

5.4 Numerical Application

In the parallel coupled line analysis, open circuit terminations at both ends are used. Therefore, all results are presented for open circuit terminations. The effects will be observed by changing the distance between the lines. The effects of other parameters will not be observed for this analysis. The parameter values that are used in this parallel coupled line analysis are given as follows:

$f = 1\,GHz$
$\varepsilon_r = 4.0$
$d = 0.02032\,cm$
$w_1 = w_2 = 0.08128\,cm$
$l_1 = l_2 = 10\,cm$

Source is located on the beginning of the left termination of line-1 which means that line-1 is active. When two terminals are open circuited, 40 basis functions are used, the distance between lines s is $7.5cm = \lambda/2$ the amplitudes of the current distributions on line-1 (active line) and line-2 (passive line) are shown in Figure-26. Since the distance between the lines is huge, the coupling effect is expected to be low and the current on the passive line is expected to be very small compared to the current on line-1.

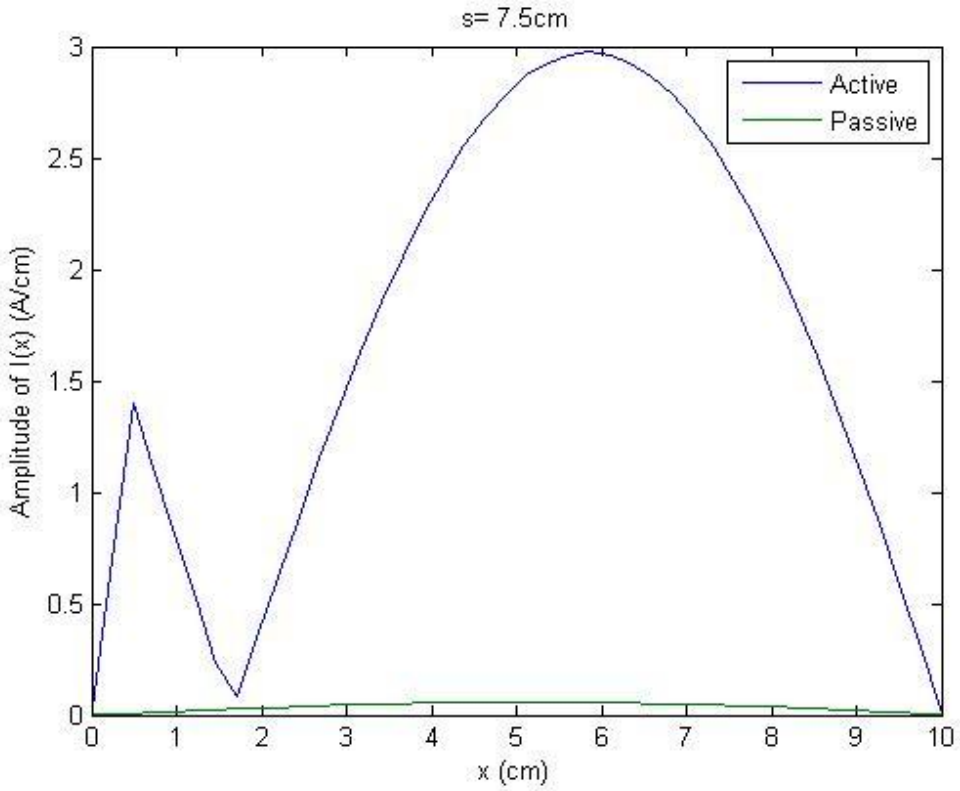

Figure-26 Amplitudes of Current Distributions on Active/Passive Lines with Open Circuit Terminations, Excited on Line-1 from Left beginning, $s = 7.5cm = \lambda/2$

Source is located on the beginning of the left termination of line-1. When two terminals are open circuited, 40 basis functions are used, the distance between lines s is $3.75cm = \lambda/4$ the amplitudes of the current distributions on line-1 (active line) and line-2 (passive line) are shown in Figure-27. While the distance between active line and passive line is decreased, it is expected to observe an increase on the passive line current. An increase on the passive line current can be observed in Figure-27 when it is compared with Figure-26.

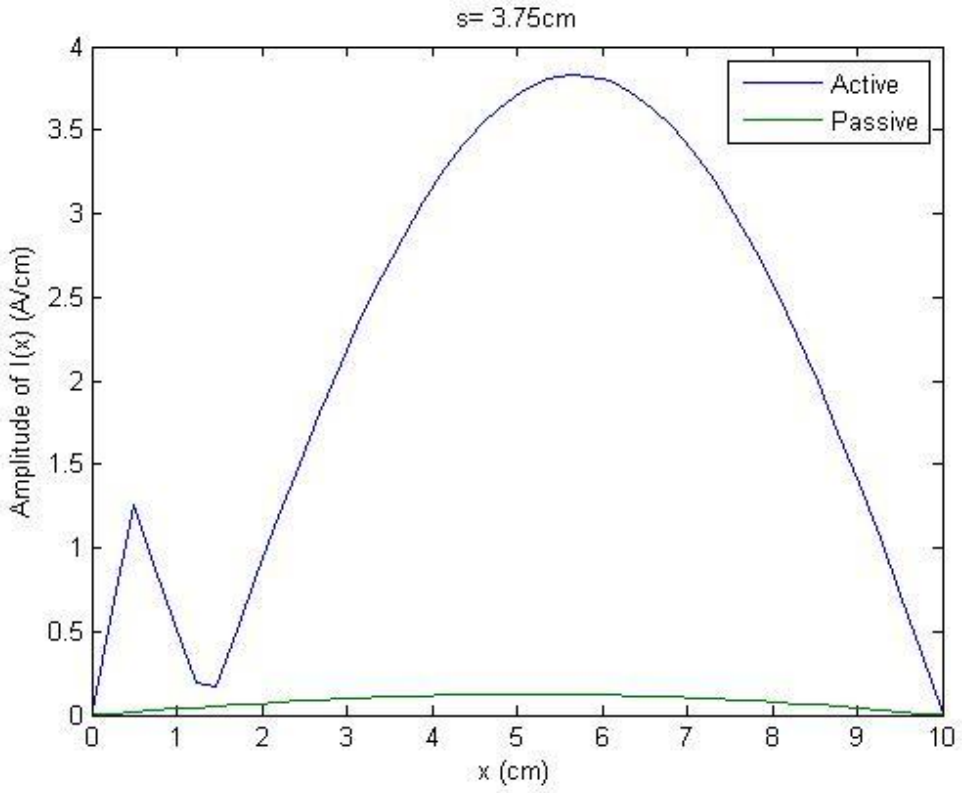

Figure-27 Amplitudes of Current Distributions on Active/Passive Lines with Open Circuit Terminations, Excited on Line-1 from Left beginning, $s = 3.75cm = \lambda/4$

Source is located on the beginning of the left termination of line-1. When two terminals are open circuited, 40 basis functions are used, the distance between lines s is $0.9375cm = \lambda/16$ the amplitudes of the current distributions on line-1 (active line) and line-2 (passive line) are shown in Figure-28. When the currents on the passive line in Figure-27 and Figure-28 are compared, an increase can be observed on the passive line current. Since the distance between the lines is decreased, the coupling effect should be increased which causes an increase on the passive line current. These theoretical expectations are almost observed in the given figures.

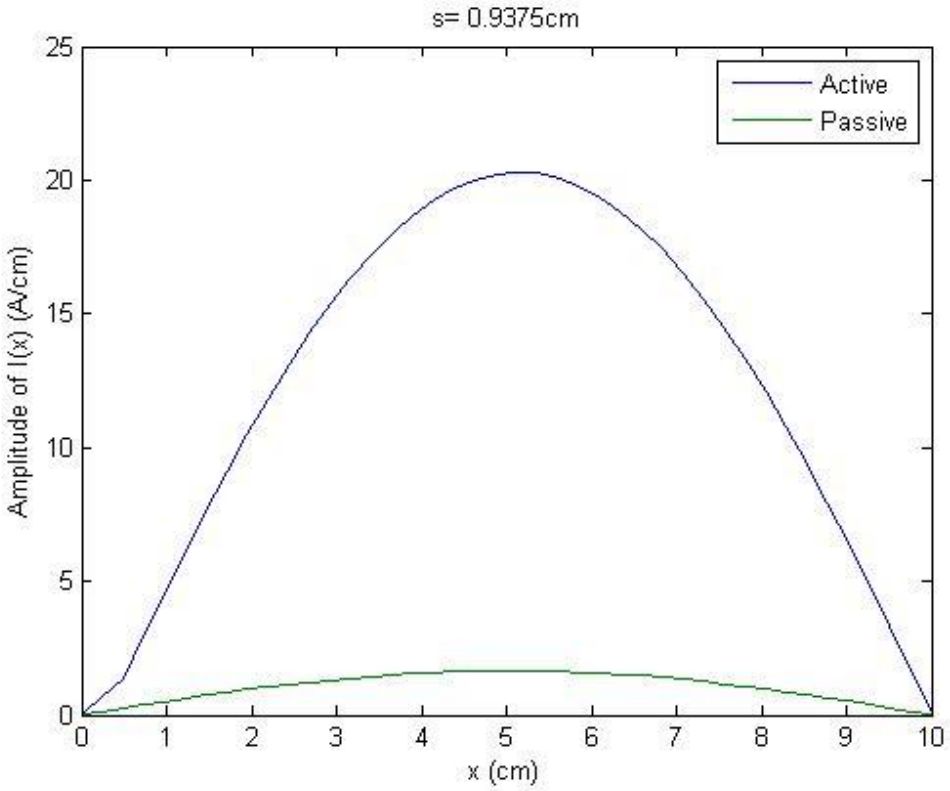

Figure-28 Amplitudes of Current Distributions on Active/Passive Lines with Open Circuit Terminations, Excited on Line-1 from Left beginning, $s = 0.9375cm = \lambda/16$

Source is located on the beginning of the left termination of line-1. When two terminals are open circuited, 40 basis functions are used, the distance between lines s is $0.234375cm = \lambda/64$ the amplitudes of the current distributions on line-1 (active line) and line-2 (passive line) are shown in Figure-29. In this figure, it is clear to observe that the current on passive line is increased compared to the current on passive line for the case of $\lambda/2$. In Figure-29, the best results can be realized. The current on the passive line is maximum for this case, since the distance is chosen as minimum.

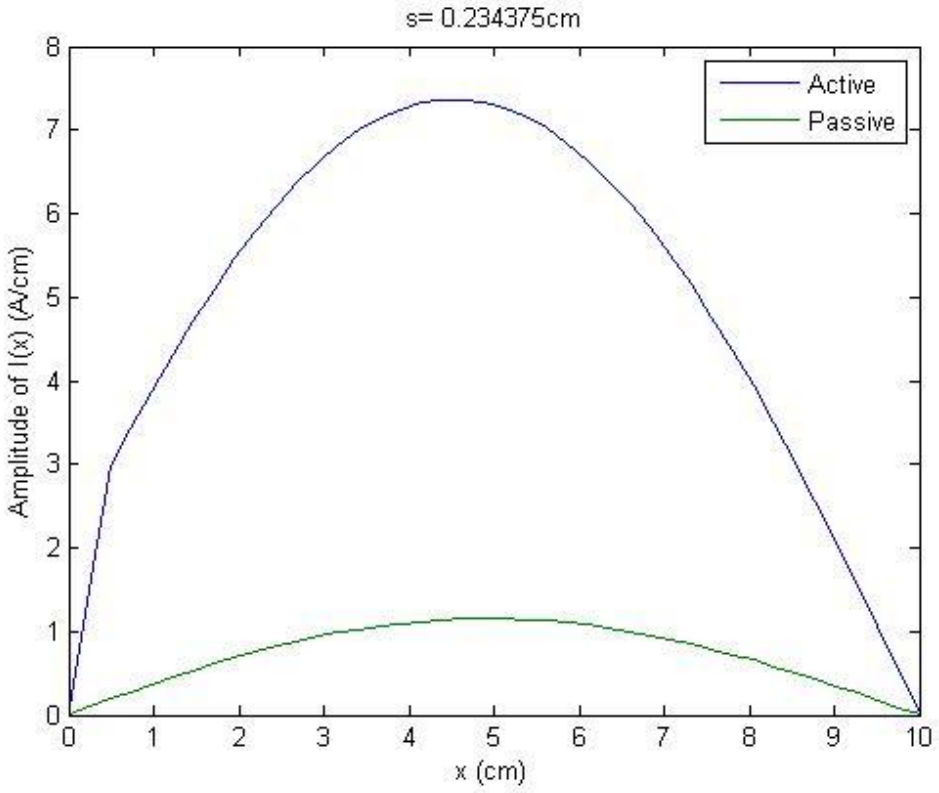

Figure-29 Amplitudes of Current Distributions on Active/Passive Lines with Open Circuit Terminations, Excited on Line-1 from Left beginning, $s = 0.234375cm = \lambda/64$

CHAPTER 6

ANALYSIS OF A PATCH ANTENNA ON PLANARLY LAYERED MEDIA

In this chapter, the current distribution on the patch antenna surface will be obtained by using closed form Green's functions in spatial domain with the application of Galerkin's MoM. First, patch antenna is defined. Afterwards, the formulation for patch antenna will be provided and the information will be given according to the transformation of this formulation into the software program. Then, the results will be analyzed.

6.1 Patch Antenna

First the difference between single line case that is described in Chapter 5 and patch antenna case should be understood. The main difference between single line case and patch antenna case is the direction of current density. In patch antenna case, the metal patch has comparable lengths in both x axis and y axis. Therefore, the y directed current density on the metal patch cannot be ignored in this case. In patch antenna case, in addition to x directed current density, the y directed current density should also be considered in the analysis. On the other hand, in Chapter 5, while analyzing the single line case only the x directed current density was considered in the analysis, since the length in y axis is relatively small compared to the length in x direction.

The patch antenna that will be analyzed in this section is illustrated in Figure-30. In this study a and b values are taken as equal.

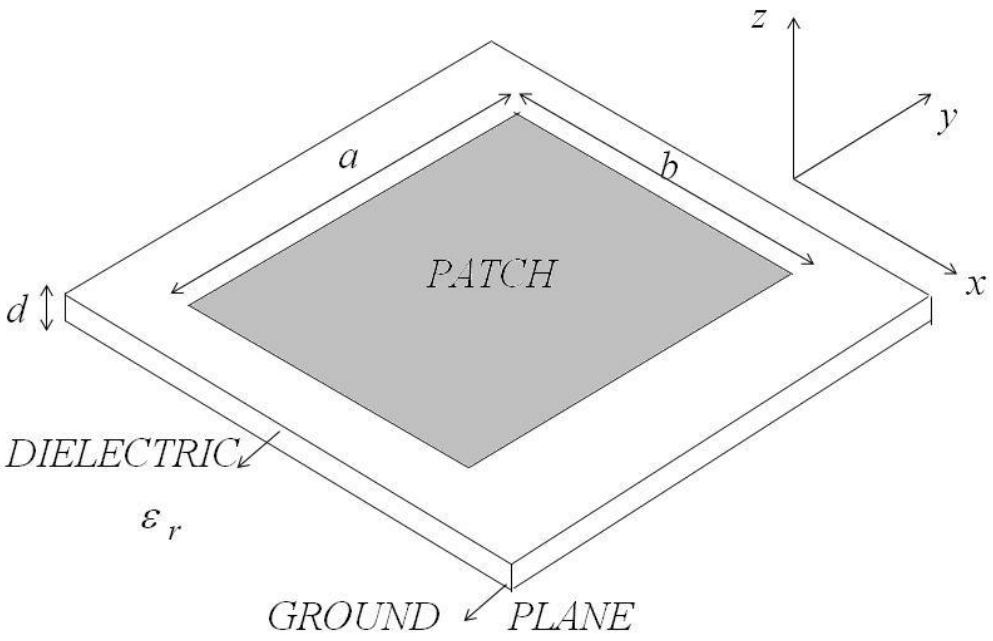

Figure-30 Illustration of Patch Antenna

Surface current density that is defined for patch antenna case is given in equation (90).

$$\bar{J} = J_x \hat{a}_x + J_y \hat{a}_y \tag{90}$$

Source current will be considered later in the analyses. It is not defined here, since the expression will become quite complex. The surface current density in equation (90) can be expanded by using basis functions J_{xn} and J_{yn}. By this way, unknown functions J_x and J_y can be expressed in terms of known functions J_{xn} and J_{yn}. In equations (91) and (92), J_x and J_y functions are expanded in terms of basis functions J_{xn} and J_{yn}, respectively. Here, A_n and B_n are the unknown coefficients of basis functions J_{xn} and J_{yn}, respectively.

$$J_x = \sum_{n=1}^{N} A_n J_{xn}(x,y) \tag{91}$$

$$J_y = \sum_{n=1}^{N} B_n J_{yn}(x,y) \tag{92}$$

Tangential electric fields are defined in both x and y directions for the patch antenna. Tangential electric field expressions for x and y directions are given in equation (93) and (94), respectively.

$$E_x = -j\omega G_{xx}^A * J_x + \frac{1}{j\omega}\frac{\partial}{\partial x}\left[G_q * \nabla.\mathrm{J}\right] \tag{93}$$

$$E_y = -j\omega G_{yy}^A * J_y + \frac{1}{j\omega}\frac{\partial}{\partial y}\left[G_q * \nabla.\mathrm{J}\right] \tag{94}$$

Tangential electric fields should equal to zero on the PEC. Since there are two tangential electric fields one in x and the other in y direction, by using testing functions J_{xm} and J_{ym} the testing expressions in equations (95) and (96) can be constructed.

$$\left\langle J_{xm}(x,y), E_x \right\rangle = 0 \tag{95}$$

$$\left\langle J_{ym}(x,y), E_y \right\rangle = 0 \tag{96}$$

The equations (95) and (96) are constructed by using testing operation. These testing equations can be simplified by processing them further. By considering the source current as well and by diving both sides to $-j\omega$, the final forms in x and y directions are given in equations (97) and (98), respectively.

$$\begin{aligned}&\sum_n A_n\left\{\left\langle J_{xm}, G_{xx}^A * J_{xn}\right\rangle + \frac{1}{\omega^2}\left\langle \frac{\partial}{\partial x}J_{xm}, G_q * \frac{\partial}{\partial x}J_{xn}\right\rangle\right\} + \\ &\sum_n B_n\left\{\frac{1}{\omega^2}\left\langle \frac{\partial}{\partial x}J_{xm}, G_q * \frac{\partial}{\partial y}J_{yn}\right\rangle\right\} = -\left\langle J_{xm}, G_{xx}^A * J_s\right\rangle - \frac{1}{\omega^2}\left\langle \frac{\partial}{\partial x}J_{xm}, G_q * \frac{\partial}{\partial x}J_s\right\rangle\end{aligned} \tag{97}$$

$$\begin{aligned}&\sum_n B_n\left\{\left\langle J_{ym}, G_{yy}^A * J_{yn}\right\rangle + \frac{1}{\omega^2}\left\langle \frac{\partial}{\partial y}J_{ym}, G_q * \frac{\partial}{\partial y}J_{yn}\right\rangle\right\} + \\ &\sum_n A_n\left\{\frac{1}{\omega^2}\left\langle \frac{\partial}{\partial y}J_{ym}, G_q * \frac{\partial}{\partial x}J_{xn}\right\rangle\right\} = -\left\langle J_{ym}, G_{yy}^A * J_s\right\rangle - \frac{1}{\omega^2}\left\langle \frac{\partial}{\partial y}J_{ym}, G_q * \frac{\partial}{\partial x}J_s\right\rangle\end{aligned} \tag{98}$$

As discussed in previous chapters, the selected basis functions are piecewise differentiable. Therefore, by using integration by parts, the order of integrals can be changed [19]. After applying this process to the equations (97) and (98), the equations in (99) and (100) are obtained, respectively.

$$\begin{aligned}&\sum_n A_n\left\{\left\langle G_{xx}^A, J_{xm} * J_{xn}\right\rangle + \frac{1}{\omega^2}\left\langle G_q, \frac{\partial}{\partial x}J_{xm} * \frac{\partial}{\partial x}J_{xn}\right\rangle\right\} + \\ &\sum_n B_n\left\{\frac{1}{\omega^2}\left\langle G_q, \frac{\partial}{\partial x}J_{xm} * \frac{\partial}{\partial y}J_{yn}\right\rangle\right\} = -\left\langle G_{xx}^A, J_{xm} * J_s\right\rangle - \frac{1}{\omega^2}\left\langle G_q, \frac{\partial}{\partial x}J_{xm} * \frac{\partial}{\partial x}J_s\right\rangle\end{aligned} \tag{99}$$

$$\sum_n B_n \left\{ \left\langle G_{yy}^A, J_{ym} * J_{yn} \right\rangle + \frac{1}{\omega^2} \left\langle G_q, \frac{\partial}{\partial y} J_{ym} * \frac{\partial}{\partial y} J_{yn} \right\rangle \right\} +$$
$$\sum_n A_n \left\{ \frac{1}{\omega^2} \left\langle G_q, \frac{\partial}{\partial y} J_{ym} * \frac{\partial}{\partial x} J_{xn} \right\rangle \right\} = -\left\langle G_{yy}^A, J_{ym} * J_s \right\rangle - \frac{1}{\omega^2} \left\langle G_q, \frac{\partial}{\partial y} J_{ym} * \frac{\partial}{\partial x} J_s \right\rangle \quad (100)$$

Now it is possible that the expressions in equations (99) and (100) can be expressed in matrix form. In equation (101), the matrix representation of equations (99) and (100) is provided.

$$\begin{bmatrix} Z_{mn}^{xx} & Z_{mn}^{xy} \\ Z_{mn}^{yx} & Z_{mn}^{yy} \end{bmatrix} \begin{bmatrix} A_n \\ B_n \end{bmatrix} = \begin{bmatrix} V_m^x \\ V_m^y \end{bmatrix} \quad (101)$$

The element values of the matrices in equation (101) are given in explicit form in equations (102), (103), (104), (105), (106) and (107).

$$Z_{mn}^{xx} = \left\langle G_{xx}^A, J_{xm} * J_{xn} \right\rangle + \frac{1}{\omega^2} \left\langle G_q, \frac{\partial}{\partial x} J_{xm} * \frac{\partial}{\partial x} J_{xn} \right\rangle \quad (102)$$

$$Z_{mn}^{xy} = \frac{1}{\omega^2} \left\langle G_q, \frac{\partial}{\partial x} J_{xm} * \frac{\partial}{\partial y} J_{yn} \right\rangle \quad (103)$$

$$Z_{mn}^{yx} = \frac{1}{\omega^2} \left\langle G_q, \frac{\partial}{\partial y} J_{ym} * \frac{\partial}{\partial x} J_{xn} \right\rangle \quad (103)$$

$$Z_{mn}^{yy} = \left\langle G_{yy}^A, J_{ym} * J_{yn} \right\rangle + \frac{1}{\omega^2} \left\langle G_q, \frac{\partial}{\partial y} J_{ym} * \frac{\partial}{\partial y} J_{yn} \right\rangle \quad (104)$$

$$V_m^x = -\left\langle G_{xx}^A, J_{xm} * J_s \right\rangle - \frac{1}{\omega^2} \left\langle G_q, \frac{\partial}{\partial x} J_{xm} * \frac{\partial}{\partial x} J_s \right\rangle \quad (105)$$

$$V_m^y = -\frac{1}{\omega^2} \left\langle G_q, \frac{\partial}{\partial y} J_{ym} * \frac{\partial}{\partial x} J_s \right\rangle \quad (106)$$

6.2 Results

The analysis described up to now are applied to an example patch antenna and results are obtained. These results are presented here. First let examine this example patch antenna geometry. In Figure-31, the example patch antenna geometry is shown together with divisions and source.

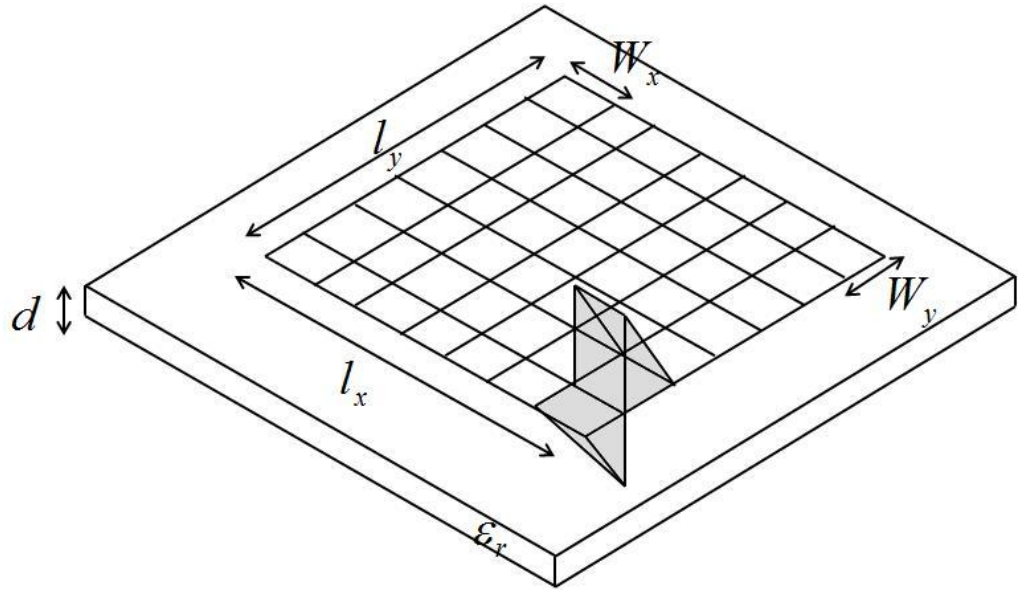

Figure-31 Example Patch Antenna Geometry

The parameter values that are used in the analysis are given below:

$f = 1\,GHz$
$\varepsilon_r = 4.0$
$d = 0.02032\,cm$
$W_x = 0.08128\,cm$
$W_y = 0.08128\,cm$
$l_x = 7.5\,cm$
$l_y = 7.5\,cm$
$m_x = 7$
$n_y = 7$

As the source model, probe is used in this analysis. However, for a realistic source model a microstrip line should be used. Microstrip line feeding will be used in the wideband patch antenna analysis in the next chapter when antenna parameters are required to be calculated. The main aim of this chapter is to obtain the general behavior of a patch antenna, so the simplest source model is used. More realistic feeding models will be used in the next chapter when antenna parameter analyses are required. In Figure-31, source location is shown arbitrarily. While analyzing the results, the location of the source is changed and the effect of the source location is observed.

In Figure-32, 2D representation of the amplitude of current distribution on the metal patch for x axis when $x_0 = 1$ cm and $y_0 = 1$ cm is shown. It is expected to obtain sinusoidal current on the edge throughout the current flowing direction. In this case, current flowing direction is through x axis. From Figure-32, currents on the edges through the current flowing direction show sinusoidal behavior as expected. Moreover, it is expected to obtain maximum current amplitudes on the edges through the direction that is perpendicular to the current flowing direction. Again, from figure it is clear that on the edges the current amplitudes are increased through the direction perpendicular to the current flowing direction. Therefore, results are roughly agreed with the expected ones.

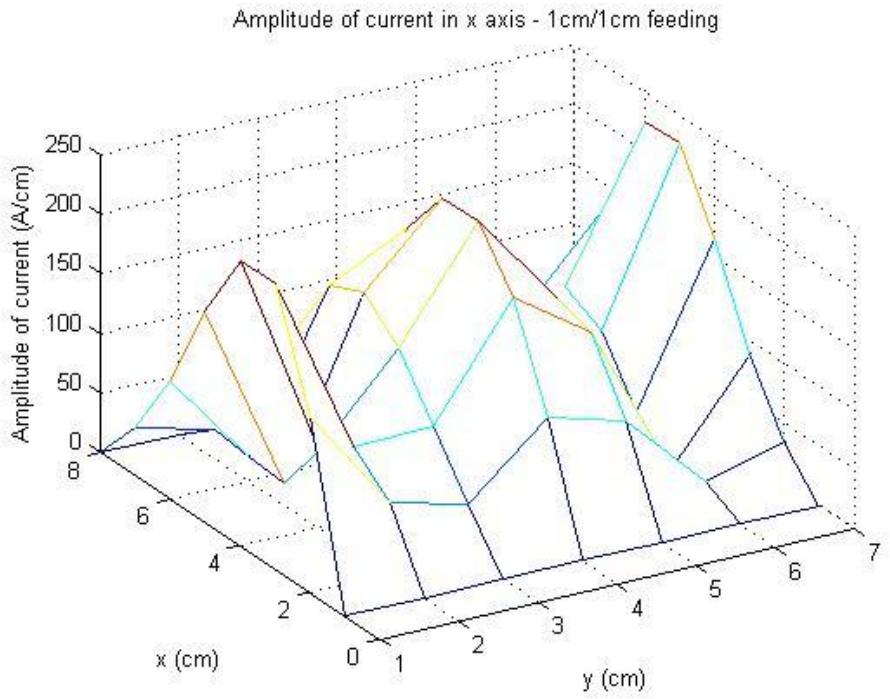

Figure-32 2D Representation of the amplitude of current distribution on the metal patch for x axis when $x_0 = 1$ cm and $y_0 = 1$ cm

In Figure-33, 2D representation of the amplitude of current distribution on the metal patch for y axis when $x_0 = 1$ cm and $y_0 = 1$ cm is shown. In this case, current flowing direction is through y axis. Therefore, currents on the edges through y direction are sinusoidal and maximum through z direction, as expected.

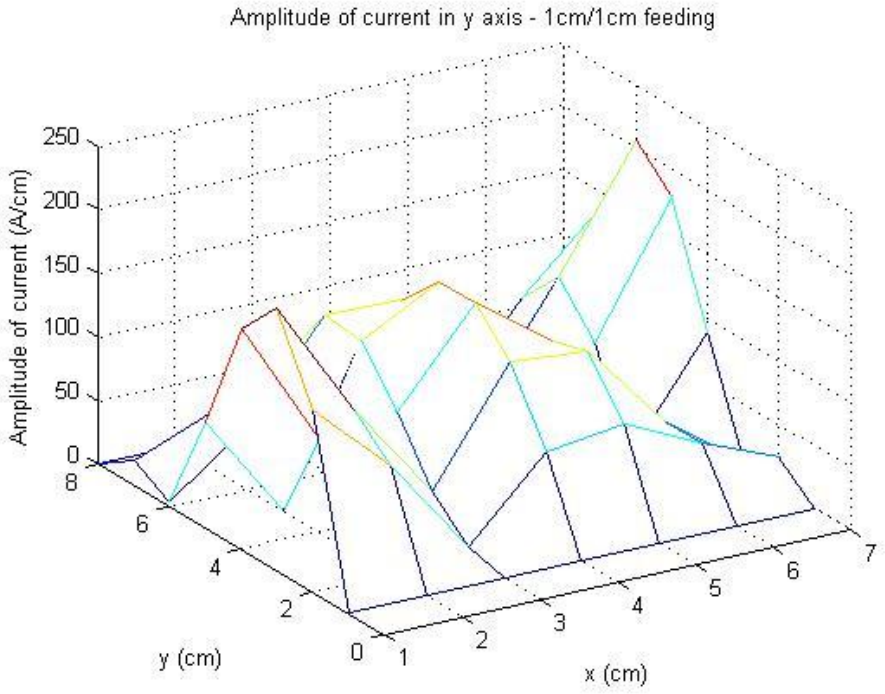

Figure-33 2D Representation of the amplitude of current distribution on the metal patch for y axis when $x_0 = 1$ cm and $y_0 = 1$ cm

In Figure-34, 2D representation of the amplitude of current distribution on the metal patch for x axis when $x_0 = 1$ cm and $y_0 = 4$ cm is shown. Again the behavior is compatible with the expected figure.

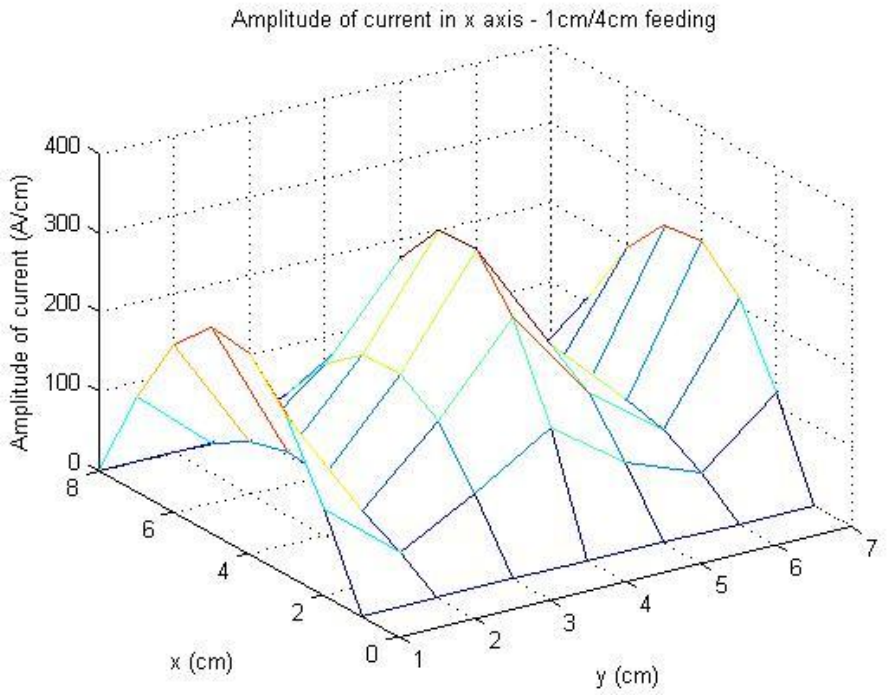

Figure-34 2D Representation of the amplitude of current distribution on the metal patch for x axis when $x_0 = 1$ cm and $y_0 = 4$ cm

In Figure-35, 2D representation of the amplitude of current distribution on the metal patch for y axis when $x_0 = 1$ cm and $y_0 = 4$ cm is shown. Here the feeding location is changed, so current distributions for x and y directions should be different. It is expected to obtain very low current levels through the y direction. Even though in Figure-35, the current amplitude levels are not small compared to the levels observed in the x direction especially in the edges, this result is due to the edge discontinuities. In the middle parts of the patch, the current levels are quite low as expected.

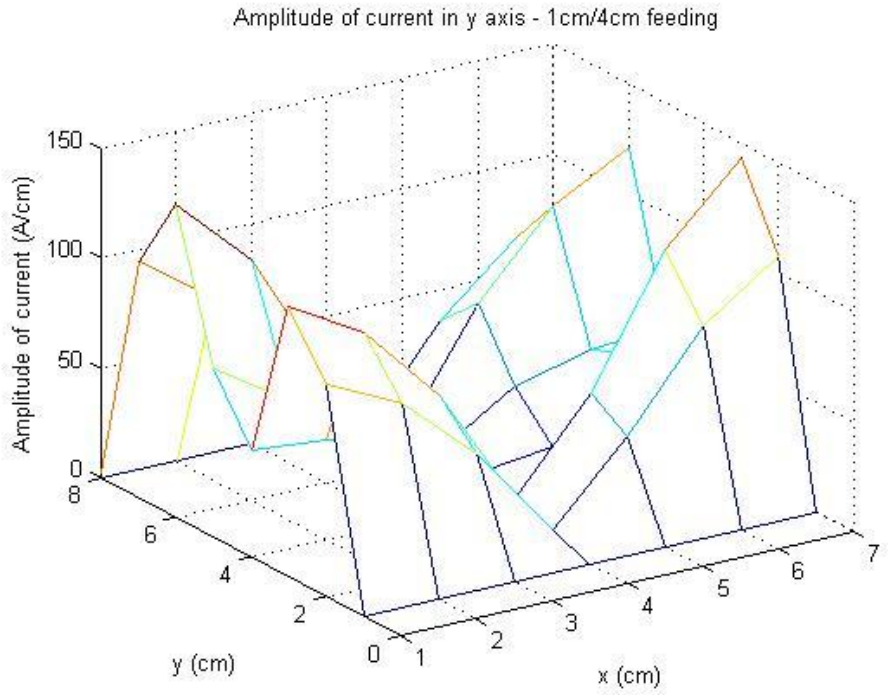

Figure-35 2D Representation of the amplitude of current distribution on the metal patch for y axis when $x_0 = 1$ cm and $y_0 = 4$ cm

In Figure-36, 2D representation of the amplitude of current distribution on the metal patch for x axis when $x_0 = 1$ cm and $y_0 = 7$ cm is shown. The current behavior is approximately appropriate. However, discontinuities may increase the current levels a little.

In Figure-37, 2D representation of the amplitude of current distribution on the metal patch for y axis when $x_0 = 1$ cm and $y_0 = 7$ cm is shown.

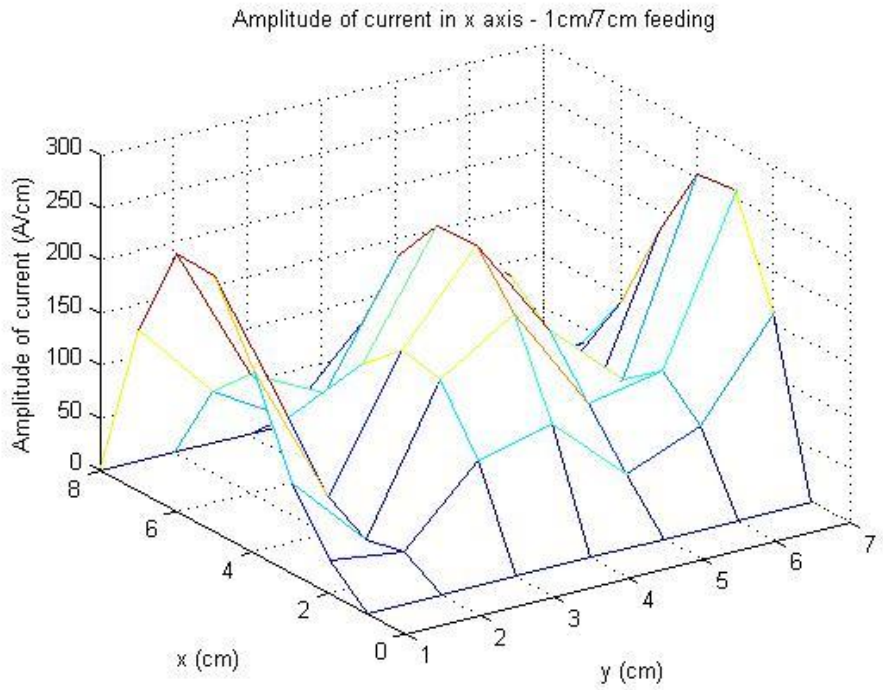

Figure-36 2D Representation of the amplitude of current distribution on the metal patch for x axis when $x_0 = 1$ cm and $y_0 = 7$ cm

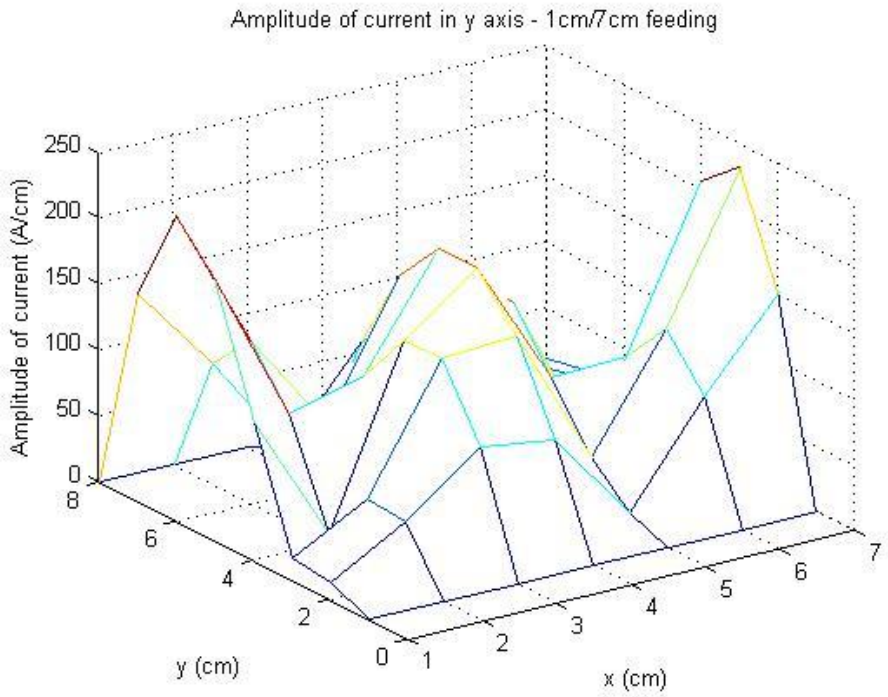

Figure-37 2D Representation of the amplitude of current distribution on the metal patch for y axis when $x_0 = 1$ cm and $y_0 = 7$ cm

6.3 Computationally Efficient Technique Used for More General Geometries

The solution procedure for a standard patch antenna was described in previous sections. However, for considering more realistic patch antenna geometry, the existing standard one should be modified. Some parts of the patch can be removed or the feeding can be more realistic such as microstrip line. Indeed, such applications are very important for this thesis study. The aim of the study is to construct a wideband patch antenna by removing slots inside a standard patch metal. As an example, by opening slots at two sides of the metal patch it is expected to obtain expansion in the impedance bandwidth. This study will be explained in the next chapter. Moreover, in order to obtain a realistic feeding, the patch antenna source will be a microstrip line in the study. All such applications require a modification on the standard patch antenna.

It is very time consuming to solve the software program for each time when a modification on the geometry is occurred. Therefore, it is not computationally efficient. The matrix entries should be redesigned for all new geometries. This means that convolution integrals should be resolved analytically that is a very exhaustive procedure. In this thesis study, a new method is used for such geometry modifications. It is computationally efficient in general. According

to this method, standard patch antenna is solved only once and then appropriate matrix row and column entries will be deleted for the related geometry modifications. By this way, the required matrix for all geometries can be obtained [39]. If a specific part is removed from the patch antenna geometry, then the matrix entries with suitable basis functions and all their relations to other basis functions are deleted from the matrix completely.

This method can be visualized with a numerical example. Let assume, the second basis function in x axis and the third basis function in y axis should be removed from the matrix according the particular geometry modification. Therefore, all interactions that include these basis functions should be deleted from the matrix. In Figure-38, this matrix row/column deleting process is illustrated.

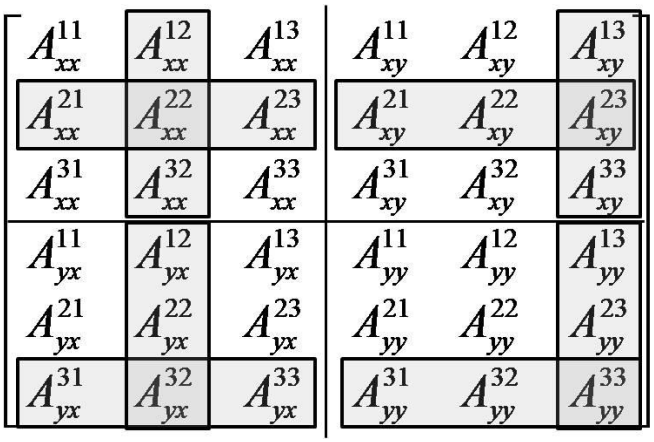

Figure-38 Example of Matrix Row/Column Deleting Process

As shown in Figure-38, all the interactions which include second basis function in x axis and third basis function in y axis are deleted.

Each geometry modification requires different entry deleting. After new geometry is obtained, the corresponding basis functions in x and y directions should be determined according to the cropped parts of patch metal. Then, deleting is performed accordingly. If this deleting procedure is not implemented, then the software code should be reconstructed for all geometries. Especially, if many geometry modifications are necessary, this method will be very useful. The benefit of this method will be understood better while analyzing the wideband patch antennas.

CHAPTER 7

FIELD ANALYSIS AND CURRENT DISTRIBUTION FOR PLANAR LAYERED MEDIA – WIDEBAND PATCH ANTENNA ANALYSIS

Patch antennas are compatible with microwave integrated circuits (MICs). This makes patch antennas very important because integrated systems can satisfy the recent technology needs with their specific features such as small size and low cost production. However, narrow impedance bandwidth is the main problem of patch antennas, especially in wireless communication applications which need wide bandwidth. The geometry and substrate parameters (relative permittivity and thickness) of the patch antenna are two factors affecting the resonance frequency and impedance bandwidth directly. Since our aim in this study is to increase the impedance bandwidth, there are two options. Either the geometry of the conventional patch antenna should be modified or relative permittivity/thickness should be changed. If the second choice is applied, for example thickness is increased and relative permittivity is decreased, the impedance bandwidth could be increased but some problems will arise. These problems can be considered as the creation of surface waves and spurious radiation, so such a design cannot be efficient. Therefore, first choice which is the modification of the existing geometry should be applied in order to increase the impedance bandwidth.

For different patch antenna geometries, different results will be obtained. For example, C-shaped patch antenna, U-slotted patch antenna, D-shaped patch antenna, L-shaped patch antenna and E-shaped patch antenna will give different results. In these different patch geometries, slots are different on the metal patch. In C-shaped patch antenna the size of the antenna can be decreased on the other hand bandwidth cannot be increased. In E-shaped patch antenna impedance bandwidth can be increased yet the size of the antenna cannot be decreased [43].

Reason behind the increase in impedance bandwidth by opening slots on the patch can be understood if the currents on the metal patch surface are analyzed. In this thesis study, patch geometry which is similar to E-shaped patch antenna is used. For such a structure, bandwidth is increased due to the creation of dual resonance. Slots are opened as being parallel to non-radiating edges. Therefore, the currents on the patch can flow throughout two different paths which create two different resonance frequencies [43]. Impedance bandwidth is generally analyzed by observing the return loss (S_{11} parameter).

In previous chapter, the current distribution on the patch antenna is obtained by using closed form Green's function in spatial domain with the application of Galerkin's MoM. Here, current distribution on the patch is obtained in the same manner. Then matrix element deleting technique will be used which is described in the previous chapter. By this way, the corresponding results could be obtained when slots are opened on the metal patch.

First patch antenna with a microstrip transmission line is explained. Then, opening slots on the patch is described. Afterwards an example patch antenna structure is presented and slots are opened on this patch antenna. The solution procedure is explained in detail here. First surface current density will be obtained for the standard patch antenna. This solution is used to obtain the currents in the case of microstrip transmission line feeding. By using this solution, current distribution for the case of parallel slots are acquired. After obtaining current distributions for microstrip fed patch antenna with and without slots, S_{11} parameter values are calculated by using resulted current distributions at different frequencies. Then, the return loss graphs are plotted separately. Obtained return loss graphs are compared with the ones that are obtained from MoM based EM simulation software IE3D by Zealand. From these graphs, the impedance bandwidths of the antennas are calculated and then they are compared. At the end of this chapter, it is expected to observe an increase in the bandwidth after modifying the patch geometry. The main aim of this chapter is to observe this bandwidth increase by opening slots on the patch.

7.1 Microstrip Transmission Line Feeding for Patch Antenna

In previous chapter, patch antenna is fed by a dipole source directly. In this chapter, microstrip line feeding as a source model is used. First, let examine Figure-39 which shows patch antenna fed by a microstrip transmission line.

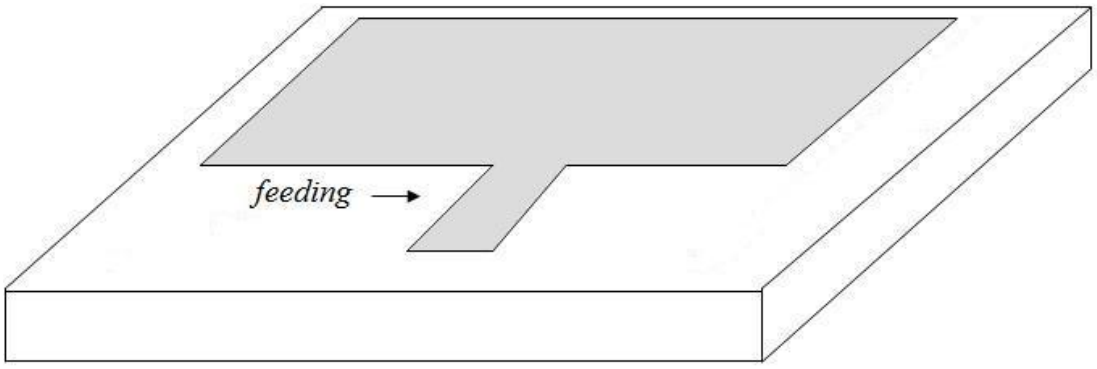

Figure-39 Patch Antenna Fed by a Microstrip Transmission Line

In order to obtain such an antenna design, the standard patch antenna geometry that is analyzed in previous should be modified. An efficient matrix deleting method that is used for

irregular and modified patch antenna geometries is defined in previous chapter. This method will be used in this chapter. Besides, the resulted matrices after solving standard patch antenna geometry in previous chapter are saved in MATLAB®. It is not necessary to solve the modified patch antenna that is shown in Figure-39. Simply the corresponding row and column entries in the existing matrices will be deleted.

First basis functions that correspond to the subtracted parts of the antenna are identified. Convolution integral relations between these basis functions and other basis functions are determined. Then, rows/columns which contain these basis functions are completely deleted from matrices. The resulted matrices have to be exactly the same as the ones that would be obtained by solving the software for the new geometry. In order to ensure this method, it is tested for coupled line geometry. First patch antenna is solved and matrices are saved. Then, geometry is modified to obtain a coupled line and corresponding rows and columns are deleted. It is observed that the resulted matrices are exactly same as the matrices for coupled line case. Therefore, this method is proven to give the exact results if the procedure would be applied correctly.

7.2 Example Wideband Patch Antenna Structure

In Figure-40, standard patch antenna geometry is illustrated with dimensions. Since matrix deleting procedure is used, first standard patch antenna should be solved and the results should be saved. Then, for each geometry modification, these matrices could be used.

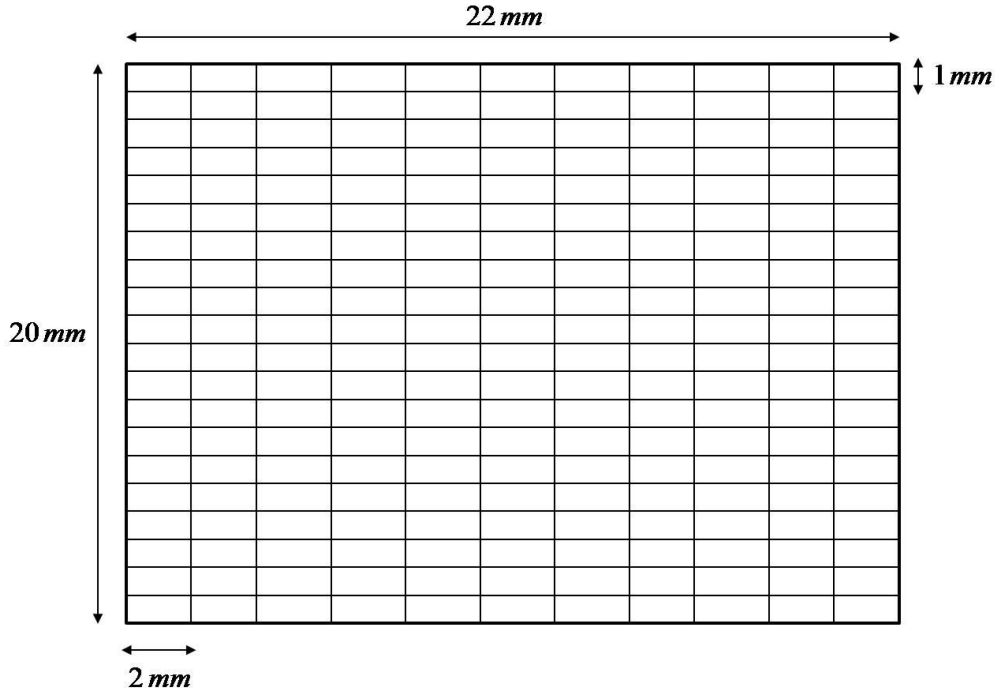

Figure-40 Standard Patch Antenna Geometry

In this patch design, the length in x direction is $22mm$ and the length in y direction is $20mm$. Patch is divided into 11 pieces in x direction and 20 pieces in y direction. Therefore, $m_x = 11$ and $n_y = 20$. In x direction, the length of the patch is $22mm$ and in x direction patch is divided into 11 parts, so $Wx = {22mm}/{11}$. In y direction, the length of the patch is $20mm$ and in y direction patch is divided into 20 parts, so $W_y = {20mm}/{20}$. The input parameters that are defined for this patch antenna are presented below:

$\varepsilon_r = 2.2$ (Relative Permittivity of the Substrate)
$d = 0.65\ mm$ (Substrate Height)
$W_x = 2\ mm$ (Length of One Division in x Direction)
$W_y = 1\ mm$ (Length of One Division in y Direction)
$l_x = 22\ mm$ (Length of Patch in x Direction)
$l_y = 20\ mm$ (Length of Patch in y Direction)
$m_x = 11$ (Number of Divisions in x Direction)
$n_y = 20$ (Number of Divisions in y Direction)

This standard patch antenna geometry is solved by these given input parameters and given dimensions for finding the current distribution on the patch. The resulted matrices are saved to MATLAB®. Therefore, for any modification on this standard patch geometry, these matrices can be used. As an example, some of these current distribution results are presented here.

In Figure-41, 2D current amplitude representation on the metal patch for x axis is presented. Here, feeding point is at $x_0 = 1$ and $y_0 = 1$. The current distribution behavior is as expected. Because of the discontinuity, large current levels are observed at the termination points through the direction perpendicular to the current flowing direction. Current distribution behavior through the current flowing direction is sinusoidal.

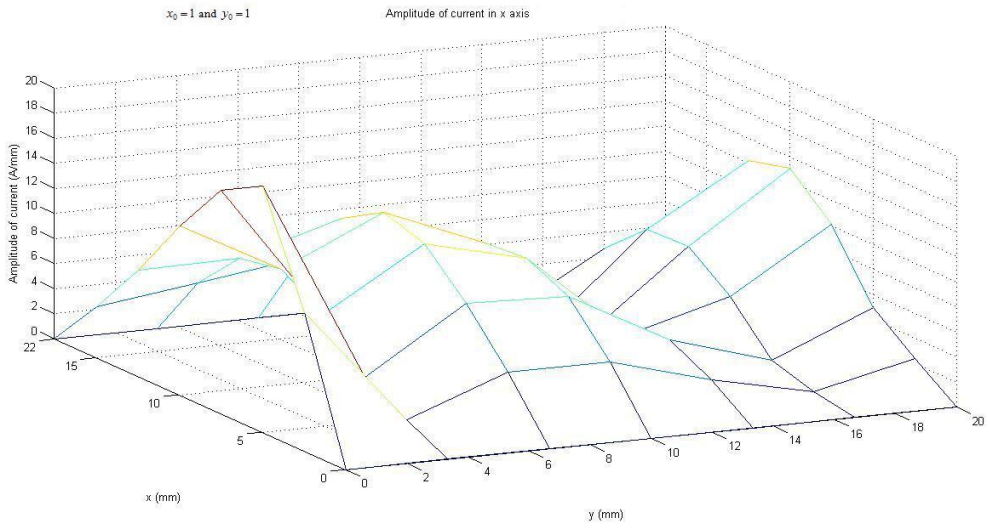

Figure- 41 2D Representation of the amplitude of the current distribution on the metal patch for x axis when $x_0 = 1$ and $y_0 = 1$

In Figure-42, 2D current amplitude representation on the metal patch for y axis is presented. Here, feeding point is at $x_0 = 1$ and $y_0 = 1$. It is expected to obtain same current behavior in y axis as well when such a feeding location is used. It can be observed that similar behaviors are obtained in x and y axes.

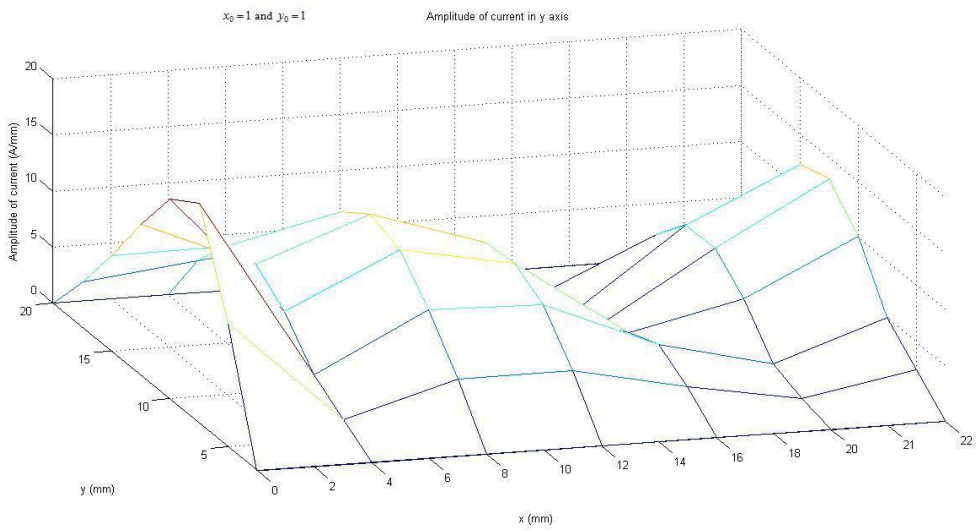

Figure- 42 2D Representation of the amplitude of the current distribution on the metal patch for y axis when $x_0 = 1$ and $y_0 = 1$

In Figure-43, 2D current amplitude representation on the metal patch for x axis is presented. Here, feeding point is at $x_0 = 1$ and $y_0 = 10$. In x direction, the behavior of the current amplitude is compatible with desired behavior.

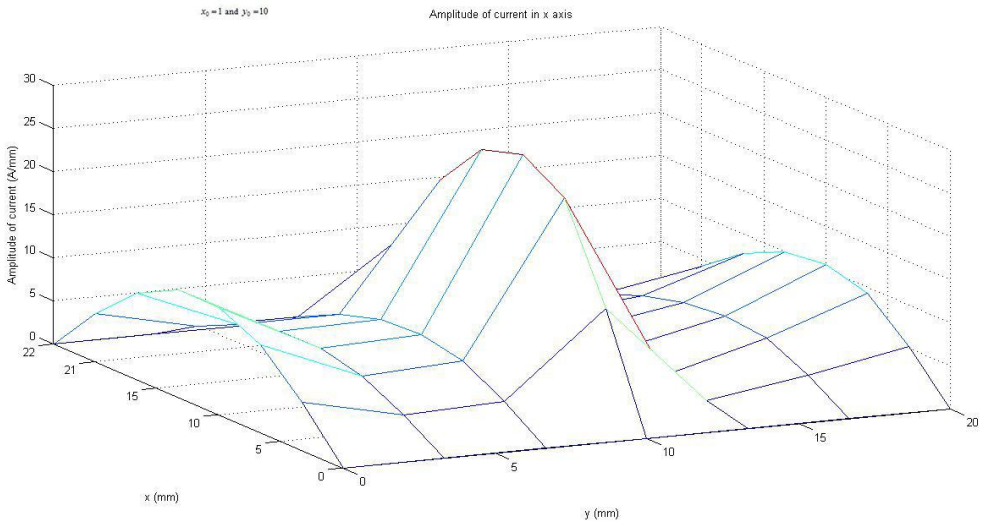

Figure- 43 2D Representation of the amplitude of the current distribution on the metal patch for x axis when $x_0 = 1$ and $y_0 = 10$

In Figure-44, 2D current amplitude representation on the metal patch for y axis is presented. Here, feeding point is at $x_0 = 1$ and $y_0 = 10$. It is expected to acquire very low current amplitude values in the y direction when such a feeding location is used. As expected, the current distribution in Figure-44 has very low current levels when compared to the one given in Figure-43.

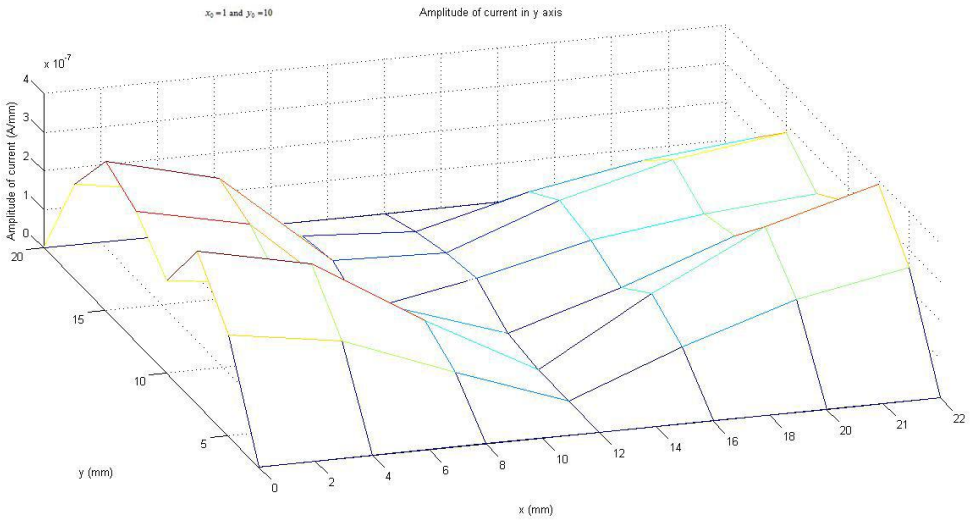

Figure- 44 2D Representation of the amplitude of the current distribution on the metal patch for y axis when $x_0 = 1$ and $y_0 = 10$

Now the patch antenna in Figure-40 is modified such that it is fed by a microstrip transmission line. Figure-45 shows the patch antenna which is fed by microstrip transmission line. This antenna is the modified version of the antenna in Figure-40. In Figure-45, the symmetric gaps are shown on the patch. The reason why small gaps are opened near the microstrip feeding is to obtain more realistic results. This antenna design is found by trying the best configuration that ensures the bandwidth increase. The design is conducted in a MoM based EM simulation software IE3D by Zealand.

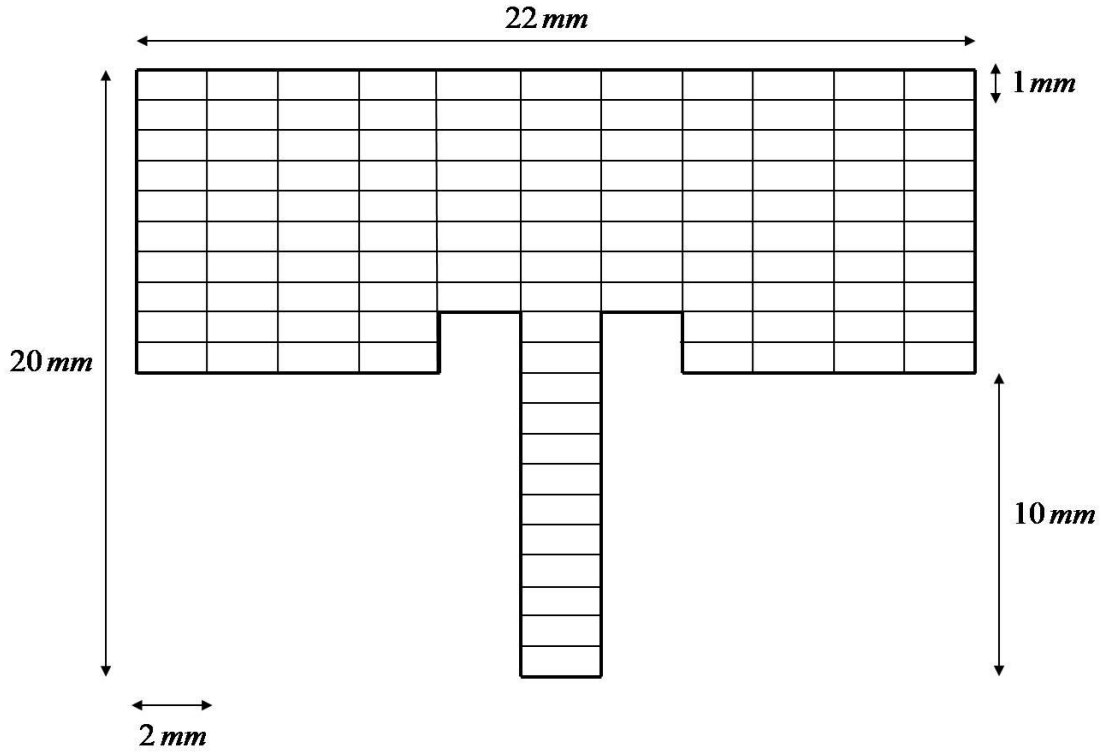

Figure-45 Patch Antenna Geometry with Microstrip Transmission Line Feeding and Two Small Gaps

In order to find the current distribution on the patch in Figure-45, the matrices that are found for the patch antenna in Figure-40 are used. The basis functions that are corresponding to the subtracted parts of the patch are determined. The rows and columns which include these basis functions are deleted completely. After this deleting procedure, the final matrices are solved as a matrix equation. Result is the current density on the patch antenna in Figure-45.

- Calculations for Obtaining Impedance Bandwidth:

First, MATLAB® program is solved for $9.1GHz$ frequency value. The parameter calculations that are described in this part are defined for this frequency value. However, same calculations should be performed to all frequencies which are in the determined frequency band. This frequency band is determined according to the MoM based EM simulation software IE3D by Zealand results and it is $8.9GHz-9.6GHz$. The designed patch antenna geometry is first solved in a MoM based EM simulation software IE3D by Zealand, then resonance frequency is determined. By considering this resonance frequency as a center frequency, a frequency band is chosen. It is important to note that MATLAB® program should be solved for each frequency in this frequency band, separately.

The current distribution on the patch for the antenna that is shown in Figure-45 is obtained for $9.1GHz$. Now, only the current on the microstrip transmission line part is used as an input to the Prony's method. The current distribution on the microstrip transmission line can be considered as a summation of currents for forward and backward propagating waves. This summation is shown in equation (107).

$$I(x) = I^{-}(x) + I^{+}(x) = c_1 e^{\beta_1 x} + c_2 e^{\beta_2 x} \tag{107}$$

c_1 is the incident wave coefficient and c_2 is the reflected wave coefficient. After applying Prony's method, two outputs are obtained as c_1 and c_2. In this thesis study, the values in equations (108) and (109) are obtained as output values for the frequency value of $9.1GHz$.

$$c_1 = -0.0016 - 0.0018i \tag{108}$$

$$c_2 = 0.0011 + 0.0004i \tag{109}$$

Reflection coefficient Γ is defined as shown in equation (110).

$$\Gamma = \frac{c_1}{c_2} \tag{110}$$

Therefore, reflection coefficient value for $9.1GHz$ can be calculated by using the formula in equation (110) and the values in equations (108) and (109). Input reflection coefficient (S_{11} parameter) value is shown in equation (111) for this thesis study at $9.1GHz$.

$$\begin{aligned} &\Gamma = S_{11} = \text{Input Reflection Coefficient} = \\ &(0.0011 + 0.0004i)/(-0.0016 - 0.0018i) = -0.4276 + 0.2310i \end{aligned} \tag{111}$$

Now, return loss value for $9.1GHz$ should be calculated. Return loss is a logarithmic ratio and the unit is dB. The formula for return loss is given in equation (112).

$$\text{Return Loss}\,(dB) = 20\log_{10}|\Gamma| \tag{112}$$

By using the formula in equation (112) and the reflection coefficient value in equation (111), return loss is calculated as shown in equation (113).

$$\begin{aligned} &\text{Return Loss}\,(dB) = 20\log_{10}|-0.4276 + 0.2310i| = \\ &20\log_{10}(0.2518) = -11.9788 \end{aligned} \tag{113}$$

Same calculations should be performed for each frequency value in the defined frequency band. All return loss values corresponding to these frequencies should be calculated. After these calculations, return loss graph can be plotted for the antenna in Figure-45. In Figure-46, return loss graph for the antenna in Figure-45 is shown.

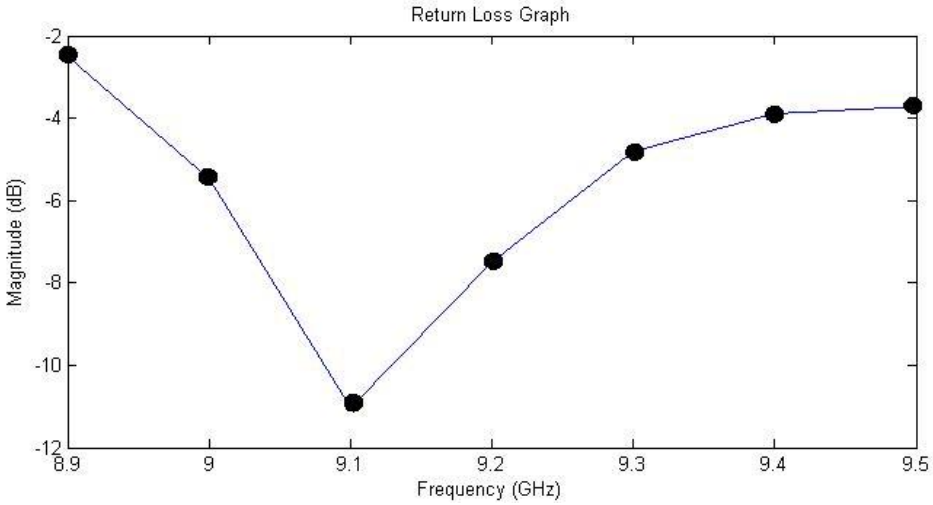

Figure-46 Return Loss Graph for Microstrip Patch Antenna that is Obtained from the MATLAB® Program

This graph is obtained by calculating return loss values for all frequencies in a defined frequency range. Return loss values corresponding to the frequencies in the defined frequency range are marked as black circles in Figure-46. In this graph, the resonance frequency can be determined approximately as $9.1GHz$. The determined frequency band is from $8.9GHz$ to $9.5GHz$. The frequencies in this range for which the return loss values are calculated can be shown from black circle markers. The analysis in this thesis study should be compared by the obtained results of MoM based EM simulation software IE3D by Zealand. Therefore, the return loss graph in Figure-46 is compared with the return loss graph that is obtained from MoM based EM simulation software IE3D by Zealand and this comparison is shown in Figure-47.

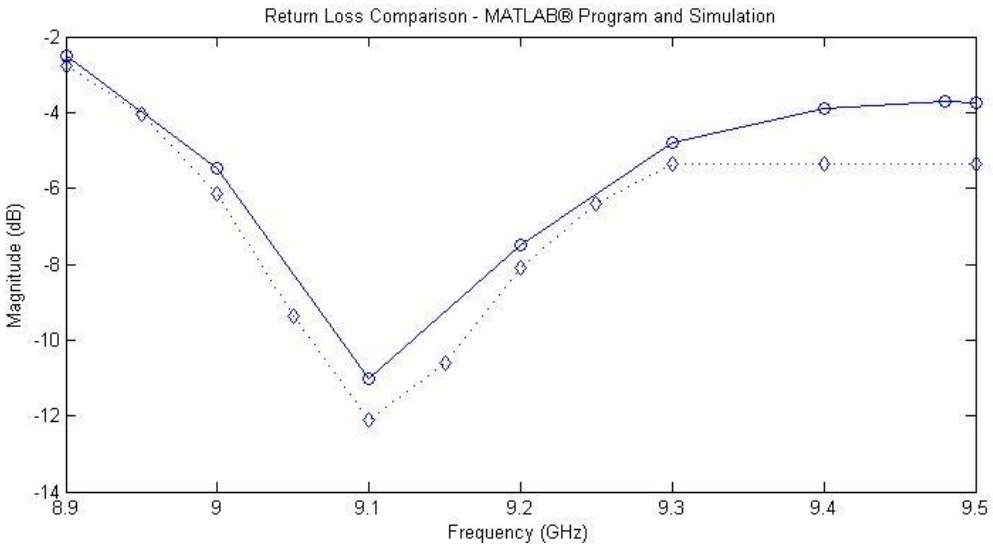

Figure-47 Comparison of Return Loss Graphs for Microstrip Patch Antenna that are Obtained from the MATLAB® Program and the MoM based EM simulation software IE3D by Zealand

By investigating the comparison in Figure-47, it can be concluded that the results are compatible with each other.

Now, by using the return loss graph in Figure-46, impedance bandwidth should be calculated. Impedance bandwidth shows a frequency range in which the antenna can work properly. This frequency range can be considered as the range of frequency which have a smaller losses than a specified loss value. The formula for impedance bandwidth is given in equation (114). Here, f_H is the highest frequency, f_L is the lowest frequency and f_C is the center frequency which corresponds to resonance frequency.

$$\text{Impedance Bandwidth} = BW = \frac{f_H - f_L}{f_C} \tag{114}$$

In this thesis analysis, $-10dB$ loss is chosen as a threshold loss value. The frequencies that have smaller loss values than $-10dB$ loss are specified. The range of these frequencies should be specified from the lowest f_L to the highest f_H. In Figure-48, f_L, f_C and f_H values are shown for $-10dB$ bandwidth.

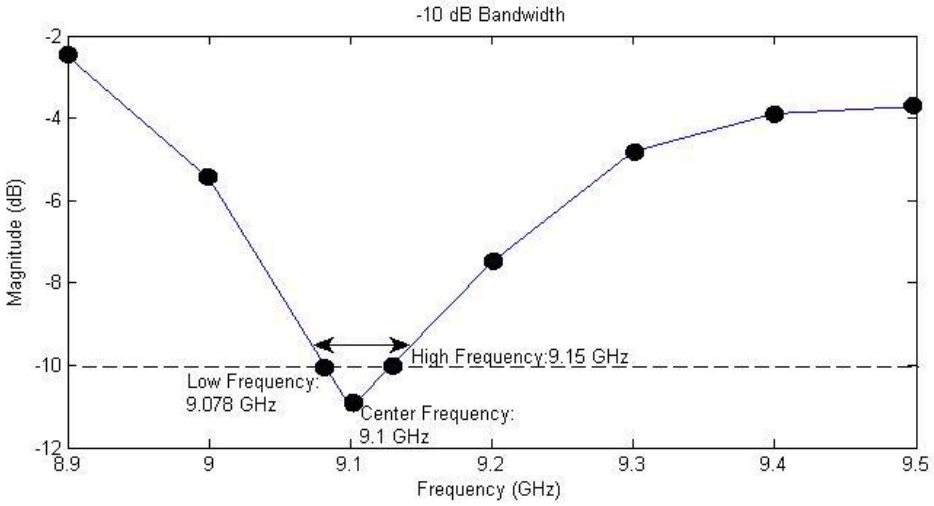

Figure-48 Return Loss Graph for Microstrip Patch Antenna that is Obtained from the MATLAB® Program with $-10dB$ Bandwidth Values

By using the Formula in equation (114), $-10dB$ bandwidth can be calculated as shown in equation (115).

$$-10dB\ \text{bandwidth} = \frac{9.15GHz - 9.078GHz}{9.1GHz} = 0.0079$$
$$= 0.0079 * 100 = \%0.79 \tag{115}$$

Up to now, the analysis for the microstrip fed patch antenna in Figure-45 is performed and the corresponding impedance bandwidth is calculated. Now, the geometry of this antenna is modified by opening parallel slots at non-radiating edges. It is aimed to design a wideband antenna by changing the geometry of the antenna in this way. This new path antenna geometry is shown in Figure-49.

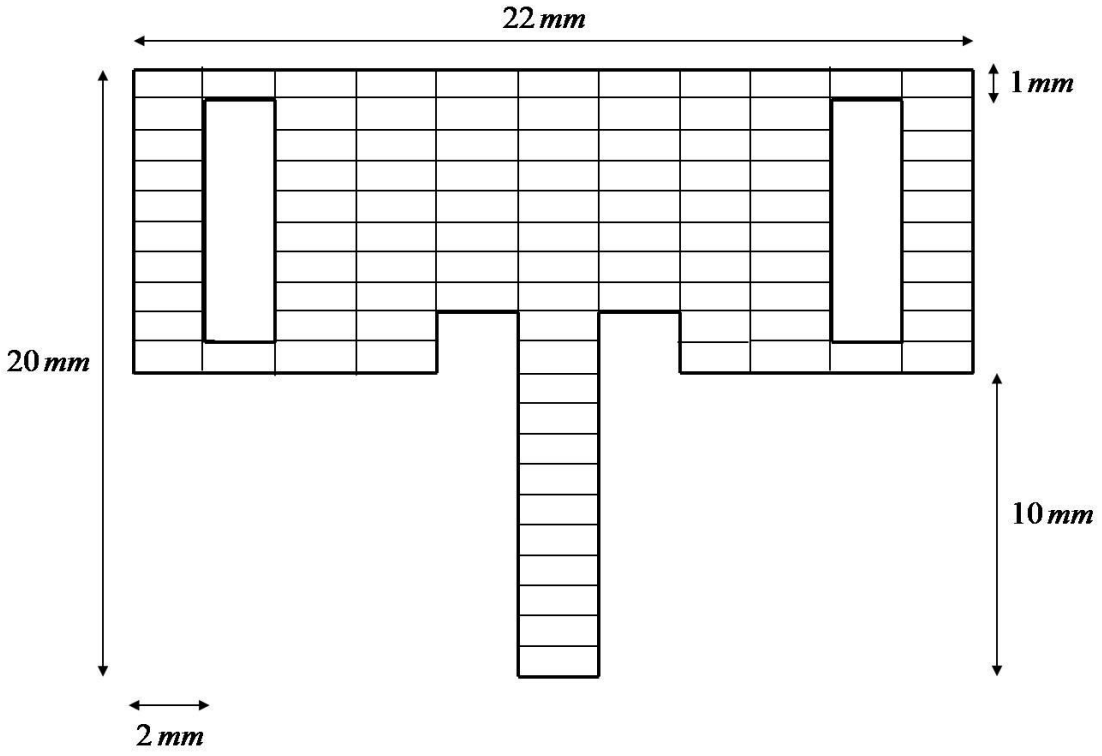

Figure-49 Wideband Patch Antenna Geometry

Since the wideband antenna geometry in Figure-49 is obtained by modifying the antenna in Figure-45, the existing matrices can be used as well. Here, slots have $2mm$ length in x direction and $8mm$ in y direction. The basis functions that correspond to the opened slots are determined. Rows and columns which include these basis functions are deleted. Then, the remaining matrices are solved. At the end, current distribution on the patch antenna in Figure-49 is found.

Again the calculations are given for $9.1GHz$ frequency level. However, same calculations should be performed for all frequencies in a specified frequency range. Afterwards, return loss values can be plotted against frequency. Calculations are similar to the ones that are defined for the antenna in Figure-45. The current distribution on the microstrip transmission line are loaded as input to the Prony's method. The outputs of the Prony's method are divided each other in order to obtain the reflection coefficient (S_{11} parameter). By using this s_{11} parameter, corresponding return loss value for $9.1GHz$ can be found and this return loss calculation is shown in equation (116).

$$\text{Return Loss} = 20\log_{10}|\Gamma| = 20\log_{10}(0.7913) = -2.0332 \qquad (116)$$

If all corresponding return loss values are calculated for the determined frequency band, return loss graph can be plotted for the wideband antenna in Figure-49. In Figure-50, return loss graph for the wideband antenna in Figure-49 is plotted.

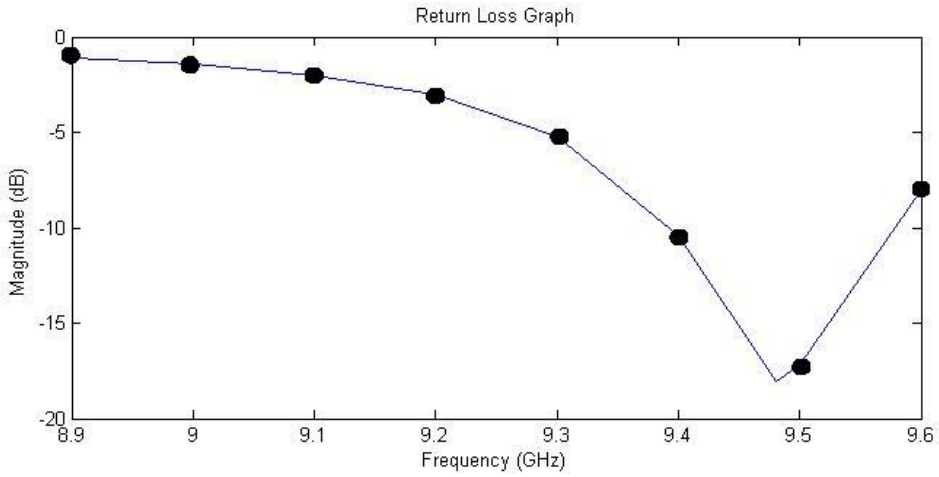

Figure-50 Return Loss Graph for Wideband Patch Antenna that is Obtained from the MATLAB® Program

Again the found return loss graph should be compared with the return loss graph that is obtained from MoM based EM simulation software IE3D by Zealand. The return loss graph in Figure-50 is compared with the return loss graph that is obtained from MoM based EM simulation software IE3D by Zealand and this comparison is shown in Figure-51. It can be said that the results are compatible with each other.

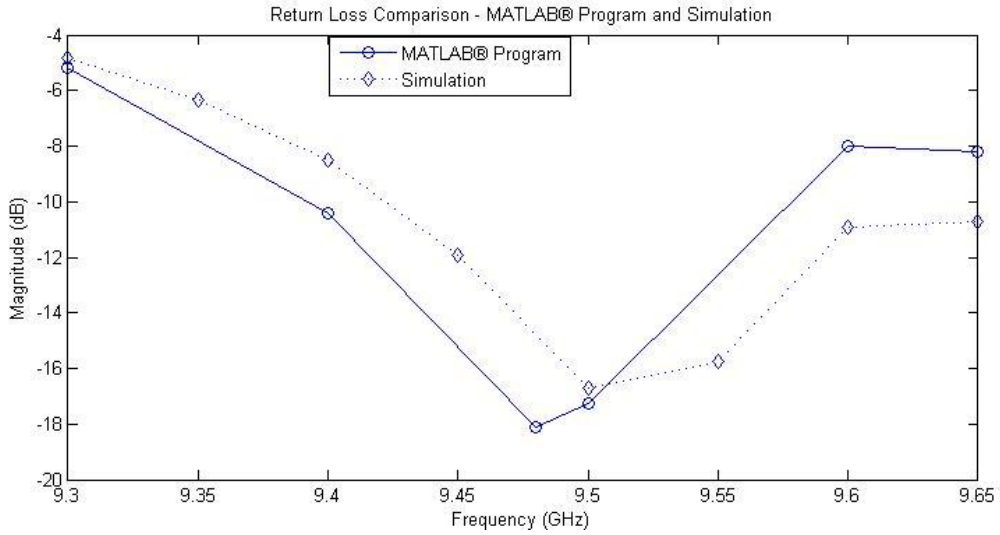

Figure-51 Comparison of Return Loss Graphs for Wideband Patch Antenna that are Obtained from the MATLAB® Program and the MoM based EM simulation software IE3D by Zealand

Now, impedance bandwidth is calculated for wideband path antenna by considering the return loss graph in Figure-50. Therefore, this graph is presented again in Figure-52 together with the corresponding frequencies of $-10dB$ bandwidth.

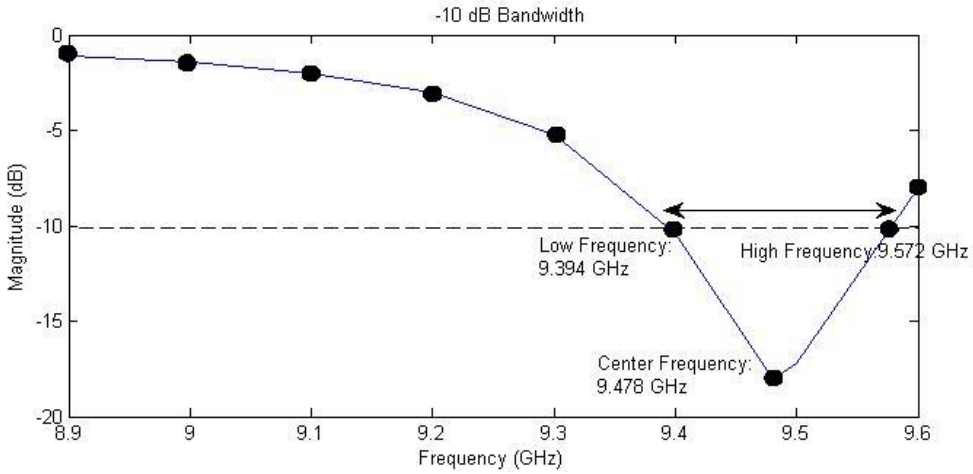

Figure-52 Return Loss Graph for Wideband Patch Antenna that is Obtained from the MATLAB® Program with $-10dB$ Bandwidth Values

For determining the lowest, highest and the center frequencies, approximate values are considered, since only few number of frequencies are used to find return losses. $-10dB$ bandwidth can be calculated as shown in equation (117) for wideband patch antenna by using the values in Figure-52.

$$-10dB\ \text{bandwidth} = \frac{9.572 - 9.394}{9.478} = 0.0187$$
$$= 0.0187 * 100 = \%1.87 \tag{117}$$

Up to now, the analysis are carried out and bandwidth values for patch antennas with and without slots are calculated. The calculation steps are presented. It is now aimed to compare the bandwidth values for these two antennas in order to determine whether there is an increase in bandwidth or not. First, return loss graphs for these antennas are plotted together in Figure-53, so the bandwidth widths can be compared visually.

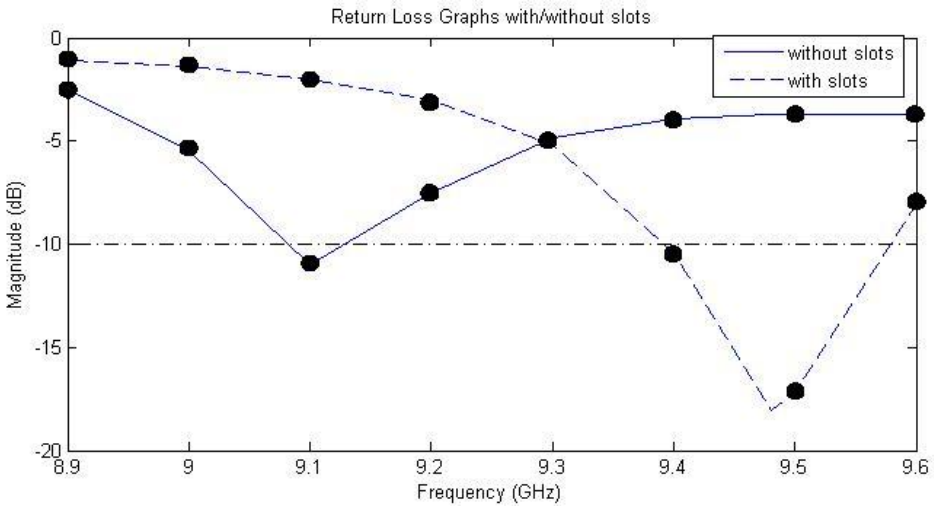

Figure-53 Return Loss graphs for Patch Antennas with/without Slots Together

As shown in Figure-53, if a horizontal line is drawn from $-10dB$ loss, the patch antenna with slots has a wider bandwidth than the patch antenna without slots as expected.

Now the calculated impedance bandwidth values can be compared. It is expected to obtain a bandwidth increase in the wideband antenna (with slots) in Figure-49 when compared to the microstrip fed antenna (without slots) in Figure-45. The antenna with slots in Figure-49 has a

bandwidth of %1.87 on the other hand the antenna without slots in Figure-45 has a bandwidth of %0.79.

These analysis are shown that if two parallel slots are opened on the patch antenna in Figure-45, an increase in $-10dB$ bandwidth value is observed. This bandwidth increase for the antenna in Figure-49 is approximately 2.3671 times greater than the bandwidth for the antenna in Figure-45. This bandwidth increase is expected, since the antenna in Figure-49 is designed to ensure a bandwidth increase. Therefore, the design is proven to increase the $-10dB$ bandwidth.

CHAPTER 8

CONCLUSION

The aim of this thesis study is analyzing various microstrip structures and finding the current distribution on these structures by using MoM in conjunction with closed-form spatial domain Green's functions. Moreover, it is aimed to design and analyze a wideband patch antenna by opening slots on a standard microstrip patch antenna. Finding the current distribution on this wideband patch antenna by using matrix deleting technique from available matrices is considered to be more efficient than re-executing the program. By using the obtained current distribution, return loss graph can be plotted and from this graph bandwidth of the wideband patch antenna can be found. Afterwards, the bandwidth values of standard and wideband patch antennas are compared in order to observe the increase in the bandwidth. The aims of this thesis study are explained. Now, the studies throughout this thesis will be summarized and the outcomes will be compared with the aims at the end of this chapter.

First microstrip structures are introduced. In general, the application areas, advantages and disadvantages of these structures are discussed. Information is given according to the development of these structures throughout the history, how and why they are used and the possible future applications. The analysis methods of microstrip structures are defined. This information about microstrip structures is given in order to recognize the structures that are studied in the thesis and investigate their historical development process. The possible subjects that could be analyzed in near future related to the microstrip structures are explained. In which areas and how they are used, in which areas they cannot be used, which features are more powerful and beneficial and which features of them should be improved are explained. By discussing such things, the aim of this thesis study could be understood better. For instance, one of the aims in this study is to increase the bandwidth of microstrip patch antenna since the bandwidth of the standard microstrip patch antenna is stated to be narrow and inadequate. Lots of studies are performed related to increase the bandwidth of patch antennas. There are many methods that could be applied; yet changing the geometry by opening slots on the metal patch seems the best one to increase the bandwidth. All these possible methods are discussed in the thesis and their related benefits are explained. In this study, wideband patch antenna is designed by opening parallel slots. Therefore, one of the disadvantages of microstrip patch antenna is chosen in this study, and it is aimed to improve this feature by designing and analyzing a wideband patch antenna. This is why introducing microstrip structures together with their features are necessary before analyses.

Full-wave analysis method is used in this thesis and MoM technique is used. Therefore, MoM technique is described in general. Firstly, the specific application of MoM technique to the problem in this thesis study is not mentioned, only the general application procedure of the MoM analysis is provided in detail.

Both spatial domain Green's functions and spectral domain Green's functions could be used in the MoM analysis. Which domain will provide more efficient analysis in MoM should be determined. Therefore, spatial domain Green's functions are explained in one chapter and spectral domain Green's functions are explained in Appendix part. The Green's functions in both domains are examined separately and the one that is more appropriate by using in conjunction with MoM is determined. If spatial domain Green's functions could be used in closed-forms, then using them in MoM analysis is computationally efficient because time consuming integral part is removed. Spatial domain Green's functions can be expressed in terms of spectral domain Green's functions and this expression is called as Sommerfeld integral, in general. If the spectral domain Green's functions in this integral could be approximated in terms of exponentials, then an identity called Sommerfeld identity can be used instead of the integral. Sommerfeld integral is very time consuming. It is aimed to eliminate this time consuming part by using Sommerfeld identity. Therefore, spatial domain Green's functions are analyzed, the procedure of how they can be expressed in terms of closed-forms is examined and how an efficient computation can be achieved by their usage in MoM analysis is demonstrated. On the other hand, spectral domain Green's functions are also discussed and it is stated that their usage in MoM analysis cannot be computationally efficient as the usage of spatial domain Green's functions. After these explanations, closed-form spatial domain Green's functions are chosen to be used in MoM analysis.

MoM analysis in conjunction with closed-form spatial domain Green's functions is used firstly for single microstrip line and the corresponding current distribution on the metal line is obtained. Single microstrip line structure is illustrated and basis functions that are used in the MoM analysis are defined. Galerkin's method is used and it is stated that this method provide symmetric matrices. The electric field expression on the metal line is given and testing procedure is applied by ensuring that tangential electric field should be zero on the metal line. Best selection of basis function that fits the behavior of current distribution on the line is rooftop function. The unknown current distributions in the electric field expression are approximated in terms of rooftop functions and it is aimed to find the coefficients of these functions. After analyses that are explained in detailed, matrix equations are obtained and transferred to a MATLAB® program. Convolution integrals are calculated analytically and the remaining integrals are calculated numerically. After the solution, current distribution on the metal line is obtained and illustrated for different cases. For instance, the location of the source on the metal line is changed in order to observe the effect on the current distribution. Furthermore, the loads at the both ends of metal line are changed such as open, short and matched then the corresponding effects are investigated.

A similar analysis is applied to the coupled microstrip line structure as well. Coupled microstrip line is illustrated and chosen basis functions are described. Galerin's MoM is used again. Loads at the ends are taken as open. There is an electromagnetic interaction between two parallel metal lines and this interaction should be taken into account in the analysis of coupled microstrip line. Active line will have an effect on the passive line and then similarly passive line will have an impact on active line. By considering this coupling effect between the lines, current distribution on these active and passive lines are found and plotted. The distance between two parallel lines is changed according to the wavelength and its effect on the current distributions is investigated. It is expected to obtain a decrease in the coupling effect when distance is decreased and an increase in the coupling effect when distance is

increased. These expectations are captured with the findings. The analysis of coupled microstrip line is very important for this thesis study, because of the coupling effect. This coupling effect should also be used in the analysis of microstrip patch antenna.

The main microstrip structure that is desired to be analyzed in this thesis study is microstrip patch antennas. First, microstrip patch antennas are analyzed, then their geometry is changed in order to increase the bandwidth. Analysis is same as the ones used in single line and coupled line cases. The important point that should be taken into account in the analysis is the current in y direction. Since the width in y direction is comparable with the wavelength as well as the width in x direction, the current distribution across the y direction should also be considered in the analysis. In the analysis, metal patch can be considered as a structure that is composed of many coupled lines. Therefore, all the coupling effects between these coupled lines should be taken into account. The distance between these coupled lines are regarded as zero. Each line has an effect on all remaining lines and this effect should be taken into account in the analysis. Basis functions are fitted on each line. The most important point is to construct the software program in MATLAB® for this case. When basic inputs are given to the program, it should consider all possible coupling effects and it should determine beginning and ending coordinates of basis functions. For instance, if the divisions in x and y directions are given as inputs to the program, then all basis function coordinates should be calculated automatically and the coupling effects should be calculated accordingly. In the analysis any number of divisions in both directions could be chosen, so these are parameters. In the first analysis, the feeding model is simply coaxial probe. Afterwards, feeding model is chosen as microstrip feeding. The location of the feeding point is changed on the metal patch and the corresponding results are observed. Since current distributions exist in both directions, results are plotted in two dimensional graphs. The current distributions on the metal patch are observed for different source locations and the effect of the location is similar to the expected results. Moreover, the software program can give fast and accurate results for any number of divisions. This program is also solved by reducing it to a coupled line case and the results are same as the ones that are obtained from coupled line analysis.

Standard microstrip patch antenna can be solved easily. However, it is not efficient to re-executing the software program for each different geometry configuration. For instance, it is time consuming to re-executing program for the case of microstrip line feeding model geometry. Instead of re-execution, the matrices that are obtained from the solution of standard patch antenna can be used in matrix deleting procedure. By this way, available matrices are used in order to find the current distribution for new geometries. This matrix deleting method is useful especially for analyzing different patch geometries where it is required to re-execute the program for many different patch configurations. The procedure of matrix deleting technique is explained and for all sorts of geometry modifications this technique is used in this thesis study.

Microstrip transmission line is used to feed the microstrip patch antenna and current distribution on the metal patch is obtained by matrix deleting technique from the results of standard patch antenna solution. Therefore, it is not necessary to re-execute the program for this new configuration with microstrip feeding. Afterwards, current distribution is used to acquire reflection coefficients for different frequencies. Subsequently, return loss graph is plotted and from this graph the bandwidth value is calculated. Next, the final patch antenna

geometry is modified. Two parallel slots are opened on the non-radiating edges of the metal patch. It is expected to an increase in the bandwidth after this geometry modification. In other words, a wideband patch antenna is designed. At the same time, this wideband patch antenna configuration is designed in a MoM based EM simulation software IE3D by Zealand and results are saved. Again matrix deleting technique is used for this new configuration. For this wideband microstrip patch antenna the corresponding current distribution is found. Then, throughout a frequency band, corresponding reflection coefficients are calculated, return loss graph is plotted and bandwidth value is calculated. Lastly, the bandwidth values of two antennas are compared and an increase in the bandwidth is observed as expected. The observed results are also very similar to the ones that are obtained and saved from a microwave simulation program. Therefore, the method I,s demonstrated to be accurate.

The explained studies up to now show that the desired aims are realized. Basically, current distributions for various microstrip structures are obtained numerically by using MoM analysis in conjunction with closed-form spatial domain Green's functions and results are plotted. Subsequently, wideband antenna is designed and current distribution is obtained in the same manner. From the results of this wideband antenna, a desired bandwidth increase is observed. By using the constructed MATLAB® program and matrix deleting technique, all sorts of different geometries can be analyzed and the corresponding parameters can be obtained.

REFERENCES

[[1] M. I. Aksun and N. Kinayman, "*Modern Microwave Circuits*", Artech House, London, 2005.

[2] R. A. Pucel, "*Design Considerations for Monolithic Microwave Circuits*", IEEE Trans. Microw. Theory Tech., vol. MTT-29, pp. 513-534, June 1981.

[3] K. B. Bhasin et al., "*Monolithic Microwave Integrated Circuits – Interconnections and Packaging Considerations*", NASA Technical Memorandum, Baltimore, Maryland, 1984.

[4] R. M. Barrett, "*Microwave Printed Circuits – The Early Years*", IEEE Trans. Microw. Theory Tech., vol. 32, pp. 983-990, September, 1984.

[5] H. Howe, "*Microwave Integrated Circuits – An Historical Perspective*", IEEE Trans. Microw. Theory Tech., vol. MTT-29, pp. 991-996, September 1984.

[6] D.M. Pozar, "*An Update on Microstrip Antenna Theory and Design Including Some Novel Feeding Techniques*", IEEE Antennas Propag. Soc. Newslett., Feature Article, October, 1986.

[7] R. E. Munson, "*Conformal Microstrip Antennas and Microstrip Phased Arrays*", IEEE Trans. Antennas Propag., vol. 22, pp. 74-78, January, 1974.

[8] N. Kınayman, "*A Novel CAD Algorithm for the Analysis of Printed Geometries*", Ph. D. thesis, Elect. and Electron. Eng., Bilkent Univ., May, 1997.

[9] Y. Liu et al., "*Some Recent Developments of Microstrip Antenna*", Internal Journal of Antennas Propag., vol.2012, Article ID 428284, January, 2012.

[10] K. Borah and N. S. Bhattacharyya, "*Magneto-dielectric Material with Nano Ferrite Inclusion for Microstrip Antennas: Dielectric Characterization*", IEEE Trans. Dielectr. Electr. Insul., vol. 17, No. 6, December, 2010.

[11] H. Kumar et al., "*Study on Band Gap Behaviour of Electromagnetic Band-Gap (EBG) Structure with Microstrip Antenna*", 14^{th} Int. Conf. on ICACT, PyeongChang, 2012.

[12] K. Mei and J. V. Bladel, "*Low-Frequency Scattering by Rectangular Cylinders*", IEEE Trans. Antennas Propag., vol. 11, pp. 52-56, January, 1963.

[13] M. G. Andreasen, "*Scattering from Parallel Metallic Cylinders with Arbitrary Cross Sections*", IEEE Trans. Antennas Propag., vol. 12, pp. 746-754, November, 1964.

[14] J. Richmond, "*Scattering by a Dielectric Cylinder of Arbitrary Cross Section Shape*", IEEE Trans. Antennas Propag., vol. 13, pp. 334-341, May, 1965.

[15] F. R. Harrington, "*Matrix Methods for Field Problems*", Proc. IEEE, vol. 55, pp. 136-149, February, 1967.

[16] F. R. Harrington, "*Field Computation by Moment Methods*", IEEE Press, New York, 1993.

[17] E. H. Newman and K. Kingsley, "*An Introduction to the Method of Moments*", Comput. Physics Commun., vol. 68, pp. 1-18, November, 1991.

[18] W. C. Gibson, "*The Method of Moments in Electromagnetics*", CRC Press LLC, New York, 2007.

[19] Ş. Ö. Piroğlu, "*Analysis of Coupled Lines in Microwave Printed Circuit Elements*", M. S. thesis, Elect. and Electron. Eng., The Middle East Tech. Univ., December, 2007.

[20] D. B. Davidson, "*Computational Electromagnetics for RF and Microwave Engineering*", Cambridge University Press, New York, 2005.

[21] T. K. Sarkar, "*A Note on the Choice Weighting Functions in the Method of Moments*", IEEE Trans. Antennas Propag., vol. AP-33, pp. 436-441, April, 1985.

[22] N. K. Saydam, "*Analysis of Microstrip Lines Using Closed-Form Green's Functions*", M. S. thesis, Elect. and Electron. Eng., The Middle East Tech. Univ., January, 1996.

[23] R. Garg, "*Analytical and Computational Methods in Electromagnetics*", Artech House, Norwood, 2008.

[24] D. G. Fang, "*Antenna Theory and Microstrip Antennas*", Taylor & Francis Group, 2009.

[25] I. Park et al., "*Numerically Efficient Analysis of Planar Microstrip Configurations Using Closed-Form Green's Functions*", IEEE Trans. Microw. Theory Tech., vol. 43, pp. 394-400, February, 1995.

[26] D. G. Fang et al., "*Discrete Image Theory for Horizontal Electric Dipoles in a Multilayered Medium*", Proc. IEEE Microw., Antennas and Propag., vol. 135, pp. 297-303, October, 1988.

[27] Y. L. Chow et al., "*A Closed-form Spatial Green's Function for the Thick Microstrip Substrate*", IEEE Trans. Microw. Theory Tech., vol. 39, pp. 588-592, March, 1991.

[28] N. Kinayman and M. I.Aksun, "*Comparative Study of Acceleration Techniques for Integrals and Series in Electromagnetic Problems*", Radio Sci., vol. 30, pp. 1713-1722, December, 1995.

[29] M. I. Aksun and R. Mittra, "*Derivation of Closed-Form Green's Functions for a General Microstrip Geometry*", IEEE Trans. Microw. Theory Tech., vol. 40, pp. 2055-2062, November, 1992.

[30] G. Dural and M. I. Aksun, "*Closed-form Green's Functions for General Sources and Stratified Media*", IEEE Trans. Microw. Theory Tech., vol. 43, pp. 1545-1552, July, 1995.

[31] M. I. Aksun, "*A Robust Approach for the Derivation of Closed-form Green's Functions*", IEEE Trans. Microw. Theory Tech., vol. 44, pp. 651-658, May, 1996.

[32] N. Kinayman and M. I. Aksun, "*Efficient Use of Closed-Form Green's Functions for the Analysis of Planar Geometries with Vertical Connections*", IEEE Trans. Microw. Theory Tech., vol. 45, pp. 593-603, May, 1997.

[33] M. E.Yavuz et al., "*Critical Study of the Problems in Discrete Complex Image Method*", IEEE Int. Symp. On Electromagn. Compat., pp. 1281-1284, May, 2003.

[34] M. I. Aksun and G. Dural, "*Clarification of Issues on the Closed-Form Green's Functions in Stratified Media*", IEEE Trans. Antennas Propag., vol. 53, pp. 3644-3653, November, 2005.

[35] F. Mesa et al., "*Closed-Form Expressions of Multilayered Planar Green's Functions That Account for the Continuous Spectrum in the Far Field*", IEEE Trans. Microw. Theory Tech., vol. 56, pp. 1601-1614, July, 2008.

[36] M. I. Aksun, "*Current Status of Closed-Form Green's Functions in Layered Media Composed of Natural and Artificial Materials*", Int. Conf. on Electromagn. in Advanced Applicat., pp. 451-454, September, 2009.

[37] A. Alparslan et al., "*Closed-Form Green's Functions in Planar Layered Media for All Ranges and Materials*", IEEE Trans. Microw. Theory Tech., vol. 58, pp. 602-613, March, 2010.

[38] A. Alparslan, "Study of Green's Functions of Potentials and Fields in Layered Media composed of Left-Handed and Right-Handed Materials", M. S. thesis, Elect. and Comput. Eng., Koç Univ., September, 2008.

[39] L. Alatan, "*Use of Computationally Efficient MoM in the Analysis and Design of Printed Structures*", Ph. D. thesis, Elect. and Electron. Eng., The Middle East Tech. Univ., June, 1997.

[40] M. I. Aksun and R. Mittra, "*Estimation of Spurious Radiation from Microstrip Etches Using Closed-Form Green's Functions*", IEEE Trans. Microw. Theory Tech., vol. 40, pp. 2063-2069, November, 1992.

[41] M. I. Aksun and R. Mittra, "*Spurious Radiation from Microstrip Interconnects*", IEEE Trans. on Electromagn. Compat., vol. 35, May, 1993.

[42] J. Kiusalaas, "*Numerical Methods in Engineering with Matlab*", Cambridge University Press, Cambridge, 2009.

[43] S. Bhardwaj and Y. Rahmat-Samii, "*C-shaped, E-shaped and U-slotted Patch Antennas: Size, Bandwidth and Cross-Polarization Characterizations*", 6^{th} Europian Conf. on Antennas and Propag., Prague, pp. 1674-1677, March, 2012.

[44] W. C. Chew, "*Waves and Fields in Inhomogeneous Media*", New York, IEEE Press, 1995.

[45] A. K. Michalski and D. Zheng, "*Electromagnetic Scattering and Radiation by Surfaces of Arbitrary Shape in Layered Media, Part I: Theory*", IEEE Trans. Antennas Propag., vol. 38, pp. 335-344, March, 1990.

[46] A. K. Michalski, "*On the Scalar Potential of a Point Charge Associated with a Time-Harmonic Dipole in a Layered Medium*", IEEE Trans. Antennas Propag., vol. AP-35, pp. 1299-1301, November, 1987.

[47] A. Erteza and B. Park, "*Nonuniqueness of Resolution of Hertz Vector in Presence of a Boundary and the Horizontal Dipole Problem*", IEEE Trans. Antennas Propag., vol. 17, pp. 376-378, May, 1969.

APPENDIX A

DETAILED GREEN'S FUNCTION ANALYSIS

A.1 Obtaining Dyadic Green's Function of Electric Field from Scalar Green's Function of Electric Field

In general, if it is aimed to find out electric field that is created by an arbitrary electric current source in homogeneous and isotropic medium, then the linear vector wave equation should be written first. This equation is obtained from Maxwell's equations and it is shown in equation (1).

$$\Delta \times \Delta \times \mathbf{E}(\mathbf{r}) - k^2 \mathbf{E}(\mathbf{r}) = -j\omega\mu\, \mathbf{J}(\mathbf{r}) \tag{1}$$

If the electric field distribution that is created by the impulse source is intended to be found, then equation (1) should be modified and electric field distribution becomes the Green's function in that case. Equation (2) shows this modified vector wave equation. Here, $\hat{\alpha}$ represents an arbitrary direction of the impulse source.

$$\Delta \times \Delta \times \overline{\mathbf{G}}^{E}(\mathbf{r}) - k^2 \overline{\mathbf{G}}^{E}(\mathbf{r}) = -\hat{\alpha}\delta(\mathbf{r}) \tag{2}$$

Dyadic Green's function for electric field in more general form can be written in equation (3). This is a very general representation which includes all possible fields that are created by an arbitrary oriented source. It can be modified and reach a specific form for each specific case.

$$\overline{\mathbf{G}}^{E} = G_{xx}^{E}\hat{x}\hat{x} + G_{yy}^{E}\hat{y}\hat{y} + G_{zz}^{E}\hat{z}\hat{z} + G_{xy}^{E}\hat{x}\hat{y} + G_{yx}^{E}\hat{y}\hat{x} + \ldots \tag{3}$$

First step is to find the Green's function by solving the equation (2). This Green's function is the electric field response that is caused from the impulse source. Afterwards, electric field that is created by an arbitrary source can be found by using convolution integral and equation (4) shows this convolution integral. Integral should be taken across source domain.

$$\mathbf{E}(\mathbf{r}) = j\omega\mu \int_{V'} \overline{\mathbf{G}}^{E}(\mathbf{r},\mathbf{r}').\,\mathbf{J}(\mathbf{r}')d\mathbf{r}' \tag{4}$$

Vector wave equation that is shown in equation (1) can be simplified. Equation (5) shows the simplified version of this equation, for the derivation reader can read the reference [1].

$$\Delta^2 \mathbf{E}(\mathbf{r}) + k^2 \mathbf{E}(\mathbf{r}) = j\omega\mu \left[\bar{\mathbf{I}} + \frac{\Delta\Delta}{k^2} \right].\mathbf{J}(\mathbf{r}) \tag{5}$$

Equation (5) is called Helmholtz equation and indeed it is composed of scalar wave equations. Three scalar wave equations that constitute equation (5) are shown in equation (6).

$$\left(\Delta^2 + k^2\right)\psi(\mathbf{r}) = 0 \qquad \text{Where} \qquad \psi = E_x, E_y, E_z \tag{6}$$

Writing the scalar wave equation separately for each direction is possible only for cartesian coordinates [1]. Then, combining electric field components that are obtained from separate scalar wave equations will result the desired electric field. By considering equation (6), scalar wave equation can be written for Green's function which is shown in equation (7).

$$\left(\Delta^2 + k^2\right) g(\mathbf{r}, \mathbf{r}') = -\delta(\mathbf{r} - \mathbf{r}') \tag{7}$$

The scalar Green's function that is found from equation (7) can be used to find the scalar function that is created from an arbitrary source. In order to obtain the scalar function that is given in equation (6), the superposition integral in equation (8) should be used.

$$\psi(\mathbf{r}) = -\int_{\mathbf{V}'} d\mathbf{r}'\, g(\mathbf{r}, \mathbf{r}') s(\mathbf{r}') \tag{8}$$

First, equation (7) should be solved for Green's function, and then this can be used in equation (8). Equation (7) should be solved for unbounded and homogeneous medium first. As seen, this equation is a differential equation and the general solution to this differential equation can be represented as the one in equation (9).

$$g(r) = C\frac{e^{-jkr}}{r} + D\frac{e^{jkr}}{r} \tag{9}$$

Now, the boundary conditions should be examined in order to find out the special solution. The source at the infinity cannot be valid physically, so in this case only outgoing waves should be present. Therefore, the coefficient D should equal to zero and the final form of the solution is shown in equation (10).

$$g(r) = C\frac{e^{-jkr}}{r} \tag{10}$$

If the boundary condition at the source point is considered, the coefficient C can be found as well. Without going into the details, the scalar Green's function that is created from an arbitrary point source can be written as the one that is shown in equation (11).

$$g(\mathbf{r}, \mathbf{r}') = g(\mathbf{r} - \mathbf{r}') = \frac{e^{-jk|\mathbf{r}-\mathbf{r}'|}}{4\pi|\mathbf{r} - \mathbf{r}'|} \tag{11}$$

These scalar Green's functions are indeed the components of vectoral Green's function in an unbounded medium. By using equation (4), convolution integral can be constructed for finding electric field and it is denoted in equation (12).

$$E(r) = -j\omega\mu \int_{V'} d\mathbf{r}' g(\mathbf{r}-\mathbf{r}') \left[\bar{\mathbf{I}} + \frac{\Delta'\Delta'}{k^2} \right] . \mathbf{J}(\mathbf{r}') \tag{12}$$

There is a relation between scalar Green's function and vectoral Green's function and this relation is shown in equation (13). For the derivation, reader can examine the reference [1].

$$\overline{\mathbf{G}}^{E}(\mathbf{r},\mathbf{r}') = \left[\bar{\mathbf{I}} + \frac{\Delta\Delta}{k^2} \right] g(\mathbf{r}-\mathbf{r}') \tag{13}$$

A.2 Obtaining Dyadic Green's Function of Electric Field from Scalar/Vectoral Potentials (MPIE)

Although the Green's function of electric field is derived from scalar Green's function of electric field in the previous section, it is also possible to derive the dyadic Green's function of electric field from scalar and vectoral potentials. It is known that electric field can be expressed in terms of scalar and vectoral potentials and the resulted integral equation is called MPIE. Electric field in terms of scalar and vectoral potentials is represented in equation (14).

$$\mathbf{E}(\mathbf{r}) = -j\omega\mathbf{A}(\mathbf{r}) - \Delta\phi(\mathbf{r}) \tag{14}$$

Moreover, equation (15) is used to find vectoral potential while equation (16) is used for scalar potential.

$$\Delta^2\mathbf{A}(\mathbf{r}) + k^2\mathbf{A}(\mathbf{r}) = -\mu\,\mathbf{J}(\mathbf{r}) \tag{15}$$

$$\Delta^2\phi(\mathbf{r}) + k^2\phi(\mathbf{r}) = -\frac{\rho(\mathbf{r})}{\varepsilon} \tag{16}$$

Since both equations (15) and (16) are expressed as wave equation, the resulted Green's functions can be used in convolution integrals in order to find out scalar and vectoral potentials. Equations (17) and (18) represent these convolution integrals.

$$\mathbf{A}(\mathbf{r}) = \mu \int_{V'} d\mathbf{r}' g(\mathbf{r}-\mathbf{r}')\,\mathbf{J}(\mathbf{r}') \tag{17}$$

$$\phi(\mathbf{r}) = \frac{1}{\varepsilon} \int_{V'} d\mathbf{r}' g(\mathbf{r}-\mathbf{r}')\rho(\mathbf{r}') \tag{18}$$

Now, if equation (14) is rewritten by considering equations (17) and (18) together with some simplifications and continuity equation, the final form of the electric field can be expressed as the one that is shown in equation (19).

$$\mathbf{E}(\mathbf{r}) = -j\omega\mu \int_{V'} d\mathbf{r}' g(\mathbf{r}-\mathbf{r}')\,\mathbf{J}(\mathbf{r}') + \frac{\Delta\Delta}{j\omega\varepsilon} \int_{V'} d\mathbf{r}' g(\mathbf{r}-\mathbf{r}')\mathbf{J}(\mathbf{r}') \tag{19}$$

Then, from equation (19), the same dyadic Green's function can be found in terms of scalar Green's function and it is shown in equation (20).

$$\overline{\mathbf{G}}^{E}(\mathbf{r},\mathbf{r}') = \left[\bar{\mathbf{I}} + \frac{\Delta\Delta}{k^2}\right] g(\mathbf{r}-\mathbf{r}') \tag{20}$$

A.3 Spectral Domain Green's Function in Layered Media

In planarly layered media, the electrical properties that are permittivity and permeability change only in z-direction. Therefore, in the source free case, vector wave equations can be reduced to two scalar wave equations. These equations represent decoupled TE to z and TM to z waves [44]. As an example, the vector wave equations in equation (21) and equation (22) can be reduced to two independent scalar equations which are given in equation (23) and equation (24), respectively. Here, all equations are considered for source free case.

$$\mu \nabla \times \frac{1}{\mu} \nabla \times \mathbf{E}(\mathbf{r}) - \omega^2 \mu\, \varepsilon\, \mathbf{E}(\mathbf{r}) = 0 \tag{21}$$

$$\varepsilon \nabla \times \frac{1}{\varepsilon} \nabla \times \mathbf{H}(\mathbf{r}) - \omega^2 \mu\, \varepsilon\, \mathbf{H}(\mathbf{r}) = 0 \tag{22}$$

$$\left[\mu(z)\frac{\partial}{\partial z}\mu^{-1}(z)\frac{\partial}{\partial z} + \underbrace{\omega^2\mu\,\varepsilon - k_x^2}_{k_z^2}\right] E_y = 0 \qquad \text{for TE-z} \tag{23}$$

$$\left[\varepsilon(z)\frac{\partial}{\partial z}\varepsilon^{-1}(z)\frac{\partial}{\partial z} + \underbrace{\omega^2\mu\,\varepsilon - k_x^2}_{k_z^2}\right] H_y = 0 \qquad \text{for TM-z} \tag{24}$$

These two scalar wave equations should be solved for each layer separately. Then, the boundary condition relations between layers are taken into account. By using boundary conditions, these separate equations for each layer can be combined to represent the overall geometry. One-dimensional equations that are given in equations (25) and (26) should be solved for each layer separately, and here subscript "i" represents the layer number.

$$\left[\frac{\partial^2}{\partial z^2} + \underbrace{\omega^2\mu_i\varepsilon_i - k_x^2}_{k_{zi}^2}\right] E_{yi}(z) = 0 \qquad \text{for TE-z} \tag{25}$$

$$\left[\frac{\partial^2}{\partial z^2} + \underbrace{\omega^2 \mu_i \varepsilon_i - k_x^2}_{k_{zi}^2}\right] H_{yi}(z) = 0 \qquad \text{for TM-z} \tag{26}$$

If transverse direction is unbounded in layered structures and the electrical properties change only in z direction, then transverse fields in each layer can be found by considering each layer as a separate transmission line [1].

In a layered media, Green's functions can be represented in closed forms only in spectral domain. Now, a layered structure is studied in which the source is in the origin and observation point is arbitrary. Figure-54 illustrates this example layered structure.

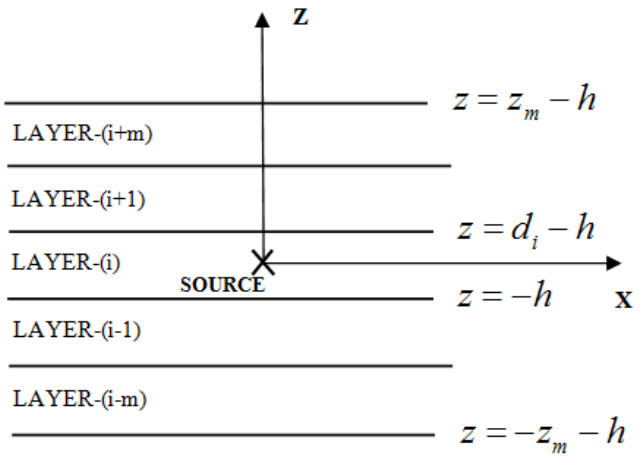

Figure-54 Example Illustration of a Layered Structure with Source in Layer-i

In order to find out the Green's functions for potentials in layered media, first of all these Green's functions should be found in unbounded media. Then, by considering the reflections and transmissions in layer interfaces, the Green's functions in layered media can be found. However, in planar interfaces reflection and transmission coefficients are only defined for plane waves [38]. Vector potential Green's functions for unbounded media can be written as the spatial derivatives of spherical waves and electric field Green's functions for unbounded media can be written in terms of spherical waves. Therefore, a process is required in order to find out reflection and transmission coefficients of spherical waves in planar dielectric interfaces. Hence, Wely identity is used to expand spherical wave representations in terms of plane waves. Equation (27) defines this Wely identity.

$$\frac{e^{-jkr}}{r} = \frac{1}{\pi}\int_{-\infty}^{\infty}\int_{-\infty}^{\infty} dk_x dk_y e^{-jk_x x - jk_y y}\frac{e^{-jk_z|z|}}{j2k_z} \qquad \text{where} \quad k^2 = k_x^2 + k_y^2 + k_z^2$$

$$\text{and} \quad |r| = \sqrt{x^2 + y^2 + z^2} \tag{27}$$

Hereby, for the summation of spherical waves in terms of plane waves, the reflection and transmission coefficients can be written. Equation (27) is the two dimensional inverse transform of spectral domain Green's function for unbounded media. Wely identity can be considered as the plane wave expansion of spherical waves. It includes both evanescent waves with $k^2 < k_x^2 + k_y^2$ and propagating waves with $k^2 \geq k_x^2 + k_y^2$. Here, by considering phase matching condition, k_x and k_y in transverse directions should equal across layers.

In layered media, non-uniqueness of potentials should be taken into account [30]. As seen in Figure-54, at least two components of vector potential are needed for an x-directed HED. This is due to the fact that the magnetic field that is created by x-directed HED has two components, one is z-directed and the other is y-directed. It is clear that the z-component is not continuous across two layers. This fact demonstrates that in contrast to the situation in unbounded media, in layered media only one component of vector potential is not enough for the solution [45, 46, 47]. Previously, the general expression for dyadic Green's function for electric field was given in equation (3). Now, dyadic Green's function for vector potential is considered. By taking into account the boundary conditions, a specific expression can be found for layered structures. It is now clear that for horizontal electric dipole, two components of vector potential should be defined. This is because the boundary conditions for electric and magnetic fields that should be satisfied across the interface cannot be satisfied with a single vector potential. As Sommerfeld indicates, vector potential for horizontal electric dipole should be considered with two vector components in layered media [1]. For vertical dipole, only one vector potential component is enough for satisfying overall boundary conditions. Therefore, it should be assumed that horizontal dipole creates two components of vector potential and vertical dipole creates only one component of vector potential. Furthermore, scalar potentials that are created by horizontal and vertical dipoles are different. In order to define all field components uniquely, 5 potential functions are necessary. The traditional form of dyadic Green's function for vector potential according to the mentioned considerations is provided in equation (28).

$$\overline{\mathbf{G}}^A = (\hat{x}\hat{x} + \hat{y}\hat{y})G_{xx}^A + \hat{z}\hat{x}G_{zx}^A + \hat{z}\hat{y}G_{zy}^A + \hat{z}\hat{z}G_{zz}^A \tag{28}$$

Spectral domain Green's functions are first found in source layer. Here, direct waves and reflected waves from the boundaries are present. Then, field in an arbitrary layer can be obtained from the field in the source layer.

A.3.1 Spectral Domain Green's Function for HED and HMD

Before the formulation, it should be remarked that because of the phase matching condition the transverse components k_x and k_y are equal in all layers. According to the previous inferences, fields can be found in the source layer first. Source region can be regarded as an unbounded medium and longitudinal components can be written for this layer. These components are indeed TM to z and TE to z components for source layer. By using equation (29) in which $\hat{\alpha}$ represents an arbitrary direction, these longitudinal components of fields can be defined which are shown in equations (30) and (32). Equation (29) is obtained by expressing electric field in terms of potentials [1].

$$\mathbf{E}(\mathbf{r}) = -j\omega\left[\bar{\mathbf{I}} + \frac{\nabla\nabla}{k^2}\right].\hat{\alpha}\mu\,\mathbf{I}l\,\frac{e^{-jk|\mathbf{r}-\mathbf{r}'|}}{4\pi|\mathbf{r}-\mathbf{r}'|} \tag{29}$$

$$E_{zi} = -\frac{jIl}{4\pi\omega\varepsilon_i}\frac{\partial^2}{\partial z\partial x}\frac{e^{-jk_i r}}{r} \tag{30}$$

$$H_{zi} = -\frac{jIl}{4\pi}\frac{\partial}{\partial y}\frac{e^{-jk_i r}}{r} \tag{31}$$

In order to satisfy the constraint conditions in layered structures, reflection and transmission coefficients are necessary [44]. These coefficients are observed in planar interfaces as indicated previously and spherical waves in hand should be expanded in terms of plane waves. It is explained previously in this thesis that this expansion is realized by using Wely identity. The longitudinal field components obtained after the plane wave expansion are provided in equations (32) and (33).

$$E_{zi} = \frac{\pm Il}{8\pi^2\omega\varepsilon_i}\int_{-\infty}^{\infty}\int_{-\infty}^{\infty} dk_x dk_y k_x e^{-jk_x x - jk_y y} e^{-jk_{zi}|z|} \tag{32}$$

$$H_{zi} = \frac{Il}{8\pi^2}\int_{-\infty}^{\infty}\int_{-\infty}^{\infty} dk_x dk_y k_y e^{-jk_x x - jk_y y}\,\frac{e^{-jk_{zi}|z|}}{k_{zi}} \tag{33}$$

$\pm$ sign is originated from the derivative of $e^{-jk_{zi}|z|}$ with respect to z. If $z>0$ it will be positive, else it will be negative.

Kernels of two dimensional Fourier transforms in equations (32) and (33) should be considered as $e^{-j(k_x x + k_y y)}$. Therefore, in the integrands of these equations, the remaining parts should be considered as Fourier transforms of longitudinal fields that are created by HED in an unbounded media. Hence, spectral domain representation of fields can be regarded as plane waves propagating in z direction [38]. Expressions in equation (32) and (33) are valid in homogeneous media. Since layered media is present in our case, these equations should be modified by considering reflection and transmission coefficients of the source layer. Here, only z propagating waves are treated, so only the field changes in the z

direction should be taken into account. By applying the modifications in layered structures, the resulted field expression is represented in equations (34) and (35). Equations (36) and (37) represent the parts in the integrands rather than the kernels.

$$E_{zi} = \frac{Il}{8\pi^2 \omega \varepsilon_i} \int_{-\infty}^{\infty} \int_{-\infty}^{\infty} dk_x dk_y k_x e^{-jk_x x - jk_y y} F_{TM} \tag{34}$$

$$H_{zi} = \frac{Il}{8\pi^2} \int_{-\infty}^{\infty} \int_{-\infty}^{\infty} dk_x dk_y k_y \frac{e^{-jk_x x - jk_y y}}{k_{zi}} F_{TE} \tag{35}$$

Where,

$$F_{TE} = e^{-jk_{zi}|z|} + A_h^e e^{jk_{zi}z} + C_h^e e^{-jk_{zi}z} \tag{36}$$

$$F_{TM} = \pm e^{-jk_{zi}|z|} + B_h^e e^{jk_{zi}z} + D_h^e e^{-jk_{zi}z} \tag{37}$$

As seen from equation (36) and (37), the field expressions in source layer can be written as the summation of incident and reflected waves. Incident and reflected waves are written by considering upper and lower boundaries and the changes are only in the z direction.

For HMD, field expressions are written by using the ones for HED and the duality principles [38]. The coefficients A_h^e, B_h^e, C_h^e and D_h^e are the coefficients of down going and up going waves in i^{th} layer. Subscripts h and e represent that the source is in horizontal direction and source type is electrical, respectively. In equations (36) and (37), it is clear that the unknown coefficients should be found. These coefficients can be found by using constraint conditions and the details for finding these coefficients can be found in the reference [44].

By using the field expressions in equations (34) and (35) and the found values of the unknown coefficients, Green's functions can be found for the z components of electric and magnetic fields. It should be stated that these expressions can be found only by using the values of the source layer. The z component expressions of spectral domain Green's functions for fields are presented in equations (38) and (39), and these are the final form of the expressions. The Green's function expressions in equations (38) and (39) are written when the source and observation points are in the same layer. Here, $\tilde{\tilde{G}}$ represents spectral domain Green's function. Additionally, in the subscript zx first index z shows the field direction and second index x shows the source direction.

$$\tilde{\tilde{G}}_{zx}^{E} = \frac{1}{2\omega\varepsilon_i} k_x \left[\pm e^{-jk_{zi}|z|} + B_h^e e^{jk_{zi}z} + D_h^e e^{-jk_{zi}z} \right] \tag{38}$$

$$\tilde{\tilde{G}}_{zx}^{H} = \frac{1}{2\omega\varepsilon_i} k_y \left[e^{-jk_{zi}|z|} + A_h^e e^{jk_{zi}z} + C_h^e e^{-jk_{zi}z} \right] \tag{39}$$

Where, propagation constant of layer i in longitudinal direction is shown in equation (40).

$$k_{zi} = \sqrt{k_i^2 - k_x^2 - k_y^2} = \sqrt{k_i^2 - k_\rho^2} \tag{40}$$

The structure is layered, so after finding the longitudinal component, these components can be used to find transverse field components. Equations (41) and (42) represent the relation between longitudinal and transverse field components.

$$\tilde{H}_t = \frac{1}{k^2 - k_z^2}\left[\frac{\partial}{\partial z}\nabla_t \tilde{H}_z + j\omega\varepsilon\,\nabla_t \times \hat{z}\tilde{E}_z\right] \tag{41}$$

$$\tilde{E}_t = \frac{1}{k^2 - k_z^2}\left[\frac{\partial}{\partial z}\nabla_t \tilde{E}_z + j\omega\mu\,\nabla_t \times \hat{z}\tilde{H}_z\right] \tag{42}$$

By using the relations in equations (41) and (42) as well as the longitudinal component expressions, the transverse field components are obtained. These transverse component expressions are provided in equations (43), (44), (45) and (46) [38].

$$\tilde{G}_{xx}^E = \frac{-j\omega\mu_i}{2\left(k_i^2 - k_{zi}^2\right)}\left[\frac{k_x^2}{k_i^2}\frac{\partial}{\partial z}F_{TM} + \frac{k_y^2}{jk_{zi}}F_{TE}\right] \tag{43}$$

$$\tilde{G}_{yx}^E = \frac{-j\omega\mu_i k_x k_y}{2\left(k_i^2 - k_{zi}^2\right)}\left[\frac{1}{k_i^2}\frac{\partial}{\partial z}F_{TM} + \frac{j}{k_{zi}}F_{TE}\right] \tag{44}$$

$$\tilde{G}_{xx}^H = \frac{k_x k_y}{2\left(k_i^2 - k_{zi}^2\right)}\left[F_{TM} - \frac{j}{k_{zi}}\frac{\partial}{\partial z}F_{TE}\right] \tag{45}$$

$$\tilde{G}_{yx}^H = \frac{-1}{2\left(k_i^2 - k_{zi}^2\right)}\left[k_x^2 F_{TM} - \frac{jk_y^2}{k_{zi}}\frac{\partial}{\partial z}F_{TE}\right] \tag{46}$$

These found expressions are all in spectral domain. As seen from these expressions that spectral domain Green's functions are expressed in closed-forms. In order to obtain the spatial domain expressions equations (34) and (35) should be solved. Indeed, they are the inverse Hankel transforms. However, it is clear that the equations in (34) and (35) include computationally expensive and oscillatory kernels and they converge slowly.

As mentioned earlier, vector and scalar potential Green's functions have higher order singularities than the electric and magnetic Green's functions. Therefore, MPIE formulation is more appropriate to the application of MoM in terms of computational efficiency. In order to find out scalar and vector potential Green's functions in spectral domain, the relations that are given in equation (47) can be used for the x-directed HED.

$$\mu\,\mathbf{H} = \nabla \times \mathbf{A} \quad \text{and} \quad \mathbf{A} = \hat{x}A_x + \hat{z}A_z \tag{47}$$

Then, the components of vector potential in x and z directions are found as shown in equations (48) and (49).

$$\widetilde{A}_x = \frac{\mu}{jk_y}\widetilde{H}_z \tag{48}$$

$$\widetilde{A}_z = -\frac{\mu}{jk_y}\widetilde{H}_x \tag{49}$$

By using the expressions in equations (48) and (49), vector potential Green's functions in spectral domain are written as provided in equations (50) and (51).

$$\widetilde{G}_{xx}^{A} = \frac{\mu_i}{j2k_{zi}}\left[e^{-jk_{zi}|z|} + A_h^e e^{jk_{zi}z} + C_h^e e^{-jk_{zi}z}\right] \tag{50}$$

$$\widetilde{G}_{zx}^{A} = \frac{-\mu_i}{j2k_{zi}}\left[\frac{k_x k_{zi}}{k_\rho^2}\left(A_h^e + B_h^e\right)e^{jk_{zi}z} + \frac{k_x k_{zi}}{k_\rho^2}\left(D_h^e - C_h^e\right)e^{-jk_{zi}z}\right] \tag{51}$$

Afterwards, by using the Lorenz gauge $\nabla.\mathbf{A}(\mathbf{r}) = -j\omega\varepsilon\mu\phi(r)$, scalar potential Green's function in spectral domain is given in equation (52).

$$\widetilde{G}_{x}^{q} = \frac{1}{j2\varepsilon_i k_{zi}}\left[e^{-jk_{zi}|z|} + \frac{k_{zi}^2 B_h^e + k_i^2 A_h^e}{k_\rho^2}e^{jk_{zi}z} + \frac{k_i^2 C_h^e - k_{zi}^2 D_h^e}{k_\rho^2}e^{-jk_{zi}z}\right] \tag{52}$$

For VED and VMD sources, same logic can be applied in order to find out spectral domain Green's functions when source and observation points are in the same layer. Since the application is similar and it is out of the content of this thesis work, the overall application is not given. The details can be found in the references [30, 38].

Up to now, the analyses are performed with the assumption that source point and observation point are in the same layer. If the source point and the observation point are in different layers, then iterative equations should be written. First, spectral domain field expressions are written for an arbitrary layer which is in most cases the source layer. Then, spectral domain Green's functions in observation layer are found for each TE-z and TM-z component by using the Green's functions in source layer [30, 44]. As an example, for an arbitrary region j TE-z field distribution can be written as shown in equation (53).

$$G_j^{TE}(z) = A_j^{-}\left(e^{jk_{zj}z} + \widetilde{R}_{TE}^{j,j-1}e^{-jk_{zj}z}e^{jk_{zj}2(-z_{-m}-h)}\right) \tag{53}$$

Where $j = i - m$

Here A_j^- is the amplitude of down-going wave in layer j. Similarly, equation (53) can be constructed for region j+1 and this is provided in equation (54).

$$G_{j+1}^{TE}(z) = A_{j+1}^{-}\left(e^{jk_{z(j+1)}z} + \widetilde{R}_{TE}^{j+1,j}e^{-jk_{z(j+1)}z}e^{jk_{z(j+1)}2(-z_{-m+1}-h)}\right) \tag{54}$$

There is a relation between region j and region j+1. The field in region j is composed of the summation of direct term, up-going waves and down-going waves. The down-going waves

in region j are the summation of transmitted part of down-going waves in region j+1 and reflected part of up-going waves in region j. By using these relations the required equations can be constructed for finding the coefficients of up and down-going waves and they are shown in equations (55) and (56). These analyses should be applied to TE-z and TM-z modes separately. Additionally, these analyses can be performed to HMD, VED and VMD sources as well as the HED source. However, the details are not given in this thesis the reference can be investigated [30].

$$A_j^- = A_{j+1}^- \frac{T^{j+1,j} e^{-j(k_{z(j+1)}-k_{z(j)})(h+z_{-m+1})}}{1-R^{j,j+1}\widetilde{R}^{j,j-1} e^{-jk_{zj}2d_j}} \tag{55}$$

$$A_j^+ = A_{j-1}^+ \frac{T^{j-1,j} e^{-j(k_{z(j-1)}-k_{z(j)})(z_{m-1}+d_i-h)}}{1-R^{j,j-1}\widetilde{R}^{j,j+1} e^{-jk_{zj}2d_j}} \tag{56}$$

Since the up and down-going wave coefficients A_i^+ and A_i^- are known, the relations in equations (55) and (56) can be used to find the coefficients in other layers iteratively. By this way, the coefficients in the observation layer can be found and then the full expressions of the fields in the observation layer can be constructed.

APPENDIX B

PRONY'S METHOD

Prony's method is similar to the Fourier transform such that it gathers lots of information from uniformly sampled data. In this method sampled data can be expressed in terms of exponentials. In this thesis study, the obtained current distribution values can be considered as sampled data, so current distribution can be approximated in terms of exponentials. By this way, information such as reflected and incident wave coefficients can be acquired from the current distribution [19]. As similar to the Fourier transform technique, by using this method valuable information can be acquired from the sampled data. The current distribution on metal can be expressed in terms of the summation of reflected and incident waves, as shown in equation (1).

$$I(x) \cong c_1 e^{\beta_1 x} + c_2 e^{\beta_2 x} \tag{1}$$

In order to obtain the current distribution values as uniformly sampled data, current distribution values should be obtained as x equally spaced points on the metal line and this uniform sampling of current distribution is provided in equation (2).

$$x = \frac{length\ of\ the\ metal\ line}{N+1} n \tag{2}$$

$$\text{where } 0 \le n \le N+1 \quad (N = Number\ of\ basis\ functions)$$

If the specific expression in equation (1) is expressed as a general form, it should be denoted as the one given in equation (3).

$$I[x] \cong \sum_{k=1}^{p} c_k e^{\beta_k x} \tag{3}$$

Where, c_k and β_k are the unknown parameters that should be found. If an exponential part in equation (3) is defined as a general variable z_k, then this variable can be expressed as the one that is shown in equation (4).

$$z_k = e^{\beta_k \frac{length of the metal line}{N+1}} \tag{4}$$

Equation (3) is redefined in equation (5) by substituting equation (2) and equation (4) into equation (3).

$$I[n] \cong \sum_{k=1}^{p} c_k z_k^n \tag{5}$$

As seen from equation (5), the expression is in the form such that it can be expressed as a matrix equation. Therefore, the matrix equation form of the expression in equation (5) is shown in equation (6).

$$\begin{bmatrix} z_1^0 & z_2^0 & . & . & z_{p-1}^0 & z_p^0 \\ z_1^1 & z_2^1 & . & . & z_{p-1}^1 & z_p^1 \\ . & . & . & . & . & . \\ . & . & . & . & . & . \\ . & . & . & . & . & . \\ z_1^{N+1} & z_2^{N+1} & . & . & z_{p-1}^{N+1} & z_p^{N+1} \end{bmatrix} \begin{bmatrix} c_1 \\ c_2 \\ . \\ . \\ . \\ c_p \end{bmatrix} = \begin{bmatrix} I[0] \\ I[1] \\ . \\ . \\ I[N] \\ I[N+1] \end{bmatrix} \tag{6}$$

Indeed, equation (5) can be considered as in the form of the solution of a homogeneous linear constant-coefficient difference equation. The general form of this difference equation is given in equation (7), where $a[m]$ values are the unknown complex coefficients and $a[0]=1$, the details can be found in the reference [19].

$$\phi(z) = \sum_{m=0}^{p} a[m] z^{p-m} \tag{7}$$

From equation (7), $(N+2-p)$ linear equations are acquired and these equations can be expressed in a matrix form which is shown in equation (8).

$$\begin{bmatrix} I[0] & I[1] & I[p-2] & I[p-1] \\ I[1] & I[2] & I[p-1] & I[p] \\ . & . & . & . \\ I[N+1-p] & I[N+2-p] & I[N-1] & I[N] \end{bmatrix} \begin{bmatrix} a[p] \\ a[p-1] \\ . \\ a[1] \end{bmatrix} = \begin{bmatrix} -I[p] \\ -I[p+1] \\ . \\ -I[N+1] \end{bmatrix} \tag{8}$$

If $N > 2p$ is assumed, method of least squares can be applied in order to find out unknown $a[m]$ coefficients [19]. Afterwards, $a[m]$ coefficients are substituted into equation (7) and equation (7) can be solved accordingly. Therefore, z_k values which are the roots of the difference equation in equation (7) can be found. Since z_k variable values are expressed in terms of β_k values in equation (4), this relation can be used to acquire the corresponding values of β_k. After this analysis, reflected and incident wave coefficient values can be obtained. Subsequently, the ratio of these coefficients will result the reflection coefficient at a given frequency. This explained Prony's method is transformed into MATLAB® program. The inputs of this software program are current distribution values and the corresponding outputs of the program are incident and reflection coefficients. Afterwards, reflection coefficient can also be found accordingly.